Gravity Data Analysis and 3D Modeling of the Caribe-South America Boundary (76°– 64° W)

Dissertation
in fulfillment of the requirements for the degree “Dr. rer. nat.”
of the Faculty of Mathematics and Natural Sciences
at Kiel University

submitted by
Javier Sanchez Rojas

Kiel, 2012

First referee: Prof. Dr. Hans-Jürgen Götze

Second referee: Prof. Dr. Wolfgang Rabbel

Date of the oral examination: 09.05.2012

Approved for publication: 10.05.2012

Abstract

During this work, a new gravity data compilation for Venezuela was processed and homogenized. Gravity values were reference to the International Gravity Standardization Net 1971. The new complete Bouguer anomaly was calculated by using the Geodetic Reference System 1980 and 2.67 Mg/m^3. Gravity maps were analyzed using different techniques, which include separation of the regional and residual Bouguer gravity fields, spectral analysis of the Bouguer anomaly, Euler deconvolution of the Bouguer gravity field, and averaged admittance function of topography and Free-Air anomaly to study the effective elastic thickness of topography and Free-Air anomaly along selected profiles (e.g. Mérida Andes).

The results of independent detailed geophysical surveys were used in conjunction with the reprocessed gravity data in the construction of 3-D density model to study of the tectonic of the Caribbean-South America plate boundary. The model was constrained by four wide-angle seismic refraction profiles, Moho depth estimations from receiver functions, and additionally seismological hypocenters, surface geology, and geodynamic information. Density values were calculated from empirical velocity-density functions, and mineralogical-chemical compositions that consider specific P/T conditions. The results of the different analyses of the gravity field and the 3D-modeling can be summarized as follows:

The separation of the regional component of the gravity anomaly was achieved by removing wavelengths greater than 200 km from the Bouguer anomaly. After the anomaly separation, regional and residual Bouguer gravity fields were then critically discussed in term of the regional tectonic features. According to the results of the power spectrum analysis of the gravity data, the averaged Moho depths for the massif, plains, and mountainous areas in Venezuela are 42, 35, and 40 km, respectively. The averaged admittance function computed across Mérida Andes showed a good fit for a regional compensation model with an effective elastic thickness of 15 km.

The 3D-model showed that the structure of the crust and lithospheric mantle under the study area can be explained by a layered model with density variations in North-South, as well as in West-East direction. This pattern of variation is mainly dominated by petrology, tectonics and thermal age. Different structural models were tested for Western and Eastern Venezuela.

The results of this investigation support the long–slab model in Western Venezuela. This geometry resulted in a good fit between observed and modeled gravity. The slab extends from the area of the Bucaramanga nest in northern Colombia to the Maracaibo block. The dip direction of the slab changes from N~150°E ± 5 in western Colombia to South in western Venezuela. This change occurs mainly underneath the Maracaibo block. The slab dip is approximately 15°, and increases up to 20° at depths greater than 100 km. Focal mechanism solutions and 3-D distribution of the recent seismicity in the region showed good correlation with the proposed geometry of the slab.

Modeling results showed that there is small contribution on the gravity field from alternative slab position underneath Eastern Venezuela Basin. The best observed-modeled gravity fitting model support the hypothesis of subduction-transform propagation mechanism which involves purely westward subduction with the slab break off along of a vertical dip-slip tear through the lithosphere.

Zusammenfassung

Im Rahmen der vorliegenden Arbeit wurde eine neue Kompilation von Schweredaten für Venezuela verarbeitet und homogenisiert. Die Schwerewerte waren im IGSN 71 referenziert. Die neue vollständige Bouguer-Anomalie war durch Verwenden des Geodätischen Referenzsystems 1980 (GRS80) und einer Referenzdichte von 2.67 Mg/m^3 berechnet worden. Die Schweredaten wurden durch verschiedene Techniken analysiert, unter anderem Wellenlängen-Filterung für die regionalen und lokalen Komponenten des Gravitationsfeldes, Spektralanalyse und Euler-Dekonvolution der Bouguer Anomalie, und Admittanz Funktion von Topographie und Freiluftanomalie entlang von Profilen zur Bestimmung der effektiven elastischen Dicke (z. B. *Mérida Anden*).

Um die Tektonik der Karibik-Südamerika Plattengrenze zu untersuchen, wurden die Ergebnisse der unabhängigen geophysikalischen Studie, zusammen mit den neuen Schweredaten wurden in einem 3D-Dichtemodell zusammengeführt. Das Modell wurde kontrolliert durch vier seismische Weitwinkel-Refraktionsprofile, Abschätzungen der Moho-Tiefe durch Receiver-Funktionen und zusätzlich durch seismologische Herdtiefen, sowie Oberflächengeologie und Geodynamik. Dichtewerte wurden aus empirischen Geschwindigkeits-Dichte-Funktionen, aus der mineralogisch-chemischer Zusammensetzung und aus spezifischen P/T-Bedingungen berechnet. Die Ergebnisse aus den unterschiedlichen Analysen des Schwerefeldes lassen folgende Interpretation zu:

Die Trennung der regionalen Komponenten der Schwerkraft-Anomalien wurden durch Entfernen von Wellenlängen größer als 200 km von der Bouguer Anomalie erreicht. Nach der Trennung der Anomalien, wurden regionale Bouguerschwerefelder und Bouguer-Restschwerefelder in Bezug auf regionale tektonische Strukturen diskutiert. Nach der Spektralanalyse der Bougueranomalie wurden die durchschnittlichen Moho-Tiefen der Massive, der Ebenen und der Bergregionen in Venezuela auf 42, 35 und 40 km bestimmt. Die über den Mérida Anden berechnete gemittelt Admittanz-Funktion zeigt eine gute Anpassung für ein regionales Kompensationsmodell mit einer effektiven elastischen Dicke von 15 km. Die Ergebnisse der 3D Modellierung lassen sich wie folgt zusammenfassen:

Das 3D-Modell zeigte, dass die Struktur der Kruste und Lithosphäre Mantel unter dem Untersuchungsgebiet durch ein Schichtenmodell mit Dichten Variation in Nord-Süd und in

West-Ost Richtung erklärt warden kann. Das Muster der Veränderung ist vor allem durch Petrologie, tektonische und thermische Alter bedingt. Verschiedene strukturelle Modellvarianten wurden für west und ost Venezuela getestet. Die Ergebnisse dieser Untersuchung unterstützen die lang-Platte in West-Venezuela. Gegenüber dem Modell mit kurzer Platte zeigt diese Geometrie eine bessere Übereinstimmung zwischen modellierten und gemessenen Schwerewerten. Die Platte erstreckt sich vom Bucaramanga Nest im Norden Kolumbiens bis zum Maracaibo-Block.

Die Streichrichtung der Platte wechselt von N ~ 150° ± 5 E im Westen Kolumbiens auf Süd-Richtung im Westen Venezuela. Diese Veränderung erfolgt überwiegend unter dem Maracaibo-Block. Der Neigungswinkel beträgt etwa 15°, mit einem Winkel bis zu 20° in Tiefen größer als 100 km. Herdmechanismen und 3D-Verteilung der Seismizität in der Region zeigen eine gute Korrelation mit der n Geometrie der Platte. Die Ergebnisse der Modelierung zeigen, daß die alternativen Modelle im Osten Venezuelas nur einen kleinen Einfluß auf das Schwerefeld ausüben. Das Modell mit der besten Übereinstimmung zwischen modellierten und gemessenen Schwerewerten unterstützt die Hypothese der Fortpflanzung der Subduktion der ozeanischen südamerikanischen Platte entlang von Transform-Störungen nach Westen unter die karibische Platte. Danach reisst die südamerikanische Platte entlang eines Systems von Transform-Störungen auf.

Resumen

Durante este trabajo de tesis, una nueva compilación de datos gravimétricos para Venezuela fue procesada y homogenizada. Los valores de gravedad fueron referenciados a la red gravimétrica internacional IGSN-71 (*International Gravity Standardization Net 1971*), y la anomalía de Bouguer completa fue calculada usando como sistema de referencia el *Geodetic Reference System 1980* (GRS80) y una densidad de Bouguer de 2.67 Mg/m^3. Mapas gravimétricos fueron analizados usando diferentes técnicas entre las que se incluyen separación de las componentes del campo de gravedad en anomalía residual y anomalía regional, análisis espectral de la anomalía de Bouguer, deconvolución de Euler y estimación del espesor elástico efectivo mediante el estudio de la función de admitancia entre datos topográficos y la anomalía de aire libre sobre perfiles trazados (*e. g.* Los Andes de Mérida).

Los resultados obtenidos a través de estudios geofísicos de alta resolución fueron compilados y conjuntamente con los datos gravimétricos usados en la construcción de un modelo de densidad tridimensional con el objetivo de estudiar la estructura tectónica en el límite entre el norte de Sur América y el Caribe. Principalmente, el modelo fue ajustado a los resultados observados en cuatro perfiles sísmicos de refracción profunda, estimaciones de la profundidad de Moho obtenidas con funciones de receptores, localización de hipocentros sísmicos, mapas de geología de superficie e información geodinámica. Los valores de densidad usados en el modelo fueron estimados mediante funciones empíricas de la relación entre la densidad y las velocidades de las ondas sísmicas y funciones que consideran la composición químico-mineralógica a condiciones P/T específicas. Los resultados del análisis y modelado 3D de los datos gravimétricos se resumen a continuación:

La separación de la componente regional de la anomalía de Bouguer fue calculada mediante la remoción de las anomalías con longitud de ondas mayores a 200 km. Los mapas de las componentes de la gravedad fueron críticamente discutidos en términos de las estructuras tectónicas a nivel regional. De acuerdo con los resultados obtenidos en el análisis espectral, las profundidades promedio del Moho en macizos, llanuras y áreas montañosas en Venezuela son 42, 35 y 40 km, respectivamente. Los valores de espesor elástico, estimados mediante la función de admitancia en perfiles, sobre los Andes de Mérida mostraron buena correlación con un modelo de corteza con un espesor elástico de 15 km.

El modelo 3D final muestra que la estructura litósferica en el área de estudio puede ser representada mediante un modelo de capas horizontales, compuestas por cuerpos con densidades con variación norte-sur y oeste-este. El patrón de variación de la densidad esta principalmente dominado por cambios petrológicos, tectónicos y de las condiciones térmicas. Adicionalmente, fueron examinados diferentes modelos existentes que explican la estructura de la corteza en el Oeste y Este de Venezuela. Por ejemplo, en el Oeste el modelo con un segmento de placa Caribe subducido (*slab*) largo mostro mejor ajuste que el modelo con un *slab* corto. Este resultado es consistente con resultados publicados por diferentes autores. El segmento subducido de la placa se extiende desde el nido sísmico de Bucaramanga al norte de Colombia hasta el bloque de Maracaibo. El buzamiento del *slab* cambia de dirección entre N~150° E ± 5 en Colombia hasta dirección sur en Venezuela. El cambio de dirección ocurre principalmente debajo del boque de Maracaibo (e. i. Sistema de fallas de Santa Marta). El buzamiento del *slab* fue estimado en 15°, dicho valor aumenta hasta 20° a profundidades mayores de 100 km. El análisis de mecanismos focales y sismicidad local mostro buena correlación con la geometría modelada del *slab*.

Los resultados del modelado en el Este de Venezuela mostraron que existe poca contribución de modelos alternativos para la posición de la placa oceánica sudamericana subduciendo debajo de la cuenca Oriental. El modelo con el mejor ajuste entre valores calculado y medidos de la anomalía de Bouguer, fue el modelo de *subduction-transform propagation mechanism,* el cual propone subducción hacia el oeste de la placa oceánica suramericana por debajo de la placa Caribe. En este modelo, la placa suramericana se rompe a lo largo de un sistema de fallas transcurrentes.

Table of Contents

1. Introduction

It is commonly accepted that the present shape of northwestern South America is the result of interactions between the South American (SA) , Nazca, and Caribbean plates (CA), which began during the Late Jurassic–Early Cretaceous (180 Ma) with the separation of the Americas and the formation of the proto-Caribbean ocean basin (Pindell 1994; Meschede and Frisch 1998). Extensive volcanism in the mid- to late Cretaceous (~90–110 Ma) resulted in the formation of the Caribbean Large Igneous Province and a thickening of large areas of the Caribbean crust (Hoernle et al. 2004). Around this time, the Caribbean plate initiated an eastward migration relative to South America (Pindell and Dewey 1982; Burke 1988; Pindell et al. 1988; Pindell and Barrett 1990; Pindell et al. 2005). The resulting variety in geologic features between the CA and SA margins includes accretionary wedges, fold and thrust belts, and extensional and foreland basins. Current relative plate motions make the boundary predominantly strike-slip, bounded in the East by the Atlantic subduction and in the west by partial subduction of the Caribbean plate under South America (Figure 1.1). The origin, tectonic structure, and the geodynamics of the Caribbean plate have remained controversial over the last few decades and are still open questions.

In recent times, several projects have been conducted to collect new geological and geophysical data which aim in a better understanding of the structure of northern South America, which is a prime location to study the processes that lead to continental crust formation and growth with an enormous economic importance for its oil fields, e.g. BOLIVAR (Broadband Ocean-Land Investigations of Venezuela and the Antilles arc Region) and GEODINOS (Recent Geodynamics of the Northern Limit of the South American Plate) projects (Levander et al. 2006). These projects aim to increase the knowledge of the current structure, geodynamics, tectonic development, and evolution in the Caribbean region. The collection, modeling and interpretation of geophysical data on a lithospheric and sub-lithospheric level constitute one of the main focuses of the projects.

I reviewed the main results and findings from the mentioned projects and used them to constrain a new 3-D density model for the entire region, using, the modeling was performed under the new gravity data collected by the GEODINOS project for modeling purposes.. This

dissertation is composed of slightly modified versions of three manuscripts, in different stages of the publication process, which show some relevant results of ongoing geophysical investigations. The first chapter is an introduction to the dissertation. This chapter summarizes the open questions, the main hypothesis driving the scientific work and methods used throughout this work. The first manuscript is presented in chapter 2, and presents the interpretation of a new Bouguer anomaly map of Venezuela by means of studying the correlation between the Bouguer anomalies, the regional geology, and the continental crustal thickness (Moho) using a spectral technique; and the spatial variations in elastic thickness (*Te)* in the mountainous areas using the coherence-admittance techniques. This manuscript was published in the International Journal of Geophysics [1]. The results of this latter work were fundamental for the development of the three dimensional density model of the southeast Caribbean-South American plate boundary that forms the chapter 3 and corresponds to the second manuscript. This manuscript studies and develops a consistent density model through testing different proposed models in eastern Venezuela in order to gain better understanding of the relationship and interactions of the mantle lithosphere and crustal features. This manuscript was written with the collaboration of Hans-Jürgen Götze and Michael Schmitz (supervisors of this thesis) and published in the International Journal of Earth Sciences [2]. The third manuscript that forms the chapter 4 of this thesis, currently under review by the *Geophysical Journal International,* studies and describes a 3-D density model of northern South America between 5° to 15°N and 67° to 78°W, encompassing parts of Colombia, Venezuela, the Caribbean Sea, and the Pacific Ocean. This manuscript was written with the collaboration of Miguel Palma. Who included important data to delimitate the geometry of the Caribbean slab based on the analysis of the seismicity of the region. Results show an outlook of the continental-scale structure of South America plate. However, this work also left several open issues that will set the precedents for further studies, as proposed in the conclusions of this dissertation.

[1] Sanchez-Rojas, J. (2011). New Bouguer gravity maps of Venezuela: Representation and analysis of free-air and Bouguer anomalies with emphasis on spectral analyses and elastic thickness. International Journal of Geophysics: 1-15. doi:10.1155/2012/731545.

[2] Sanchez, J., et al. (2011). A 3-D lithospheric model of the Caribbean-South American plate boundary. International Journal of Earth Sciences 100(7): 1697-1712. doi: 10.1007/s00531-010-0600-8.

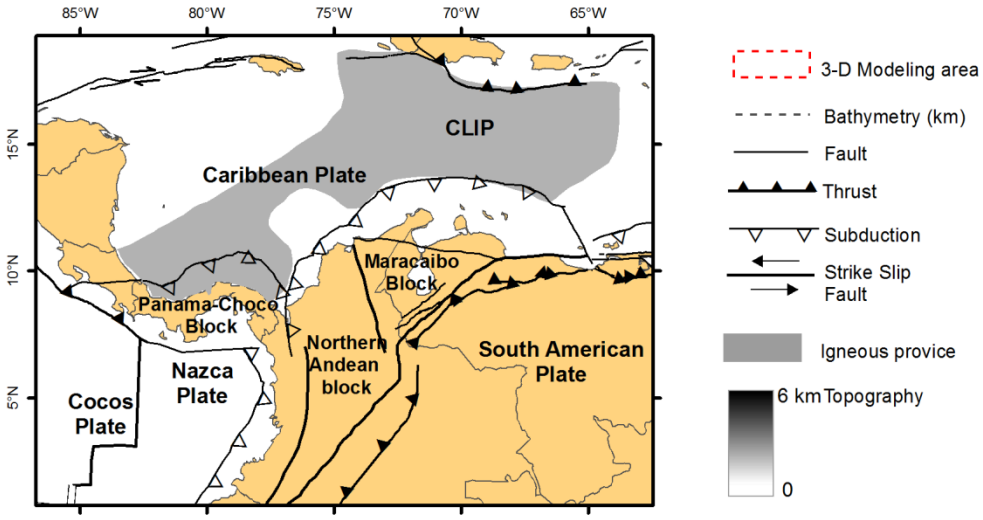

Figure 1.1 Tectonic overview of the Caribbean plate and neighboring regions. Extent of thickened Caribbean oceanic crust (crustal thickness >10 km), modified after Mauffret and Leroy (1997).

1.1. Interactions among South American plate and surrounding plates short outline of the evolution

In the early Jurassic, the Pangaea continental crust broke up, and South American plate rifted away from North America. The northern South America plate margin is the result of a long interaction among the Caribbean, North America and Nazca plates. Nowadays, the Caribbean plate is bounded in the West by the Middle American subduction zone and in the East by the Lesser Antilles subduction zone. The northern and southern boundaries are not as well defined. Furthermore, southeastern Caribbean plate interaction zone is described as a 600 km wide and 800 km long diffuse boundary, bounded to the north and south by oppositely verging folds, thrust belts and foreland basins, and it is traversed in the middle by the San Sebastian-El Pilar dextral strike-slip fault system and the Boconó dextral strike-slip fault system (Audemard and Audemard 2002), which dominates the tectonics of the plate boundary.

Two different models have been presented of how the Caribbean might have formed. The Pacific models (Figure 1.2a) propose a Late Mesozoic origin of the Caribbean oceanic crust in the Pacific region and drift into its present position between the two Americas (Wilson 1965; Malfait and Dinkelman 1972; Burke K et al. 1978; Pindell and Dewey 1982; Ross and

Scotese 1988; Stephan et al. 1990; Pindell 1994). Alternative models (Figure 1.2b) propose formation of the Caribbean crust to the west from its present position but still an intra-plate history of the Caribbean between both Americas (Ball and Harrison 1969; Aubouin et al. 1982; Sykes et al. 1982; Donnelly 1985; Klitgord KD 1986; Frisch et al. 1992; Meschede 1998; Meschede and Frisch 1998). Conflicts between the differing views of plate-tectonic evolution arose from timing of events, plate configuration, origin of blocks and terranes (e.g. Greater Antilles), and paleomagnetic data. Both models converge towards the beginning of the Cenozoic.

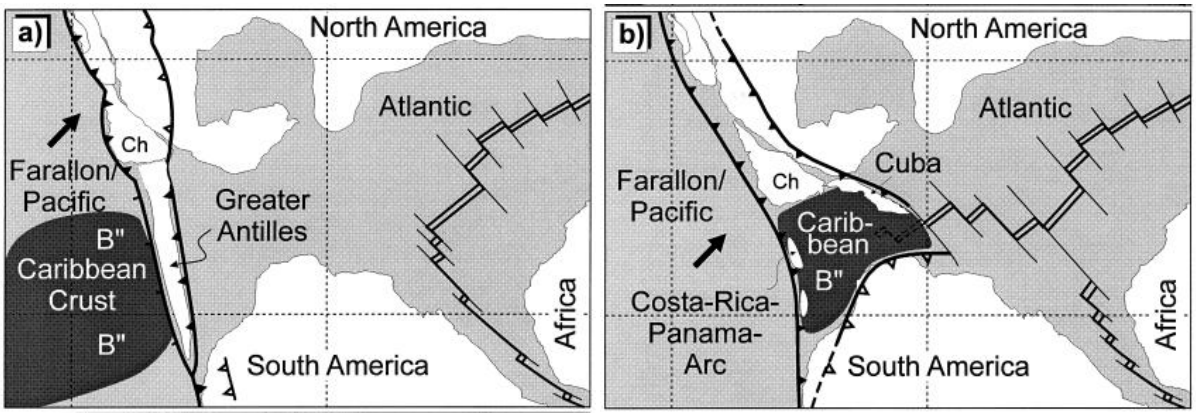

Figure 1.2 Two families of hypotheses to explain the origin of the Caribbean lithosphere (comparison of palinspastic reconstructions of the Albian, 100 Ma): (a) 'Pacific model', modified after Pindell (1994) Caribbean crust (B'' reflector) formed in the Pacific realm. (b) Alternative hypothesis; formation of the Caribbean crust in an inter-American position.

Early models of the tectonic evolution of the Nazca plate were established by means of reconstruction of magnetic anomalies and bathymetric data (Hey 1977; Lonsdale and Klitgord 1978). These models suggested that major plate reorganization took place in the region around 25 Ma, breaking the ancient Farallon plate into the Cocos–Nazca plate and the Juan de Fuca plate. Differential stresses between the Cocos segment and the Nazca segment near the Galapagos hot spot later evolved into N–S seafloor spreading (Cocos–Nazca Spreading Center) along the two segments and originating from both Nazca and Cocos plates.

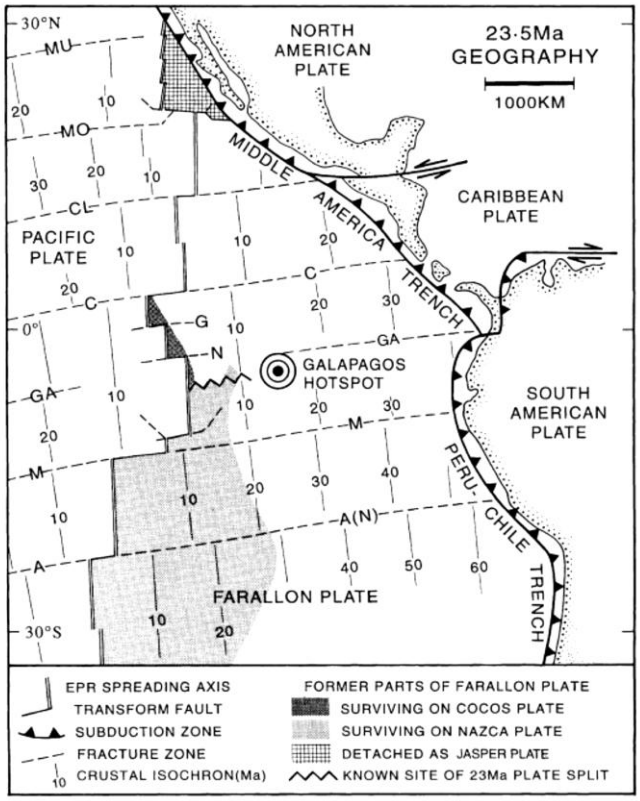

Figure 1.3 Reconstruction of the geography of the Farallon plate just before splitting into the Cocos and Nazca plates. Note that most of the plate has subsequently been lost by subduction (Lonsdale 2005).

Several seismological studies indicate that a continuous slab built as part of the Caribbean lithosphere subduct beneath Northern Colombia and NW Venezuela, and extends along the entire width of Mérida Andes (Van der Hilst and Mann 1994; Malavé and Suárez 1995; Perez et al. 1997; Colmenares and Zoback 2003). Another hypothesis assumes a tear fault along San Sebastian-El Pilar fault system (Taboada et al. 2000). Based on records of intermediate depth seismicity, the dip angle and dip direction of the slab are estimated to be 17°±3° and 50°±20°, respectively (Van der Hilst and Mann 1994).

1.2. Focus and working hypothesis

The work of this thesis focuses on the establishment and description of a 3-D density model of northern South America between 5° to 15°N and 67° to 78°W (Figure 1.1) encompassing parts of Colombia, Venezuela, the Caribbean Sea, and the Pacific Ocean. The

model obtained of the study area get use of up- to-date existing geophysical and geological data, which include topography, bathymetry, wide-angle seismic studies, seismicity distribution, deep boreholes, and surface geology.

The main hypothesis analyzed throughout this dissertation are that a continuous Caribbean slab subducted beneath Northern Colombia and NW Venezuela, and extends along the entire width of Mérida Andes and that south American oceanic crust in eastern Venezuela break off beneath western Gulf of Paria as a subduction-transform propagation model with purely westward subduction.

This work is by no means a conclusive final answer, it is part of a road toward a better understanding of this much debated margin, and provides some answers to outstanding questions, adds new constraints, and point towards new directions for new researches.

1.3. Previous work

In order to avoid ambiguity in the gravity model, independent information has to be used for constraining the model. Results from methods such as reflection and refraction seismic, seismology, magnetotellurics and receiver function methods represent the major contributions to the final model. They provide information on the structure of the Earth's interior and their physical parameters (velocities, susceptibilities, depths of boundaries of studied structures, seismicity etc.). Cartography geology, provide information about structures, tectonic setting, deformation processes that take place in a study area. Petrology and geochemistry indicate of the composition of subsurface structures. All of this information provides constraints necessary for density modeling.

The main independent information used in this work came from the GEODINOS and the BOLIVAR projects, among that information are wide angle seismic measurements, conformed by four refraction profiles, fairy distributed in northern Venezuela (Schmitz et al. 2008). The BOLIVAR (Broadband Ocean-Land Investigation of Venezuela and the Antilles arc Region) project was designed to image the structure of the lithosphere along the entire southeastern Caribbean margin (Levander et al. 2006).

1.3.1.1. Earlier gravity modeling in Venezuela

For many years, in Venezuela and surrounding countries have been carried out gravity surveys and also have been presented gravity models, now days there are more than 40 two dimensional (2-D) gravity models (Figure 1.4).

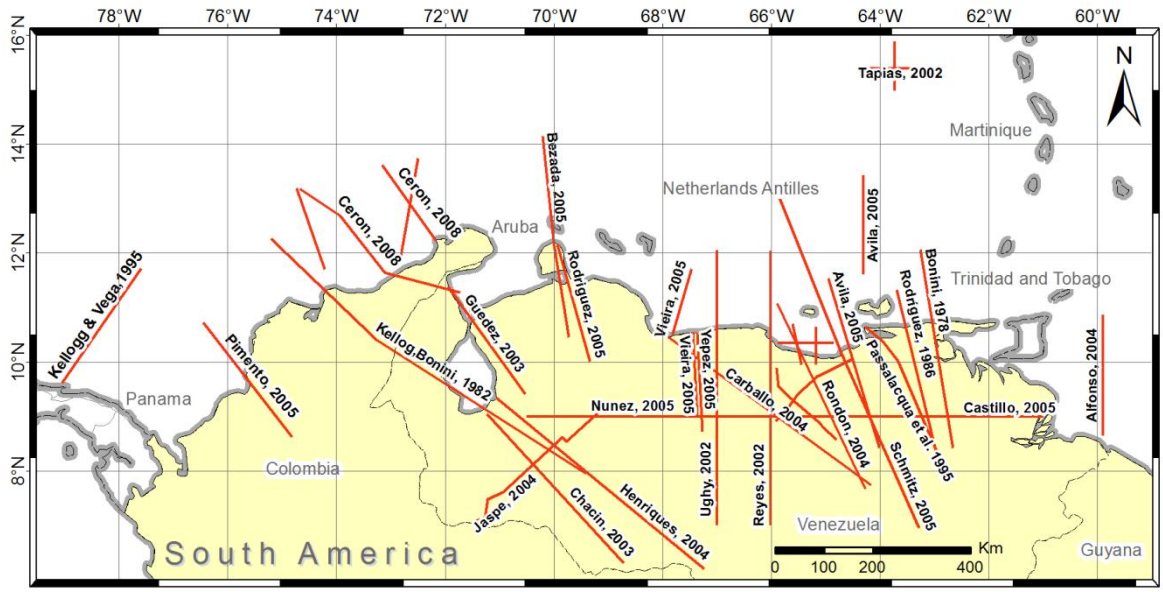

Figure 1.4 Map of the distribution of previous 2D gravity models in Venezuela (Bonini et al. 1977; Kellogg and Bonini 1982; Rodríguez 1986; Kellogg and Vega 1995; Passalacqua et al. 1995; B.Sc.Ughi 2002; Reyes 2002; Tapias 2002; Chacín 2003; Guédez 2003; Alfonso 2004; Carballo 2004; Henriques 2004; Jaspe 2004; Rondon 2004; Ávila 2005; Castillo 2005; Núñez 2005; Schmitz et al. 2005; Sousa et al. 2005; Vieira 2005; Yépez et al. 2005; Pimiento 2007; Bezada et al. 2008; Ceron 2008).

1.4. Methods

The methodology used in this thesis comprises two main steps: Analysis of existing gravity data to study the gravity response of the first order structure, and construction of a lithospheric-scale three-dimensional (3D) model constrained by all available geological and geophysical information about the structure of the Caribbean–South America boundary.

2. New Bouguer gravity maps of Venezuela: Representation and analysis of free-air and Bouguer anomalies with emphasis on spectral analyses and elastic thickness

A new gravity data compilation for Venezuela was processed and homogenized. Gravity was measured in reference to the International Gravity Standardization Net 1971, and the complete Bouguer anomaly was calculated by using the Geodetic Reference System 1980 and 2.67 Mg/m^3. A regional gravity map was computed by removing wavelengths higher than 200 km from the Bouguer anomaly. After the anomaly separation, regional and residual Bouguer gravity fields were then critically discussed in term of the regional tectonic features. Results were compared with the previous geological and tectonic information obtained from former studies. Gravity and topography data in the spectral domain were used to examine the elastic thickness and depths of the structures of the causative measured anomaly. According to the power spectrum analysis results of the gravity data, the averaged Moho depths for the massif, plains, and mountainous areas in Venezuela are 42, 35, and 40 km, respectively. The averaged admittance function computed from the topography and Free-Air anomaly profiles across Mérida Andes showed a good fit for a regional compensation model with an effective elastic thickness of 15 km.

2.1. Introduction (Earlier gravity mapping in Venezuela)

Gravity surveys have been carried out in Venezuela since 1945 with the intensification of oil exploration. Thus, gravity surveying was first confined to the oil-producing sedimentary basins (i.e., Maracaibo and Eastern Venezuela basins). The first precise gravimetric survey covering the whole country was carried out as late as 1970 under the framework of the Latin American Gravity Standardization Network (McConnell et al. 1979), which established a national network. The Venezuelan National Geographic Institute published the first gravity map of the entire country after 1988 (Graterol 1988). Since then, several Venezuelan universities and official institutes have cooperated with international institutes to improve the coverage of the national network. In addition, the Venezuelan National Oil Company (PDVSA) has released a large amount of data for educational purposes. In this context, Izarra

et al. (2005) presented the last gravity data compilation from Simon Bolívar University in 2005. However, due to the extent of the country and the presence of inaccessible areas such as the Amazon forest and Mérida Andes, general improvement in the data coverage has been slow.

The purpose of this work is to present a new Bouguer anomaly map of Venezuela using the data available thus far. This study has four main aims: (1) to study the correlation between the Bouguer anomalies and the known regional geology by means of regional and residual gravity anomaly separation; (2) to estimate the continental crust thickness (Moho) using a spectral technique and to correlate it with Moho estimations derived from independent geophysical techniques (i.e., P-wave velocity models, which stem from wide-angle refraction seismic and the results from receiver function methods); (3) to use the coherence-admittance techniques to determine the spatial variations in elastic thickness (*Te)* in the mountainous areas; and (4) to provide a new updated gravity database for future investigations.

2.2. Geological setting

Different theories have been proposed about the origin of the Caribbean Plate (Pindell 1994; Meschede and Frisch 1998). Nowadays, it is commonly accepted that extensive volcanism in the mid- to late Cretaceous (~90–110 Ma) resulted in the formation of the Caribbean Large Igneous Province and a thickening of large areas of the Caribbean crust (Hoernle et al. 2004). Around this time, the Caribbean plate (CA) initiated an eastward migration relative to South America (SA) (Pindell and Dewey 1982; Burke 1988; Pindell et al. 1988; Pindell and Barrett 1990; Pindell et al. 2005). The resulting variety in geologic features between the CA and SA margins includes accretionary wedges, fold and thrust belts, and extensional and foreland basins (Ostos et al. 2005). Current relative plate motions make this margin predominantly strike-slip; it is limited on the east by subduction of oceanic (Atlantic) SA beneath the Lesser Antilles island arc (Weber et al. 2001) and in the west by partial subduction of the Caribbean plate under South America (Figure 2.1). On the continental deformation front observed along the Venezuela coastline, the important (large oil-producing) Barinas-Apure and Eastern basins have been formed. Barinas-Apure is mainly a foreland basin generated by the flexural response to the Mérida-Andes Mountain load (Chacín et al. 2008). On the other hand, the Eastern basin can be considered to be the result of (a) flexural loading of the Cordillera de la Costa range; (b) large and continuous deposition of

continental material from the Guyana shield; and (c) subduction dynamics in the east (Jácome et al. 2003). The Barinas-Apure and Eastern Venezuelan sedimentary basins are separated by a geomorphologic-structural high called El Baúl High, formed by an igneous-metamorphic complex. This massif was described by Bellizzia (1961), who differentiated several granitic, volcanic and metasedimentary units and subunits. For instance, the Maracaibo basin is a foreland basin separated from Barinas-Apure by the emplacement of the Mérida Andes. This basin is bounded on the north by the Oca-Ancon fault system, Sierra de Perijá to the west, and the Mérida Andes mountains to the south and east. Mérida Andes (MA) is a NE–SW trending mountain chain about 420 km long and with a maximum height of 5 km. This uplifted block was formed as a consequence of the convergence of the Panama arc and western South America (Stephan 1982; Audemard 1991; Colletta et al. 1997; Audemard and Audemard 2002). According to Schubert (1984) and Kohn et al. (1984) this convergence has the main period of shortening during the Oligocene-Miocene, and evidence suggest that there is still significant present day deformation.

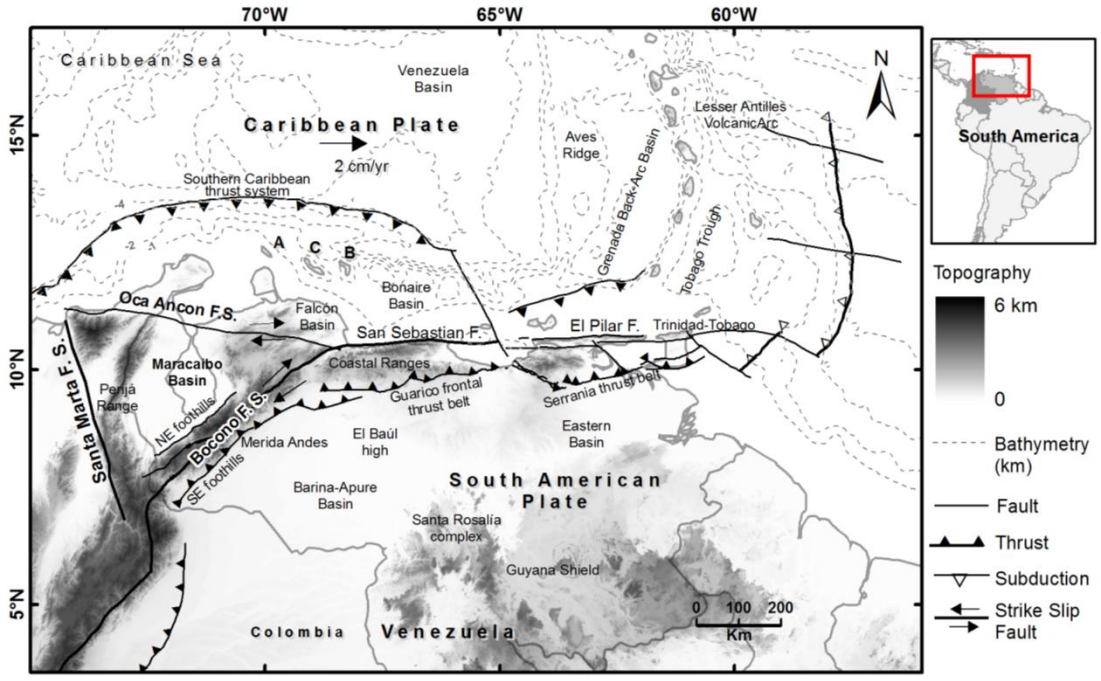

Figure 2.1 Study area and general tectonic and kinematic features of the northern margin of South America setting (modified from Audemard and Audemard (2002) on a digital elevation map. Arrows indicate relative regional motions. Texts indicate the name of geological or tectonic features. A, B, and C mean Aruba, Bonaire, and Curazao (ABC islands).

Due to the large amount of interactions and its complexity between the CA–SA plates, the location of the plate boundary is controversial. Thus, this boundary has been interpreted as a 300 km wide plate boundary zone (Avé Lallemant 1997) that forms an orogenic float. This orogenic float is represented by the Mérida Andes; it is linked to the north with the Northern Cordilleras of Venezuela (i.e., Cordillera de la Costa range) and goes as far as the Trinidad-Tobago islands to the east. The boundary zone is limited by the Southern Caribbean thrust system on the north and the Mérida Southern Foothills, Guárico Frontal thrust belt, and Serranía thrust belt on the south (Audemard and Audemard 2002). The Cordillera de la Costa range is formed by different geological provinces containing (from north to south) late Jurassic to early Cretaceous basic and ultrabasic rocks, Precambrian and Paleozoic basement rocks, Jurassic to Cretaceous lower crust–upper mantle fragments, volcano-sedimentary sequences and basaltic to rhyolitic rocks, and late Cretaceous–Paleocene molassic sediments and flysh sequences (Beck 1985; Bellizzia 1986; Navarro et al. 1988; Donnelly et al. 1990; Ostos 1990; Giunta et al. 2002).

The stable South American crust is represented by the Guyana Shield. This massif outcrops as sialic Precambrian continental crust composed mainly of metasedimentary and metaigneous rocks at amphibolite to granulite facies that have been intruded by granites (Feo-Codecido et al. 1984). The reported ages of these crystalline rocks range from 3600 to 800 Ma (González de Juana et al. 1980).

2.3. Gravity database

A new gravity data compilation is presented here that includes data from early compilations by Simon Bolivar University (Izarra et al. 2005) and data from the National Geophysical Data Center (NGDC). In order to improve the quality and coverage of onshore data, new high-resolution gravity surveys from the Venezuelan Foundation for Seismological Research (FUNVISIS) were included. Offshore data coverage was improved by new measurements from several marine surveys provided by the Marine Geoscience Data System (MGDS) (Carbotte et al. 2004).

(1) The Simon Bolivar University database consists of datasets from different Venezuelan institutions, oil companies, universities, and international surveys. Most of the data are evenly spaced; however, the compilation includes data with high accuracy (1×10^{-5} m/s^2 or less for gravity and 0.5 m or less for height) and an average station spacing of less than 100 m. This dataset has coordinates measured through the use of precise leveling methods, which were mainly collected by oil companies. In contrast, for data collected by universities, in some cases, the stations coordinates and heights were derived by reading from topographic maps. These data have elevation errors of several meters and errors of higher than 1×10^{-5} m /s^2 for the observed gravity. In addition, this dataset does not cover oil-producing areas and rugged mountainous terrains with limited accessibility. Thus, it cannot be completely discharged.

(2) The NGDC dataset was made available by the National Geophysical Data Center (NGDC), which belongs to the US Department of Commerce. This dataset includes offshore gravity data collected during research cruises from 1953 to the present from several oceanographic institutions and government agencies worldwide. As a consequence, the resolution and accuracy of this data are very variable.

(3) The MGDS dataset was made available by the Marine Geoscience Data System, which serves different communities of National Science Foundation–funded researchers and provides direct access to data (http://www.marine-geo.org). The collected data include research cruises from 1977 to 2004.

(4) The FUNVISIS dataset includes more than 4000 observations collected by a Scintrex CG-5 gravimeter combined with GPS system. The resolution and accuracy of this gravity data are 0.5×10^{-5} m/s^2 for gravity and ±1 m for station heights with average station spacing of 500 m.

Presently, the gravity compilation contains about 80,000 onshore observations and more than 40,000 offshore stations (Figure 2.2). The average station interval is less than 1 km, which results in an average station density of 1 station/km^2 or higher.

2.3.1. Data processing

A comparison of the different datasets showed that the gravity datasets and surveys in the compilation refer to different datum levels and exhibit variable quality and accuracy. Therefore, data homogenization focusing on the gravity datum and calibration and the coordinate determination and anomaly equations was required for anomaly reduction. After processing, the data were manually edited to remove erroneous measurements. Stations with outlier gravity values were removed after interpolating a high resolution gravity map.

Additionally, stations with erroneous coordinates and/or heights have been removed after comparing the station heights with those obtained by a high resolution digital terrain model (90 m spacing). Stations with heights differences of 50 m or higher were also removed. In total, more than 2000 stations were eliminated from the original database (Izarra et al. 2005).

The Bouguer anomaly was calculated using the following assumptions:

- The horizontal coordinates and elevations of the gravity stations based on the Geodetic Reference System 1980.
- Absolute gravity datum is referred to International Gravity Standardization Net 1971 (IGSN71).
- Theoretical gravity calculated at the normal ellipsoid: Somigliana's formula (Moritz 1980).
- Topography correction calculated for a spherical cap of up to 167 km radius (Hayford zone O2) (Kwang-Sun et al. 2007) assuming a constant density of 2670 kg/m^3. This value is close to the mean density of the surface rocks in the investigated area and the standard value used in the Bouguer anomaly correction. The digital terrain model used was based on the Shuttle Radar Topography Mission (SRTM) with a grid spacing of 90 m (onshore), and Gtopo30 (offshore).
- Bouguer correction equation for spherical Earth (Karl 1971).
- Height correction estimated by a Taylor series expansion of normal gravity up to 2nd order (Heiskanen and Moritz 1967).

Taking into account all the different sources of errors in the databases, the accuracy of the computed Bouguer anomaly values was estimated to be about ±1–5 × 10^{-5} m/s^2 (1 × 10-5 m/s^2= 1 mGal). Additional details about the Venezuelan gravity network and the dataset can be found in Drewes et al. (1991) and Izarra et al. (2005).

2.1. Gravity maps

The calculated anomaly map consists of Bouguer anomalies (BA) onshore (correction density of 2.67 Mg/m3) and Free Air anomalies (FAA) offshore (Figure 2.3). Anomaly values ranges from –225 to 225 × 10^{-5} m/s^2. Offshore, in the Venezuela Basin (VB), magnitudes of the FAA barely reach low positive values. In contrast, the South Caribbean accretionary prism shows a broad gravity low with a WNW–ESE trend. A gathering of local anomaly highs separated by relative low gravity values appears as local highs along the Leeward Antilles (Aruba, Bonaire, and Curazao). The highest FAA values (more than 200 × 10^{-5} m/s^2) are

caused by the subduction in northeastern Venezuela (i.e., Lesser Antilles volcanic arc), which extends further eastward. In the area of the Grenada basin (GrB) and Tobago trough (TT), gravity values decrease down to -80 × 10^{-5} and -45 × 10^{-5} m/s^2, respectively. Onshore, the most relevant BA is the prominent anomaly low observed in the Eastern Venezuelan basin (EVB) mostly caused by a large amount of infill sediments. The BA has NE–SW trending positive values in the area between the Guárico basin (GB) and Guyana shield (i.e., Precambrian rocks).

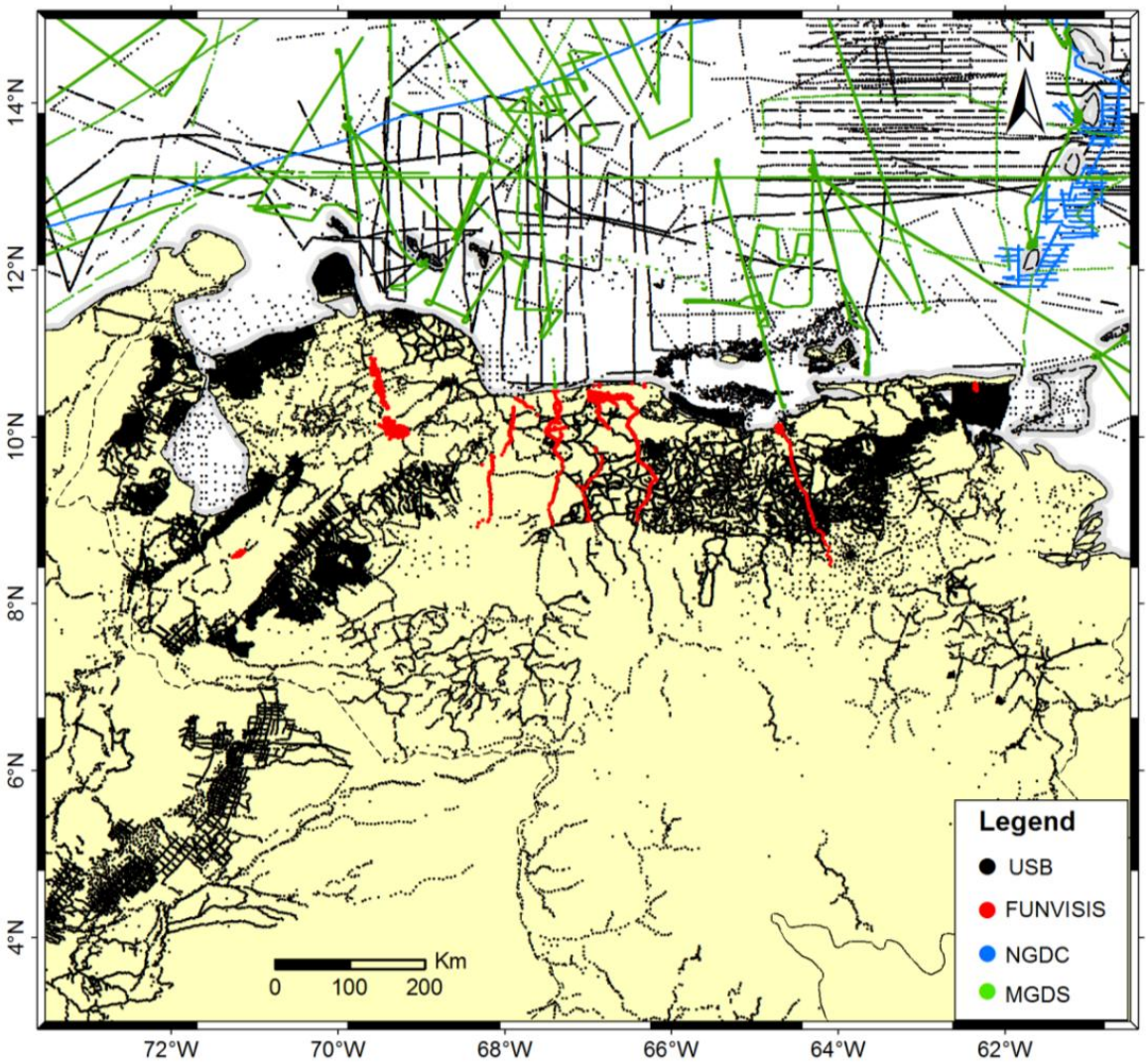

Figure 2.2 Station distribution map of gravity stations used for the new gravity anomaly map of Venezuela.

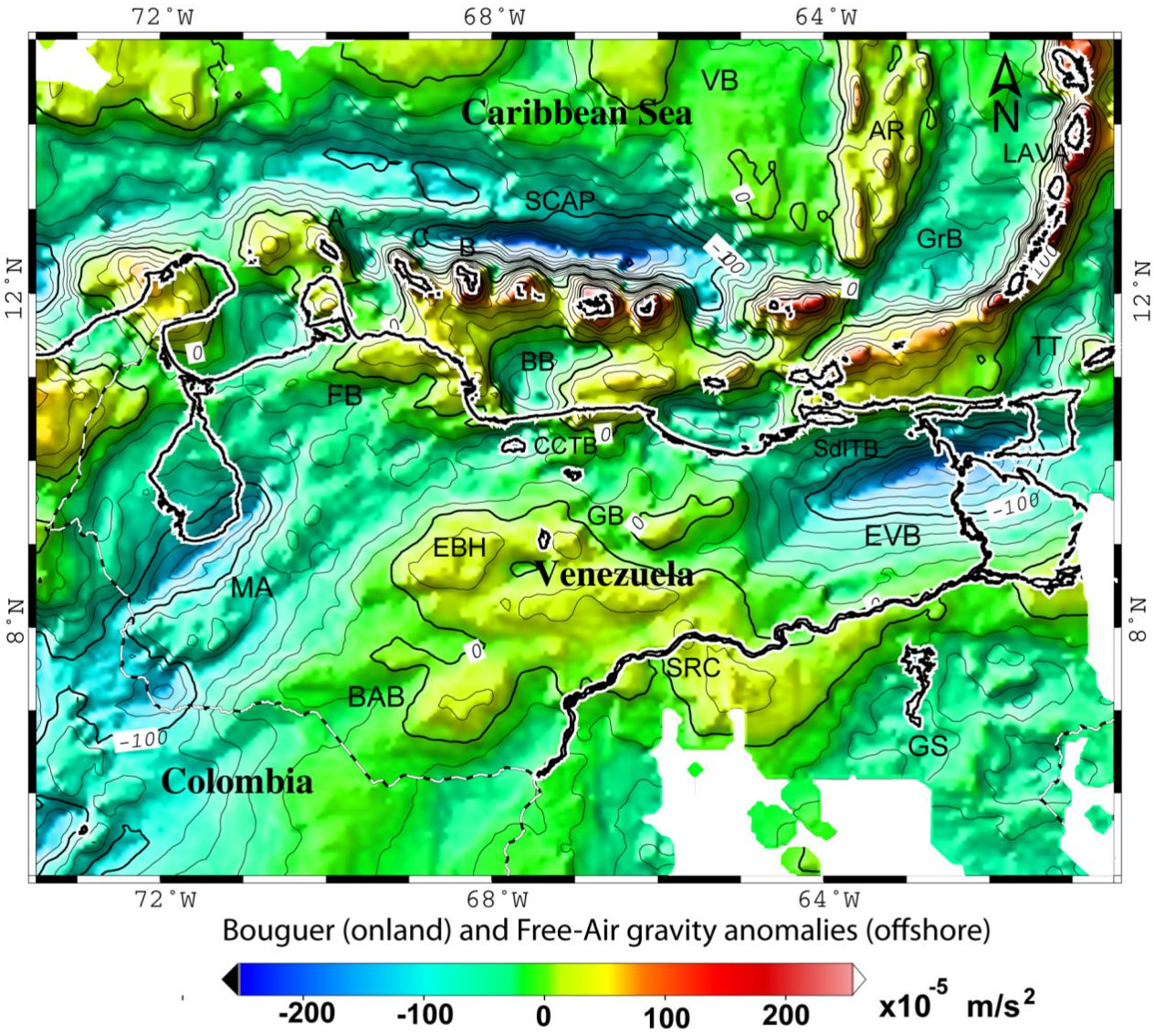

Figure 2.3 Gravity anomaly map of Venezuela. Complete Bouguer anomalies are given on land, and Free Air anomalies are offshore. The Bouguer reduction density was 2.67 Mg/m3. Contour interval: 20 × 10^{-5} m/s^2. Geographical coordinates. Geological features labeled are: BB: Bonaire basin, BAB: Barinas Apure basin, CCTB: Coastal Cordillera thrust belt, EBH: El Baúl high, EVB: Eastern Venezuela basin, FB: Falcon basin, GB: Guárico basin, GS: Guyana shield, GrB: Granada basin, LAVA: Lesser Antilles volcanic arc, MA: Mérida Andes, SCAP: South Caribbean accretionary prism, SdITB: Serranía del Interior thrust belt, SRC: Santa Rosalía complex, and TT: Tobago through.

2.1.1 Regional and residual gravity maps

In order to analyze the anomalies, a set of wavelength filters were applied to progressively separate local effects from regional effects within the gravity field. Here, the concept of the Butterworth band-pass filter was applied in the frequency domains to separate regional and residual fields. The Butterworth filter is a spectral domain filter with a roll-off and requires an order (n) to implement the transition between the passing and rejected portions of the data spectrum; the higher the order, the steeper the transition. Based on the analysis of the radial power spectrum (Figure 2.4), the wavelength cutoff adopted here retained short-wavelength components for the observed data of 200 km, and the order was set at 3.

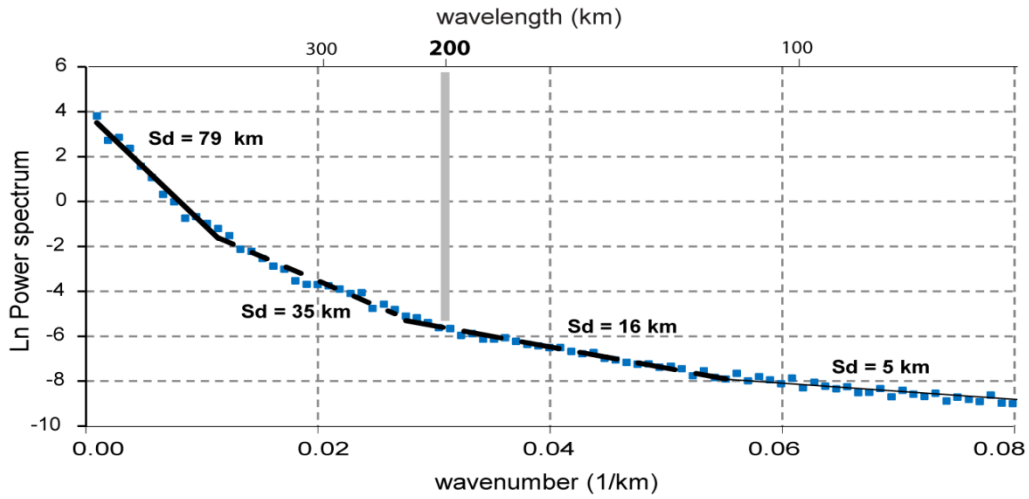

Figure 2.4 Graph representing the natural logarithm of the radially averaged power density spectrum versus the radial wavenumber and wavelength for the Bouguer anomaly map (blue points). The straight lines present the power spectra of mass points located at a maximum estimated depth. Four sources were recognized with estimated depths (Sd) of 79, 35, 16, and 5 km

2.2. Power spectral analysis

The application of Fourier analysis to the interpretation of potential field data is common and is frequently used to obtain the regional/residual field components of the gravity field. Here, the complete Bouguer gravity anomaly was used to get estimated depths for the structures that cause the measured anomaly. The methodology assumed that for large samples, the logarithm of the power spectrum (E) of the gravity field of a monopole source versus the

wave number (radial/distance) may show a linear relationship. The slope of the straight line is proportional to the depth to the top of the corresponding body causing the gravity anomaly. Thus, if *k* denotes the wavenumber and *S(k)* denotes the power spectrum of the gravity field, the depth (d) to the source can be estimated from the relation *S(k)* = f(k) by employing the formula:

$$\ln S\ k\ = -2 * k * d \qquad \text{Equation 2.1}$$

The power spectrum analysis was carried out through the 2D fast Fourier transformation of the gravity field. Due to the two-dimensional character of the dataset, radial averaging of the power spectrum was performed to obtain a one-dimensional representation (Spector and Grant 1970; Mishra and Naidu 1974; Bhattacharyya and Leu 1977; Dimitriadis et al. 1987; Tselentis et al. 1988). Confidence limits for the depth estimations were calculated from the standard errors of the slopes of the best fitting lines for the linear segments.

The gravity data of the study area, covering a surface area of 900 × 900 km^2, was interpolated to produce a grid with a node spacing of 4 km. Results of the power spectrum analysis for this dataset showed four tendencies for the correlation between the energy (E) and wavenumber (radial/distance) (Figure 2.6a). The most regional part of the spectrum resulted in greater depths of about 79 km. The local part of the spectrum resulted in depths of ~16 km. The main aim of the spectral analysis was focused on the intermediate depths of about 35 km because this depth could correspond to the crust–mantle boundary (Moho). The effect of shallower sources (~5 km) may account for local wavelengths of the gravity field in the area of study. The characteristics and origin of these sources were not investigated because they were outside the main aim of this work.

In order to perform the same analysis over all anomalies in the study area, a data block (window), measuring 300x300 km each, was used for the calculation of Moho depths across the N-S and E-W directions. The window size of 300 km^2 corresponds to six times the expected source depth (Moho) to assure a depth-estimation error of <10% according to

Rengan and Hinze (1976). Figure 2.6a-d show results for windows over the anomalies observed in the Barinas-Apure basin, Mérida Andes, Maracaibo basin, Guárico basin, Eastern basin, and Leeward Antilles. The final results are shown in figure 2.7 and figure 2.8.

2.3. Effective elastic thickness determination

The correlation between gravity observations and sea floor topography has been well documented. This relationship can be analyzed by using a linear transfer function called admittance. The basic techniques for determining the admittance function between the gravity and bathymetry data have been discussed in detail by McKenzie and Bowin (1976) and Watts (1978).

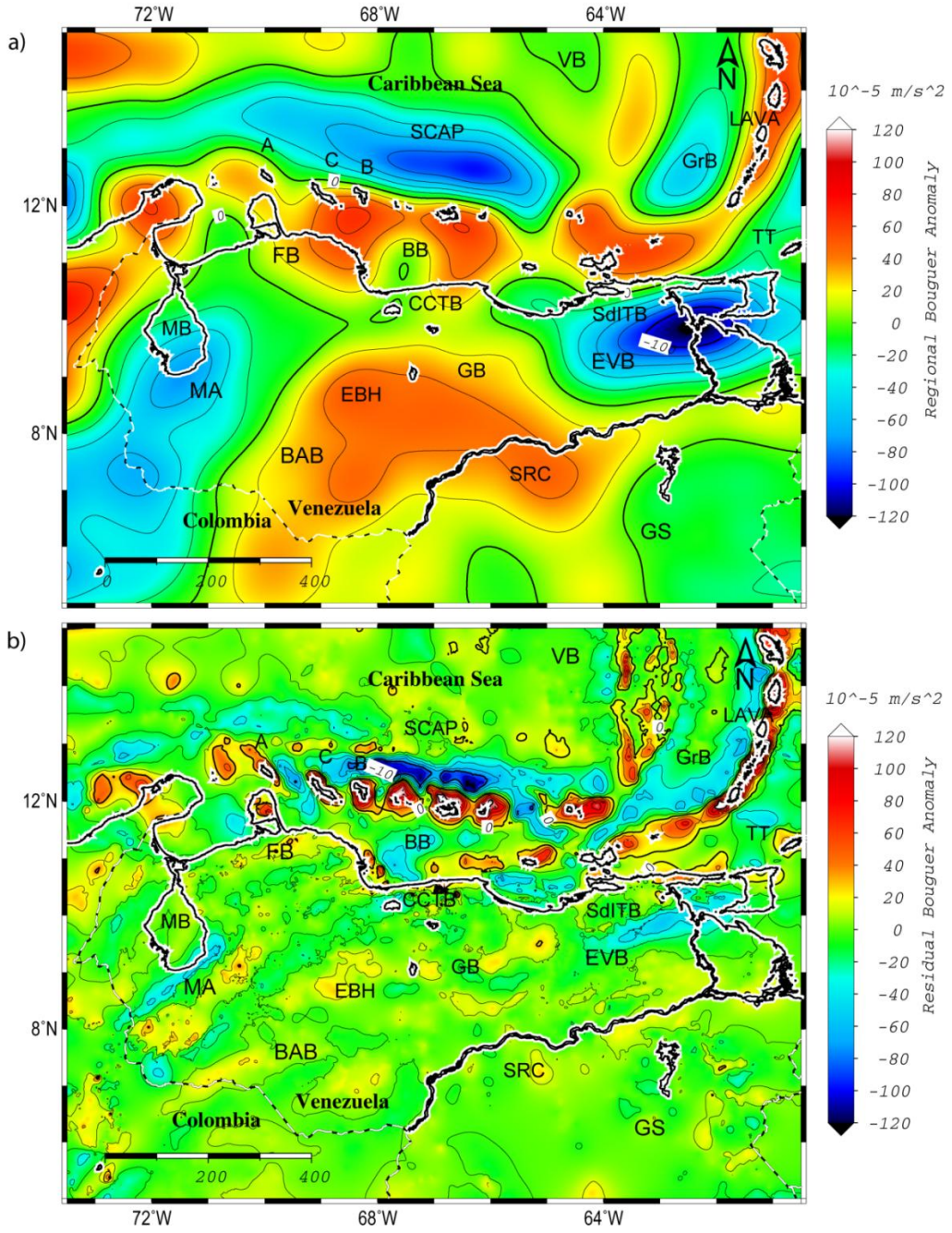

Figure 2.5 a) Regional gravity map obtained by applying a Butterworth filter defined by results of the spectral analysis (Figure 2.4) of the gravity anomaly map. b) Residual gravity map obtained by subtracting the regional gravity map from the observed gravity map in figure 2.3. Both maps: contour interval = 5×10^{-5} m/s^2. Graphical indications as described in the Figure 2.3

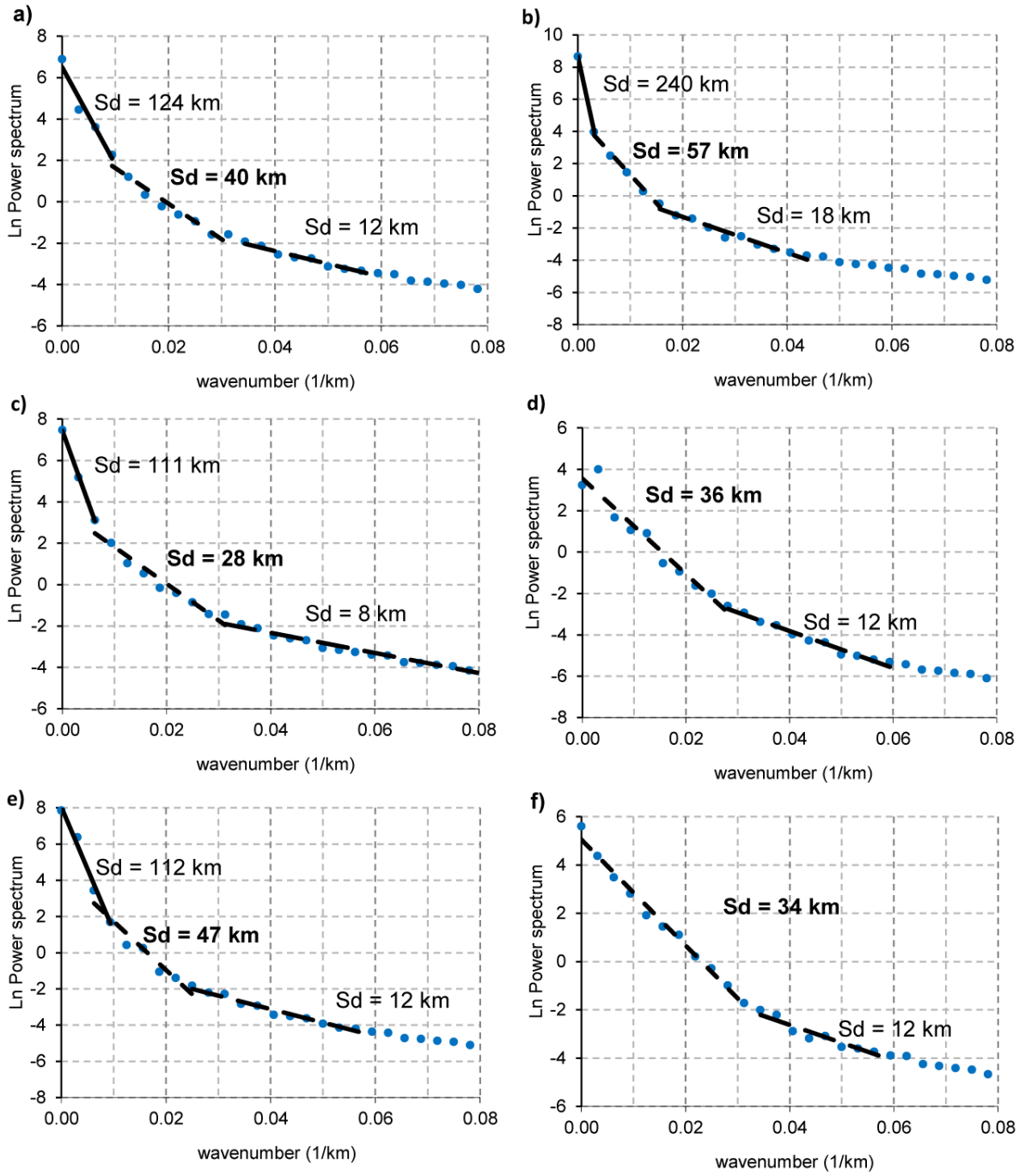

Figure 2.6 Results for the power spectrum analysis of the Bouguer gravity field using 2D fast Fourier transform. Black lines represent the trends of the linear regression separating the spectrum of mass points (blue points) located at a maximum estimated depth: a) Barinas-Apure basin, b) Mérida Andes, c) Maracaibo basin, d) Guárico basin, e) Eastern basin, and f) Leeward Antilles. Estimated depth (Sd).

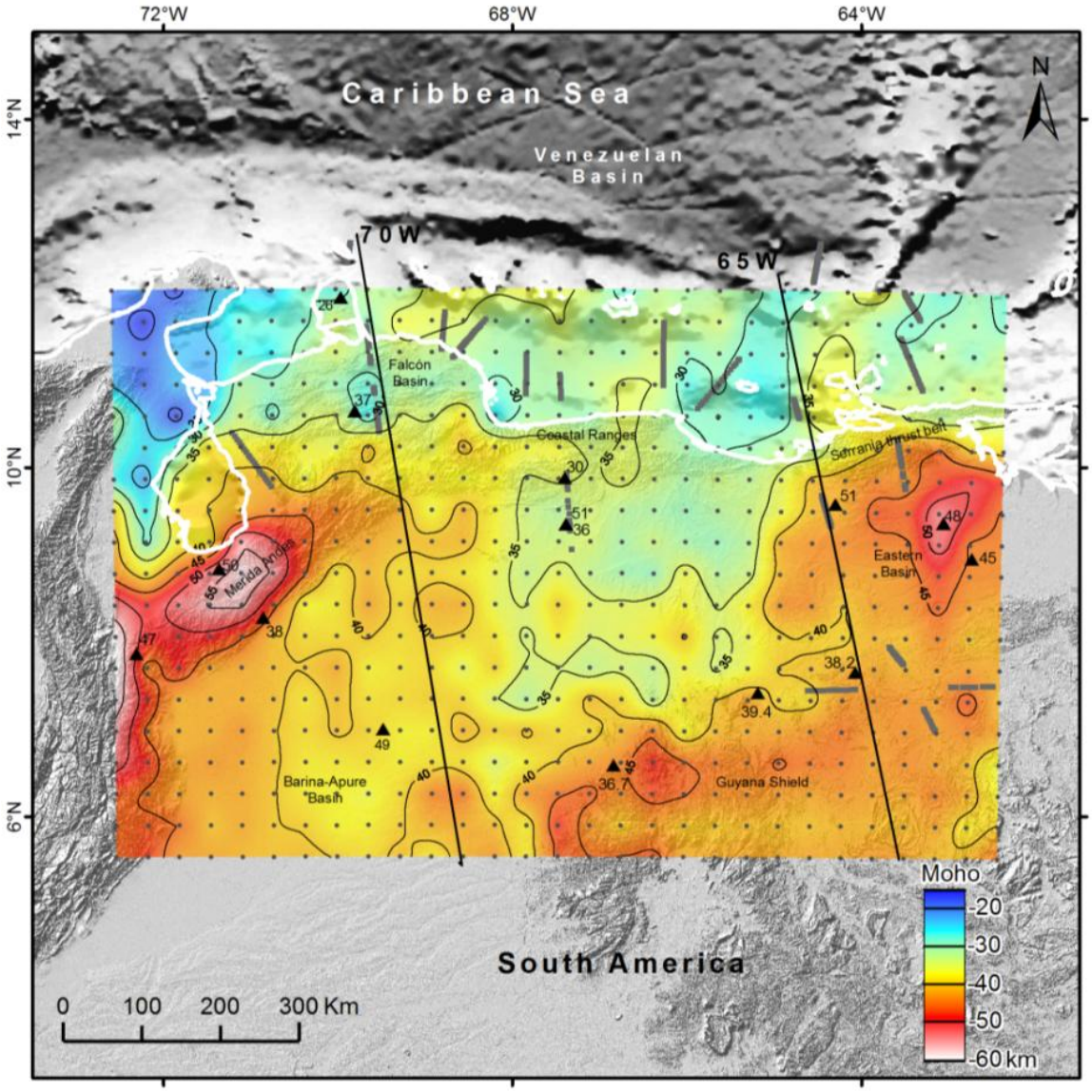

Figure 2.7 Map of source-depth estimation (Moho) obtained by spectral analysis of gravity data. Triangles are the receiver function Moho depth estimations in kilometers (Niu et al. 2007). Gray lines are Moho depths estimated from seismic studies (Schmitz et al. 2008). Location of profiles are shown as black lines labeled by 70 W and 65 W.

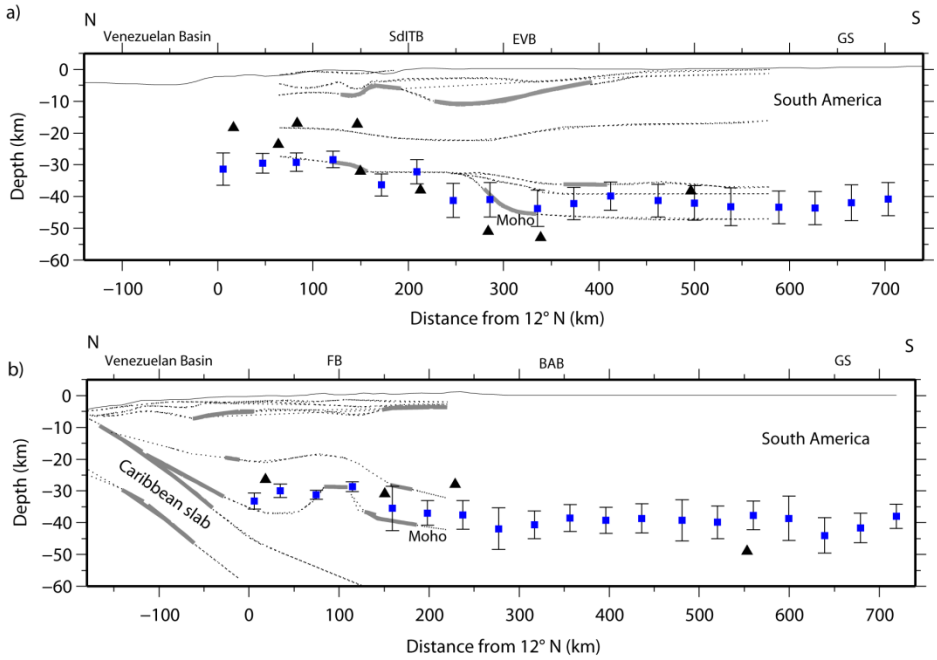

Figure 2.8 Moho depths cross sections along N-S (blue boxes) with associated errors. a) Profile 70W. b) Profile 65W. Triangles are Receiver Function Moho depth estimations (Niu et al. 2007). Gray lines are Moho depths estimated from seismic studies (Schmitz et al. 2008). See Figure 2.7 for location. BAB: Barinas Apure basin, EVB: Eastern Venezuela basin, FB: Falcon basin, GS: Guyana shield, SdITB: Serranía del Interior thrust belt.

The method assumes that free-air gravity anomalies are caused by topography, and its compensation attempts to determine a function when convolved with topography produce the gravity anomaly. The advantage of this method is that the admittance function may be derived from the observed data independent of a particular isostatic model and can be interpreted in terms of simple models of isostasy.

The isostatic response method simply involves deriving a filter that, convolved with the bathymetry in space domain, produces a series that resembles the observed gravity, again in the space domain. This process can be represented in the space domain by using the convolution operator *:

$$g(x) = f(x) * h(x) \qquad \text{Equation 2.2}$$

where h(x), f(x), and g(x) are the series representing the topography, filter, and free-air gravity, respectively. The above convolution in the space domain is equivalent to multiplication in the spatial frequency domain.

$$G\ k\ = Z\ k\ H\ k \qquad \text{Equation 2.3}$$

where G(k), Z(k), and H(k) are the discrete Fourier transforms of g(x), f(x), and h(x), respectively. Z(k) is known as the admittance or transfer function and the wavenumber k = $2\pi/\lambda$ = n2 π /L, where n = 0, 1, 2,…, L/2$\Delta\zeta$, L is the length of the Fourier series, $\Delta\zeta$ is the distance between two consecutive sampling points, and λ is the wavelength. Eq. 2.3 can be rewritten as:

$$Z\ k\ = G\ k\ /H\ k \qquad \text{Equation 2.4}$$

However, the function Z(k) obtained in this way is influenced by noise in the gravity field, particularly at short wavelengths. The noise present in any data may be due to measurement errors, the data reduction procedure, or variations in the structure of the linear system under consideration. In the presence of noise, a better estimate of Z(k) (McKenzie and Bowin 1976) can be obtained from:

$$Z\ k\ = \frac{C\ k}{Eb\ k} \qquad \text{Equation 2.5}$$

Where

$$C\ k\ = \frac{1}{N}\ \sum_{r=1}^{N} G_r\ k\ H_r^*\ k \qquad \text{Equation 2.6}$$

and

$$Eb\ k\ = \frac{1}{N}\ \sum_{r=1}^{N} H_r\ k\ H_r^*\ k \qquad \text{Equation 2.7}$$

N is the number of profiles, and C(k) is the complex cross-spectrum of bathymetry and gravity. Eb(k) is the power spectrum of bathymetry.

* denotes the complex conjugate.

The quality and reliability of the admittance amplitudes were controlled by means of four additional parameters: the coherence, phase of admittance, and the coherent and incoherent energies:

$$\emptyset\ k\ = \tan^{-1}\ \frac{Im\ Z\ k}{Re\ Z\ k} \qquad \text{Equation 2.8}$$

$$\gamma^2\ k\ = \frac{N\ \frac{C\ k}{EbEg}\ -1}{N-1} \qquad \text{Equation 2.9}$$

$$\text{Coherent energy} = \gamma^2\ k\ Eg\ k \qquad \text{Equation 2.10}$$

$$\text{Incoherent energy} =\ \ 1-\gamma^2\ k\ \ Eg\ k \qquad \text{Equation 2.11}$$

where φ(k) is phase of admittance. Im[Z(k)] and Re[Z(k)] are the real and imaginary parts of Z(k). Υ^2(k) is the coherence. Eg(k) is the power spectrum of gravity.

The observed admittance curve was compared with a set of theoretical admittance curves for the Airy and Flexure models, which contain the mean crust (Tc) and elastic plate thickness (*Te*) parameters. The final values of *Te* and Tc were obtained through the selection of the lowest mean square error between the observed admittance curve and each of the theoretical curves.

The theoretical curves for the admittance of the free air anomaly for Airy isostatic compensation ($Z(k)^{Airy}$) and for the flexure or plate isostatic compensation model ($Z(k)^{Flex}$) were calculated following the method given by McKenzie and Fairhead (1997).

$$Z(k)^{Airy} = 2\pi G\rho_c \ 1 - e^{-kTc} \qquad \text{Equation 2.12}$$

$$Z(k)^{Flex} = 2\pi G\rho_c \ 1 - \frac{e^{-kTc}}{A} \qquad \text{Equation 2.13}$$

where

$$A = 1 + \frac{Dk^4}{g\ \rho_m - \rho_c} \qquad \text{Equation 2.14}$$

and

$$D = \frac{ET_e^3}{12\ 1-\upsilon^2} \qquad \text{Equation 2.15}$$

G is the gravitational constant, E = is Young's modulus, υ is Poisson's ratio, g is acceleration due to gravity, ρc and ρm are the average crustal density and density of material below the assumed flexed elastic plate, Tc is the effective depth of compensation, and Te is the effective elastic thickness.

For the admittance analysis, in the present work, three areas were selected: Mérida Andes (Zone A), the Cordillera de la Costa range (Zone B), and the Guyana shield (Zone C). For each area, a maximum of nine profiles were extracted from the free air anomaly map and topography map, each of ~500 km (Figure 2.9). Elevation data profiles were extracted from the Shuttle Radar Topography Mission (SRTM) with a grid spacing of 90 m. Each data set along each profile was regularly spaced at intervals of 0.5 km. The coherence, phase of admittance, and energies (equations 2.8-2.11) for each area were plotted with respect to wavenumber and are shown in Figure 2.10.

The observed admittance was computed from equation 2.5 for 2n samples, where n was taken as 9, which correspond to half of the longitude of the regularly spaced profiles. Theoretical admittance curves were computed (equation 2.13 for *Te* values between 5, 10, 15, 20, 25, and 30 km. *Te* values were obtained after studying the square medium errors (RMS) of the correlation between observed and theoretical admittance curves. A best fit was considered whenever RMS dropped below a minimum value with the correlated theoretical *Te* value.

Finally, the observed and theoretical admittance curves were plotted with respect to wavenumber (Figure 2.11).

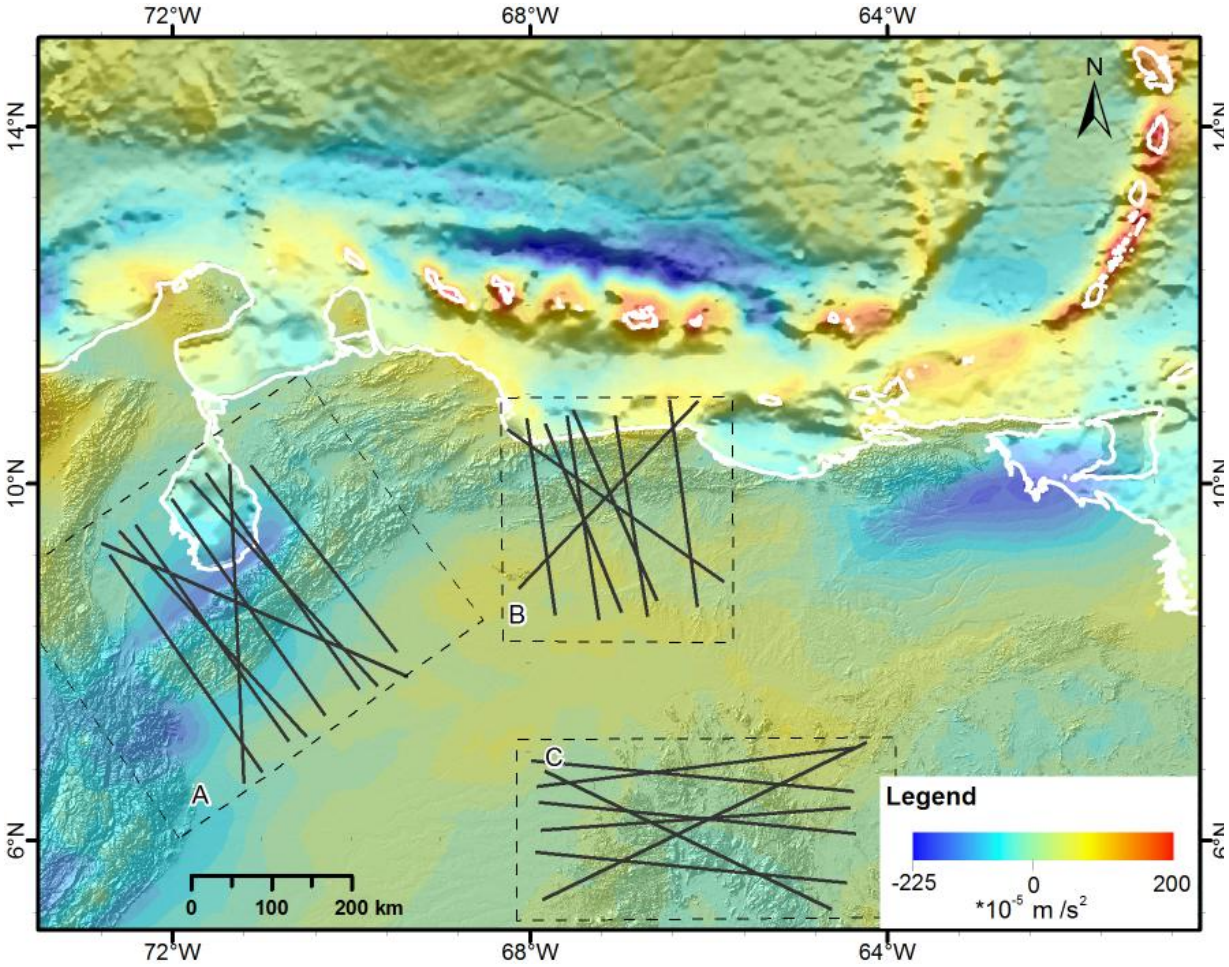

Figure 2.9 FAA and topography/bathymetry maps. Black-dotted boxes labeled as A, B, and C are selected regions for the estimation of elastic thickness: A) Mérida Andes, B) the Cordillera de la Costa range, and C) the Guyana shield. Black straight lines are location of the selected profiles.

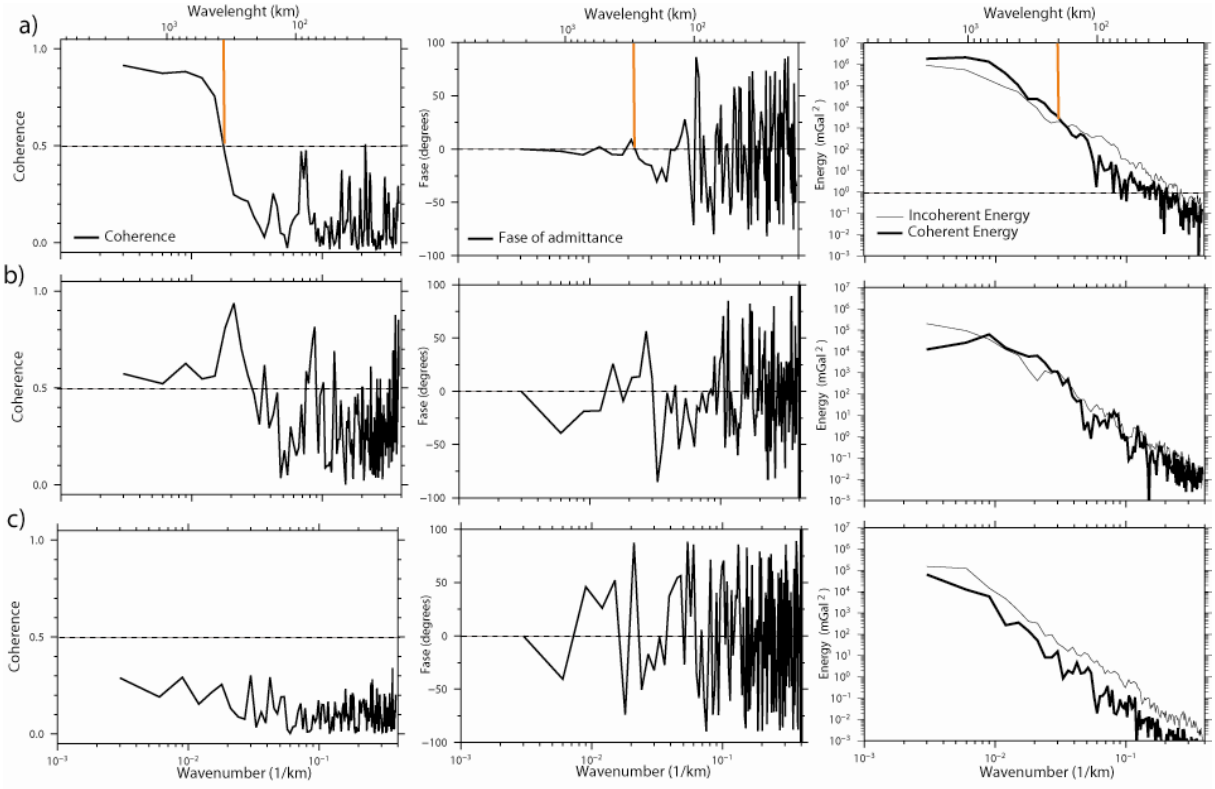

Figure 2.10 Observed admittance values computed from FAA and topography for areas A, B, and C in figure 2.8. Red lines indicate cutoff values for coherence, phase, and coherent (thick line) and incoherent (thin line) energies. a) For Mérida Andes, the coherence is high for $k < 0.04$, the estimated phase is close to zero for $k < 0.08$, and the coherent energy is higher than the incoherent energy for values of $k < 0.08$.

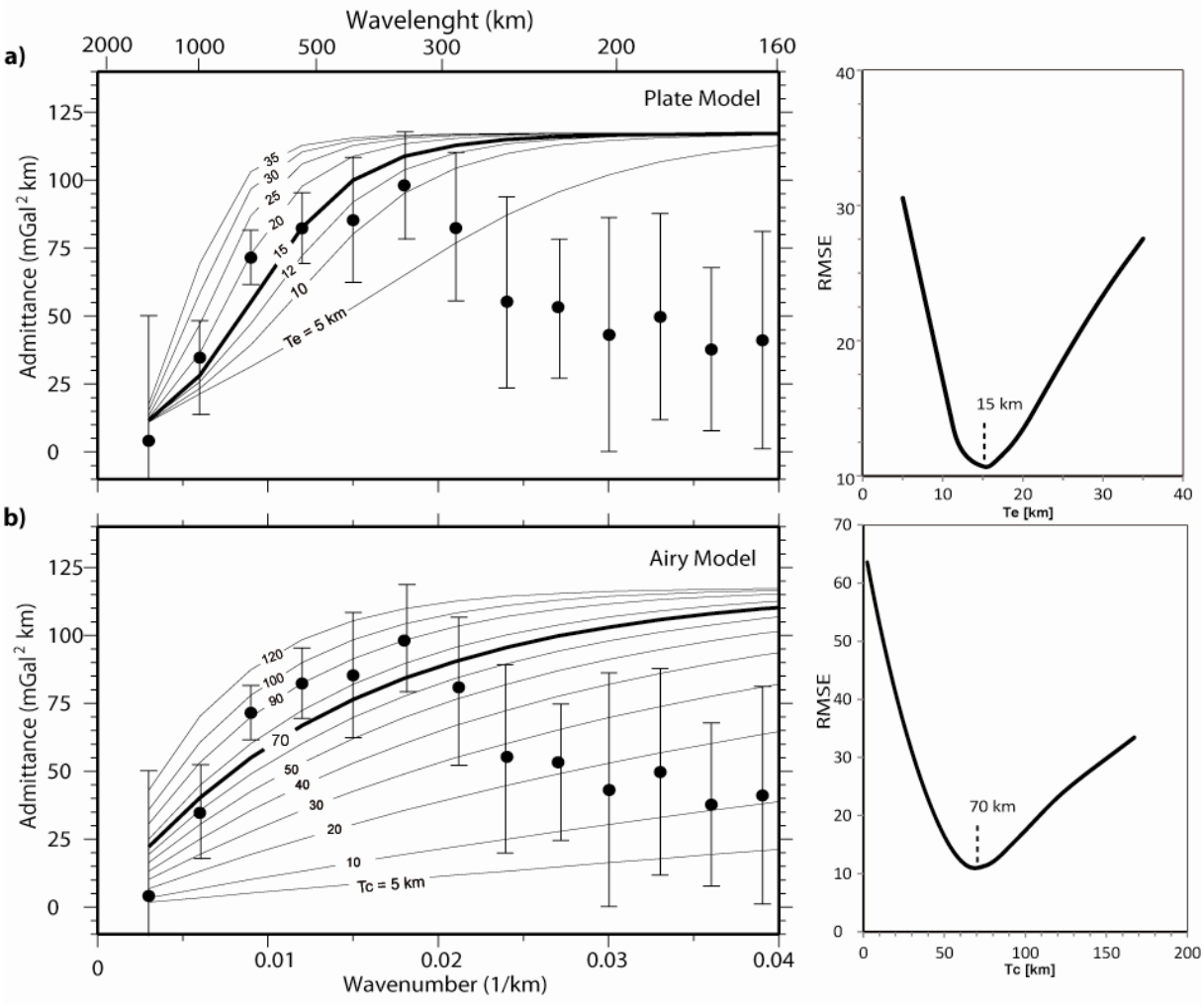

Figure 2.11 Observed admittance values computed from the FAA and topography profiles in figure 2.9 for low wavenumbers, where k = 0.0–0.04. Observed (solid circles) and theoretical (solid curves) admittance for the a) Flexure model, where *Te* is the effective elastic thickness; and b) Airy isostatic model, where Tc is the mean thickness of the crust as a varying parameter of the model. Admittance errors were computed from the coherence (Watts 1978). The best fitting curve for Mérida Andes was the simple flexure model of the lithosphere with *Te* = 17±3 km

2.4. Results and discussion

2.4.1. Regional and residual gravity anomalies and their correlation with major tectonic provinces

The 3-min resolution maps shown in Figure 2.5 can be used to identify gravity anomalies associated with geological bodies approximately 50 km or greater in size. These maps are therefore suitable for correlating gravity with tectonic provinces having dimensions of several hundred kilometers. In addition, in the southern part of Venezuela, large areas have poor coverage of gravity observations, especially in the Amazon region (i.e., Guyana shield).

Considering major topography and gravity changes, the study areas were separate in major topography/gravity provinces. The offshore provinces encompass the Venezuelan basin, South Caribbean accretionary prism, Aves Ridge, Grenada back arc basin, Lesser Antilles arc, Bonaire basin, and Tobago trough. The onshore provinces include the Guyana shield, Barinas-Apure basin, Maracaibo basin, Falcón basin, East Venezuela basin, Perijá-Mérida, and coastal ranges.

Large areas of negative residual anomalies onshore (Figure 2.5b) are associated with Mesozoic and Cenozoic sedimentary basins (Figure 2.1). These intracratonic Mesozoic basins such as the Barinas-Apure, Maracaibo, Falcón, and East Venezuela basins have distinct gravity signatures. For instance, the Barinas-Apure basin is characterized by long wavelength anomalies with low amplitude (-20 to +20 $\times$ 10^{-5} m/s^2). Another negative residual anomaly, near inland, but not as large in magnitude, is a FAA low through Bonaire basin. This basin has a quasi-rectangular shape with low negative residual anomalies which are emphasized by the surrounding gravity highs associated with the coastal ranges and the Leeward Antilles arc.

The negative Bouguer anomaly observed in the Eastern Venezuelan basin (Figure 2.3) is characterized by a SW-NE trending of a negative residual anomaly (~-50 $\times$ 10^{-5} m/s^2) (Figure 2.5b). This gravity low is associated with Cenozoic sediments, which accommodates the result of thrust-sheet loading (i.e., Serranía thrust belt) that forced the American continental lithosphere to flex downward between the Guyana shield and El Pilar fault (Roure et al. 1994). Schmitz el al. (2005) used seismic refraction data to estimate a maximum of 10–13 km of sedimentary infill for this basin. According to Jácome et al. (2003), the amount of

sediments is the result of multiple processes: (a) flexural loading of the Cordillera de la Costa range; (b) large and continuous deposition of continental material from the Guyana shield as the main source; and (c) the subduction dynamics of oceanic South America underneath the Caribbean plate. The spectral analysis of the Bouguer anomaly (Figure 2.6d) estimated an anomaly source located 12 km deep that may correspond to the top of the basin basement.

In the Mérida Andes, the residual gravity map (Figure 2.5b) showed a SW-NE trending of positive residual anomalies (~40 × 10^{-5} m/s^2) flanked on both sides by negative anomalies(-20 to -40 × 10^{-5} m/s^2), that are associated with Barinas-Apure basin in the south and the Maracaibo basin. These gravity highs are associated with exposed Archean to Lower Proterozoic high-grade metamorphic basements within the mountain range. Relative maximums follow dikes (diabase) that intruded the Precambrian and Paleozoic rocks of Mérida Andes, which formed as a consequence of the convergence of the Panama arc and western South America, which initiated the formation of this mountain range (Stephan 1982; Audemard 1991; Colletta et al. 1997; Audemard and Audemard 2002). Negative residual anomalies flanking the Mérida Andes showed similar shapes but very different amplitudes. These anomalies are mainly caused by strong flexes of the crust and the infill sediments of the Barinas-Apure basin in the south, and the Maracaibo basin in the north, in association with a chain-scale thrust and back thrust systems along the Mérida foothills. The northern flank has lower amplitude (<-40–40 × 10^{-5} m/s^2) with a relative maximum located in the northwest. In contrast, the southern flank barely reaches -40–40 × 10^{-5} m/s^2 in the most southeastern area of the anomaly. These anomalies were interpreted by Audemard and Audemard (2002) to be the consequence of the rheological characteristics of two different continental crusts (the crust underneath the Maracaibo basin and the South American crust underneath the Barinas-Apure basin). In other words, the Maracaibo crust underwent a more recent tectonic and thermal event due to continental rifting during the Jurassic than the long-cooled Precambrian crust of the SA craton in the south. In summary, the Andes of Venezuela is a floating orogen involving incipient, gently NW-dipping continental subduction that generates a shallow foreland basin on the Barinas-Apure basin side, while it strongly flexes the Maracaibo crust on the forearc-equivalent side, where a deep flexural basin develops in association with a chain-scale backthrust along the Maracaibo foothills on the northwest (Audemard and Audemard 2002).

Other regions where positive residual anomalies were observed were the Lesser Antilles arc and the Aves ridge. They were characterized by shorter wavelengths (<100 km) but high amplitudes (>100 × 10^{-5} m/s^2) in the residual anomalies map. These pronounced gravity highs and steep gradients were the combined effect of the steep slope of the bathymetric and high-density volcanic rock outcroppings in these localities, which displayed a wide range of compositions.

The regional gravity anomaly map provided a general view of the areal extent of the gravity response from the major geological units and reflects the gross crustal structure of the area. The calculated regional anomaly map displayed several well-defined gravity highs and lows of varying dimensions and relief. For instance, under the Guyana shield, the regional gravity field showed no evidence of significant crustal thickness variations (Figure 2.5b). This result is consistent with seismic studies that indicate a crust thickness of ~45 km (Schmitz et al. 2008). In this region, regional and residual gravity maps suggest that the observed anomalies can be explained by upper crustal lateral density variations alone rather than by changes in the thicknesses of the lower crust and Moho. This is supported by the small range of ~20 to ~-20 ×10^{-5} m/s^2 for the regional field in this area.

A conspicuous gravity high (~40 × 10^{-5} m/s^2) in central Venezuela trending from NE to SW separates the Barinas-Apure basin and Eastern Venezuela basin. This anomaly extends from the El Baúl high to granitic rocks of the Santa Rosalía complex in the Precambrian Guyana shield, which crop out in the southwestern margin of the Orinoco River. In addition, Viscarret et al. (2009) determined U–Pb zircon ages and interpreted the El Baúl massif to be a Paleozoic basement belt, which shows more affinity with the Mérida Andes than with rocks of the Guyana shield. Therefore, this long wavelength anomaly is very likely created by the overlapping of anomalies caused by the El Baúl high and the Santa Rosalía complex.

After the separation of the regional component of the BA, the Eastern Venezuelan basin still has the most relevant anomaly. This pronounced negative Bouguer gravity anomaly has been studied by several authors (Bonini et al. 1977; Russo and Speed 1992; VanDecar et al. 2003; Izarra et al. 2005; Sanchez et al. 2010). The negative gravity anomaly is roughly parallel to the arc platform extension, but it does not extend west of Gulf of Paria. According to gravity and recent seismic refraction studies, this negative gravity anomaly is indicative of the very large load on the South American lithosphere here as well as the large amount of sediments in the basin.

Regional gravity anomalies of the South Caribbean accretionary prism and Leeward Antilles arc (i.e., ABC Islands) form a positive-negative gravity pair characteristic of subduction zones. The high-density rock in the Leeward Antilles islands are characterized by residuals with very high amplitudes of 100–120 × 10^{-5} m/s^2, but regional field anomalies also have very high amplitudes. Whereas, the gravity anomalies caused by strong density contrast in the masses that form these volcanic bodies, that are or are being accreted to the continent, produce local anomalies that are very emphasized by the steep bathymetry. This interpretation is similar to the one by Bonini et al. (1977), based on gravimetric data.

2.1.2 Effective elastic thickness and Moho depth

The admittance and coherence results presented here for the Mérida Andes (Figure 2.11) best fit a flexural model with *Te* = 15 km. The Airy model fits the observed admittance when the mean crustal thickness is 70 km. This value is incompatible with the estimates of the typical continental crust thickness (35–40 km). Consequently, the Airy model cannot be accepted as a possible isostatic compensation mechanism. A simple plate flexure model with *Te* = 15 km is more reasonable.

Along the Cordillera de la Costa range, the admittance calculation agrees more closely with the theoretical values calculated for a plate thickness of 10 km. *Te* is around ~10 km north of the Eastern Venezuelan basin (i.e., along the Cordillera de la Costa range), indicating that low rigidity amplified the subsidence of the basin.

Coherence, phase of admittance, and coherent and incoherent energies calculated for the Cordillera de la Costa range and Guyana shield showed poor quality and reliability for *Te* estimations. In other words, the phase of the admittance was not close to zero, the coherence was less than 0.5, and incoherent energy was higher than coherent energy for all wavenumbers in the selected profiles (Figure 2.9). The admittance estimates for the set of profiles crossing Mérida Andes showed a noticeable data scattering at wavelengths longer than 160 km. this scattering could be caused by the wide variability of the thickness of sediments and also by very short wavelength anomalies that could considered as noise.

Tassara et al. (2007) used a wavelet formulation of the classical spectral isostatic analysis to invert satellite-derived gravity and topography/bathymetry for *Te* over South America. According to their calculations, Mérida Andes, which is the region located between the

coastline (i.e., Cordillera de la Costa range) and Colombian Eastern Cordillera, exhibits variable *Te* from 35 to 40 km with an uncertainty of ±10 km. Beneath the Cordillera de la Costa range, *Te* decreases to ~35±10 km. This high *Te* value in the Cordillera de la Costa range may reflect the combined effect of the strength of the upper continental and the partially subducted Caribbean oceanic lithospheres. Beneath the Eastern Venezuela basin, the elastic thickness ranges between 40 and 50 km with an uncertainty of ±10 km. The Guyana shield shows *Te* as low as 10 km, although with an uncertainty of up to 25 km.

The *Te* values estimated in this study did not match the elastic plate thicknesses estimated by Tassara et al. (2007). These discrepancies between the admittance results are the most probable cause for the presence of a considerable amount of loading from the top, which corresponds to stacking of thrust sheets and uplifts of basement rocks in coastal ranges, and from the bottom, i.e., the partially subducted Caribbean slab. Another factor to consider is the size of the window used to compute admittance. According to Pérez-Gussinyé et al. (2004) windows that are too small introduce spurious spatial variations, and windows that are too large tend to average the spatially varying *Te* values and smooth the true structure. These discrepancies could be caused by the large and tectonically heterogeneous area required by the admittance technique, which would tend to bias their result towards a weaker plate (Forsyth 1985).

The results obtained in the spectral analysis confirm the previously established value of 35 km as the mean reference Moho depth (Schmitz et al. 2008). In addition, the crust thickness is not homogeneous. For instance, the Moho topography shows a NE–SW depression beneath the Mérida Andes with a maximum depth of ~55±5 km; this value gradually decreases toward the south and north of the main strike of this feature. The maximum crustal thickness in Mérida Andes (Figure 2.7) was partially constrained by the receiver function analysis (Niu et al. 2007), which shows Moho depths of 50 and 47 km near this maximum. The Maracaibo basin seems to have a crustal thickness of 35-40 km. The estimated Moho geometry under the area of the Falcón basin agreed well with the refraction seismic data modeled along the 70°W profile, which indicates a crustal thickness of ~27 km (Bezada et al. 2008). The crustal thickness beneath the Eastern Venezuela basin ranges from ~50 to ~40 km. The Guyana shield is regionally underlain by a crust of ~45 km. Northwards beneath the Guárico and Barinas-Apure basins, the crustal thickness reaches ~40 km. Along

the coastline, the Caribbean Mountain System crustal thickness oscillates around 30 km and decreases slightly toward the Leeward Antilles (Figure 2.7 and Figure 2.8).

Figure 2.8 shows that there are significant differences among Moho values estimated with spectral analysis and Moho estimated with receiver function. On the other hand, Moho depth values in Figure 2.7 and closely match the values estimated by Schmitz et al. (2008) and also produces the best fits to the observed Bouguer gravity data (Sanchez et al. 2010). According to Schmitz et al. (2008) the mismatch between seismic Moho and receiver function Moho is caused by the resolution of these technics.

2.5. Conclusions

A new Bouguer gravity map of Venezuela was developed based on an up-to-date dataset available in the country. All data were reprocessed and homogenized according to gravity processing standards, and the effects of the topography were corrected with digital topographic maps. The final dataset was comprised of more than ~80,000 observation points that are now available for future detailed interpretations and future crustal investigations, such as 2D and 3D gravity modeling.

The results obtained in the Bouguer gravity map presented in this work can be greatly improved by adding more gravity data in areas where scarce and poor quality data are the only data available, such as in mountain ranges (e.g. Andes) and the Amazon forest (e.g. Guyana shield).

The Free-Air gravity and topography admittance analysis of the data windows over the Mérida Andes provided elastic thicknesses in the range of 30–35 km.

Finally, *Te* values presented in this work using the admittance method were found to be lower than *Te* calculations carried out in previous studies on the scale of South America and surrounding plates. These differences in the *Te* calculation could be caused by tectonical heterogeneities and problems associated with the admittance technique (window size, data coverage and presence of noise), but these arguments are still in discussion. It is possible that satisfactory results for this area that has a very complicated structure could only be obtained by a more sophisticated approach.

3. A 3-D lithospheric model of the Caribbean-South American plate boundary

A 3-D structural model of the Caribbean-South American plate boundary was constructed by gravity modeling. The model was constrained by four wide-angle seismic refraction sections, Moho depth estimations from receiver functions, and additionally seismological hypocenters, surface geology, and geodynamic information. Density values were calculated from empirical velocity-density functions, and mineralogical-chemical composition considering specific P/T conditions.

We tested different structural models for Western and Eastern Venezuela. In the final model, the fit of the measured and modeled gravity fields for a long Caribbean slab in Western Venezuela was better than the fit obtained for a short one. This interpretation is consistent with the constraining data. The slab is interpreted to extend further to the south beneath Northern Colombia and culminates in the area of the seismic cluster of the Bucaramanga nest. The modeling estimates a slab dip angle under Maracaibo and Mérida Andes of 15°, which increases to 32° below 100 km depth. The dip direction of approx. N150°E ± 5 increases lightly eastward. In Eastern Venezuela, considering its short wavelength, lineaments analyzed from gravity data (by curvature methods and Euler deconvolution) seem to be related to shallow structures and density contrast in the Serranía del Interior and not from a deep detached slab beneath the continental crust. It is deduced from modeling results that this slab configuration has a very small influence on the gravity field. The slab was modeled according to the subduction-transform propagation model with purely westward subduction and a slab break off along a vertical dip-slip tear through the lithosphere.

3.1. Introduction

The current Caribbean-South American plate configuration results from a transpressive evolution that began in the Tertiary and continued in the Quaternary (Pindell 1994; Meschede and Frisch 1998). The lithosphere structure of Western Venezuela shows a very complex geodynamic setting, where the South America, Nazca and Caribbean plates and several smaller crustal blocks are interacting (Audemard 1993; Audemard 1998). The Caribbean plate

moves eastward with a rate of about 2 cm/yr (Perez et al. 2001; Weber et al. 2001) relative to the South American continent in a compressive, extensional and strike-slip tectonic regime (Figure 3.1a). These regimes are associated with important topographic reliefs. For example, Mérida Andes, which is the northeastward topographic prolongation of the Eastern Cordillera of the Colombian Andes, and also La Costa and Interior ranges that run along the central and eastern portions of Venezuela's northern coast. Eastward, the most recent evolutionary stage of Caribbean plate is still active. Here, Atlantic/South America oceanic lithosphere subducts under the Caribbean plate with about 4 cm/yr (DeMets et al. 1994) in the last 5 Ma (Audemard and Audemard 2002).

In recent times, several projects have been conducted to collect new data which aim in a better understanding of the structure of this plate boundary, which is a prime location to study the processes that lead to continental crust formation and growth with an enormous economic importance for its oil fields, e.g. BOLIVAR (Broadband Ocean-Land Investigations of Venezuela and the Antilles arc Region) and GEODINOS (Recent Geodynamics of the Northern Limit of the South American Plate) (Levander et al. 2006). These projects increased the knowledge of the structure in the Caribbean region, which is crucial for insights into the geodynamics in the region and its tectonic development. In the present study, findings from the mentioned projects are used to constrain a new 3-D density model for the entire region. Our main aim was to develop a consistent density model through testing different proposed models in the region in order to gain better understanding of the relationship and interactions of the mantle lithosphere and crustal features.

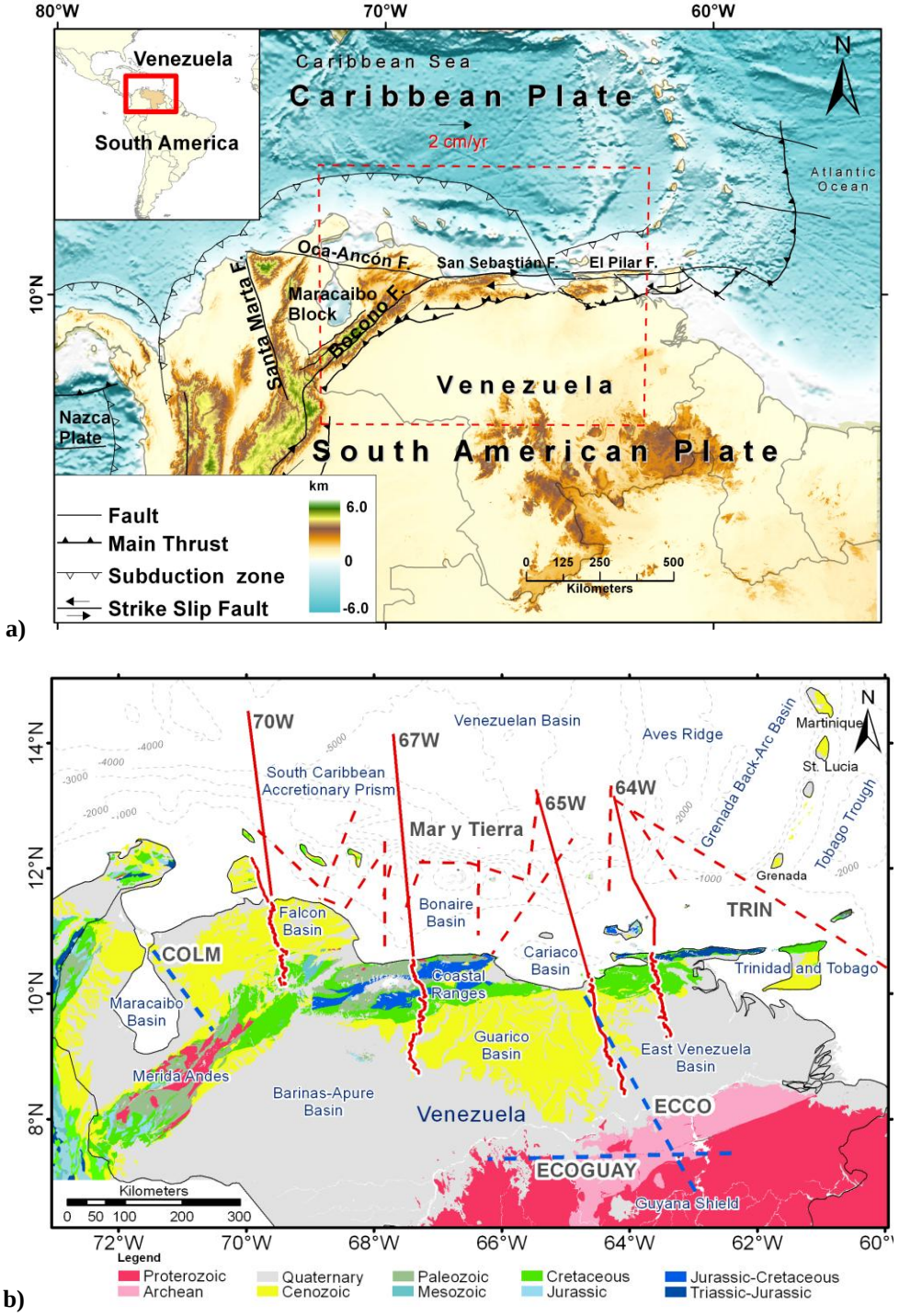

Figure 3.1 a) General tectonic and kinematic features of the northern margin of South America. Study area in stippled red box. Arrow with red numbers indicates relative regional motion. Color bar indicates topography and bathymetry. Black letters indicate geological/tectonic features and general information. b) Simplified geologic map of the 3D density model region (red stippled line in Figure 1.1a). Red lines show the position of main seismic cross-sections in the study area. Red and blue dashed lines indicate secondary seismic cross-sections (Schmitz et al. 2008). Black and blue letters indicate name of seismic profiles and geological/tectonic features. Black dashed lines with numbers indicate bathymetry (meters). Black lines are Coastlines and political boundaries

3.2. Geological setting

The interaction between the Caribbean and South American plates began in the Late Jurassic-Early Cretaceous (180 Ma) with the separation of the Americas and the formation of the Proto-Caribbean ocean basin (Pindell 1994; Meschede and Frisch 1998). However, the plate-tectonic structure and geodynamic of the Caribbean plate has been controversially discussed during the last decades, and the discussion is still going on. This research will contribute to this discussion by testing different theories with 3D density models.

The Southern Caribbean plate margin is the result of a long interaction between the Caribbean and South America plates, two heterogeneous plates characterized by different lithospheric thicknesses, and petrological compositions. Today, Southeastern Caribbean plate interaction zone is described as a 600 km wide and 800 km long diffuse boundary, bounded to the north and south by oppositely verging folds, thrust belts and foreland basins, and it is traversed in the middle by the San Sebastian-El Pilar dextral strike-slip fault systems and the Boconó dextral strike-slip fault system (Audemard and Audemard 2002), which dominate the tectonics of the plate boundary.

The plate boundary in the area of Eastern Colombia and Western Venezuela is composed by a set of different blocks which move independently among the main larger plates (Caribbean, South America and Nazca plate) (Figure 3.1a). These blocks are limited by major strike-slip fault and thrust systems (Audemard and Audemard 2002). Several seismological studies indicate that a continuous slab built as part of the Caribbean lithosphere subduct beneath Northern Colombia and NW Venezuela, and extends along the entire width of Mérida Andes (Van der Hilst and Mann 1994; Malavé and Suárez 1995; Perez et al. 1997; Colmenares and Zoback 2003). Another hypothesis assumes a tear fault along San Sebastian-El Pilar fault system (Taboada et al. 2000). Based on records of intermediate depth seismicity, the dip angle and dip direction of the slab are estimated to be 17°±3° and 50°±20°, respectively (Van der Hilst and Mann 1994). These studies are focused on subduction beneath Northern Colombia, where intermediate seismicity indicates the hypothetical geometry and kinematics of the subducted Caribbean Plate.

The Eastern Andean front fault system and the Boconó fault zone coincide with changes in the direction of the slab's dip in the Bucaramanga swarm area. The Northern Venezuela orogeny is attributed to oblique Caribbean-South America collision and consists of a thrust belt made up of several first-order imbricated oceanic and continental tectonic units, accreted

with general south-vergence since the Late Cretaceous (Beck 1985; Bellizzia 1986; Ostos 1990) (Figure 3.1b). At the eastern part of the Caribbean plate boundary, the Atlantic oceanic lithosphere is subducting northwestward beneath the Caribbean Plate. Here, seismicity indicates at least 200 km depth of subducted oceanic South American plate beneath the island arc (Molnar and Sykes 1969; Russo et al. 1992). This slab extends over the entire margin (Van der Hilst 1990; Russo and Speed 1992; Russo et al. 1992) however, intermediate-depth seismicity, which defines the top of the slab, ceases abruptly beneath the western Gulf of Paria (VanDecar et al. 2003). This observation makes it difficult to describe the actual tectonic setting of this region.

Tomographic images from VanDecar et al. (2003) show an aseismic continuation of the subducted and detached South American lithosphere toward the southwest beneath Serranía del Interior. In their interpretation, this detached oceanic slab contributes to the unusual low in the gravity anomaly that occurs in the Serranía del Interior, and it is interpreted as a larger subsurface load build by continental lithosphere that depresses and displaces the mantle below. Moreover, Clark et al. (2008) integrate results from new seismic surveys and explain the slab break off beneath western Gulf of Paria as a subduction-transform propagation model with purely westward subduction, where the south edge resists tear propagation pulling the plate downward.

3.3. Database

3.3.1. Gravity data

Data from different institutions e.g. Simon Bolivar University (Izarra et al. 2005), National Geophysical Data Center (NGDC) and Venezuelan Foundation for Seismological Research (FUNVISIS) have been recompiled for the purpose of 3-D modeling of the gravity field.

The Simon Bolivar University database consists of data sets from different Venezuelan institutions, oil companies, universities and international surveys. Most of the data are evenly spaced. However, the compilation includes data with high accuracy (1×10^{-5} m/s^2 or less in gravity and 0.5 m or less in height) and an average station spacing of less than 100 m. This data set was mainly collected by oil companies. In contrast, some data have elevation errors of some meters and errors higher than 1×10^{-5} m /s^2 in the gravity.

NGDC data set was made available by the "National Geophysical Data Center (NGDC), which belongs to the US Department of Commerce. This data set includes offshore gravity data collected during research cruises from 1953 to present, from several oceanographic institutions and government agencies worldwide.

FUNVISIS data set includes more than 1000 observations along the main seismic lines, collected by a Scintrex CG-5 gravimeter and GPS-navigation. The resulting accuracy and resolution of the gravity data consist of 0.5×10^{-5} m/s^2 in gravity and ±1 m for station heights, and an average station spacing of 500 m.

A comparison of the different data sets show that the main errors found are related to uncertainties in positioning of the observations; this holds for most of the old data. Unfortunately, in this data set no meta-data is available. In cases where no correction was possible, data were eliminated. The estimated accuracy and resolution of the recompiled data is not better than 5×10^{-5} m/s^2 to 15×10^{-5} m/s^2. However, for a regional model with relevant wavelengths of the gravity field greater than some hundred kilometers, we considered this uncertainty in the gravity data as acceptable.

3.3.2. Constraints

To constrain the density model several independent information was taken into account from the BOLIVAR and GEODINOS projects. Four deep seismic wide angle profiles closely located to longitudes 64°W, 65°W, 67°W and 70°W, and extending roughly from latitudes 14°N to about 8°N were used to constrain the final 3-D density model (Figure 3.1b). 2-D velocity models show that crustal thickness in the Guayana Shield reaches 45 km. Northwards crustal thickness decreases reaching about 40 km. Along the coastline, corresponding to the Caribbean Mountain System the derived crustal thickness oscillates around 35 km and decreases slightly toward the Leeward Antilles up to 26 km. There are two regions with anomalous crustal thickness: (1) On the Eastern Venezuela Basin, a crustal thickness up to 50 km is observed. Here, high velocity anomalies are observed in the lower crust. Schmitz (2008) interpreted this anomalous velocity as reworked lower crustal and upper mantle material associated to the plate interactions of the South American and the Caribbean plates. (2) In Western Venezuela, the Falcón Basin shows a remarkable crustal thinning from 35 km to 27 km, which extends eastwards into the Bonaire Basin (Bezada et al. 2008).

Receiver functions indicate a typical crustal thickness value at the Guyana Shield around 38 km. Beneath the Maturin Basin, the Moho (crust/mantle boundary) steadily deepens to 48 km northwards. Toward the plate boundary, the receiver function interface steps upward to 30 km beneath the Serranía del Interior, and shallows more gradually to 26 km beneath the strike-slip system (Niu et al. 2007).

Seismicity in Venezuela is characterized mainly by shallow earthquakes of moderate and low magnitude. However, some events have been recorded for depths exceeding 150 km in Eastern and Western Venezuela. They have been attributed by means of focal solutions and seismic tomography to subduction processes (McCann and Pennington 1990; Van der Hilst 1990; Malavé and Suárez 1995; Perez et al. 1997; Corredor 2003). Southwest Venezuela, seismicity is characterized by the Bucaramanga Nest composed by intermediate depth events gathering in small volume, eastward the seismicity is dominated by Boconó and Oca-Ancón fault systems with several shallow depths but with some deep seismicity. Over the years, several authors have postulated about the direction and dip of the structures: Dewey (1972) concluded that these seismic events occurred at the same slab with strike N10°E and dipping eastward, Pennington (1981) reports N109°E dip direction, dipping 25-30°, Kellogg and Bonini (1982) and Kellogg and Vega (1995) proposed a zone dipping ~30° which ends at 200 km, Schneidar et al. (1987) defines a Wadati Benioff zone up to 190 km striking N10°E and dipping ~30°. In their interpretation, Van Der Hills and Mann (1994) showed a 3-D tomography model revealing a slab at depths of 275 km with changes in dipping and digging. After that, Malavé and Suarez (1995) using focal depths ranging from 60 km to 180 km extended the slab geometry eastward in a NNE-SSW direction and dipping approximately 25°-32°. Taboada et al. (2000) concludes that the Bucaramanga nest may correspond to an inflexion zone or hinge in the slab.

3.4. Data processing and modeling

All available gravity observations have been compiled, resulting in about 80000 observations onshore and more than 20000 stations offshore. The whole dataset was reprocessed according to standard procedures using the 1980 Geodetic Reference System and a crustal reference density of 2.67 Mg/m^3. Topographic corrections were calculated up to 167 km (Hayford zone O2), using a digital terrain model based on the Shuttle Radar Topography Mission (SRTM) with a grid spacing of 90 meters. Taking into account all sources of error in

the database, the accuracy of the computed Bouguer anomaly values are estimated in the range of ± (5–15)×10^{-5} m/s^2 (1×10^{-5} m/s^2= 1 mGal).

The calculated anomaly map consists of Bouguer anomalies onshore (correction density of 2.67 Mg/m3) and Free Air anomaly offshore (Figure 3.2). The overall magnitudes of the anomalies range from –205 to +225 x 10^{-5} m/s^2. This wide range of anomalies do not shows a simple trend o pattern which reflects the structural and density complexity in this region. On shore, the most relevant features in the map are: a prominent anomaly low observed in the East (mainly caused by a large amount of sediments deposited in the Eastern Venezuelan Basin), and a regional NE–SW negative trend which runs parallel to the strike of Mérida Andes. In this trend are located two minimums, one on the Mérida Andes northwestern flank and another on the southeastern flank. They are related to the gravity effect of light sedimentary infill in the Maracaibo and Barinas-Apure Foreland Basins, respectively. In the area of Guárico Basin the Bouguer anomaly has NE–SW trend with low positive values. The Guayana Shield (i.e. Precambrian rocks) is characterized by low negative gravity values with no simple regional trend.

Offshore, a broad gravity low with WNW–ESE trend is caused by the subduction zone in Northern Venezuela. The anomaly in the area of the Leeward Antilles appears as elongated local highs separated by gravity lows which are caused by sedimentary basins located between the islands and the positive topography onshore (e.g. Bonaire basin and Cariaco trough). The highest gravity values (more than 200×10^{-5} m/s^2) are caused by the subduction in northeastern Venezuela (i.e. Lesser Antilles volcanic arc). In the area of the Grenada basin and Tobago trough gravity values decrease to -80×10^{-5} m/s^2 and -45×10^{-5} m/s^2, respectively. In the Venezuela Basin magnitudes of the Bouguer anomaly barely reach low positive values.

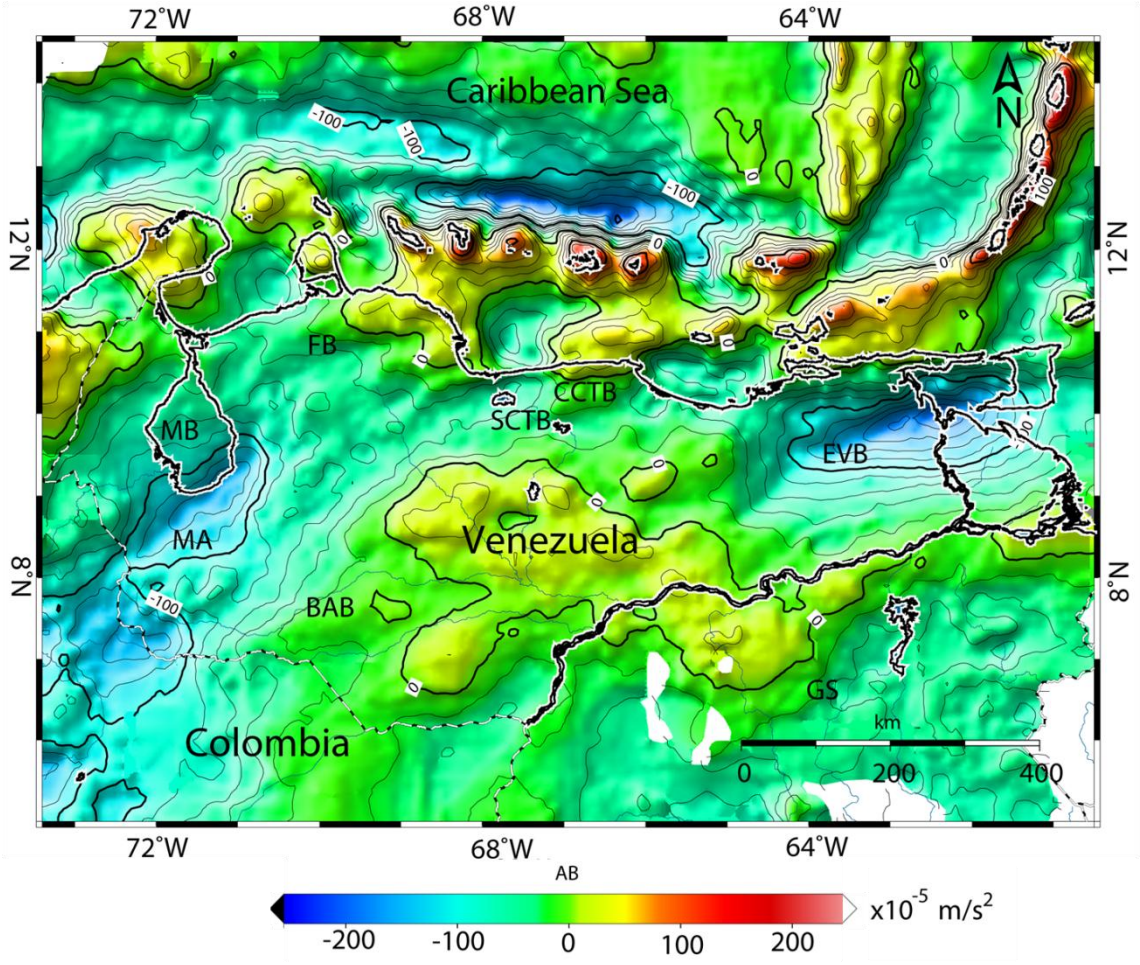

Figure 3.2 Bouguer anomaly map onshore (2.67 Mg/m^3) and free air anomaly map of Northern Venezuela and the Southern Caribbean Sea. Thin lines are contour lines 20×10^{-5} m/s^2 spacing. EVB: Eastern Venezuela Basin, MA: Mérida Andes, FB: Falcon Basin, BAB: Barinas Apure Basin, MB: Maracaibo Block, CCTB: Coastal Cordillera Thrust Belt, SCTB: Serranía del Interior Thrust Belt, GS: Guyana Shield. Thick lines show contour lines 100×10^{-5} m/s^2. For more detailed information refer to corresponding text.

3.4.1. Curvature analysis

Curvature techniques were applied to analyze directional patterns of the observed gravity anomaly and highlight principal features within the studied area. If we consider a point on a curve, curvature is the reciprocal of the radius of the circle which makes the greatest possible contact with the curve at this point. This two-dimensional concept of curvature can be easily extended into three-dimensions. The 3-D concept of curvature describes the bending of a surface from a straight plane at particular line. There is, of course, an infinite number of

planes and hence an infinite number of curvatures which can be extracted. These curvatures can be combined in a number of different ways to define important curvature properties relating to the surfaces. These properties are present through attributes which are computed directly from the surface itself. Details on its formulation and calculus can be found in Roberts (2001). The most commonly used attributes are the first derivative types, which includes dip angle, azimuth, minimum and maximum curvature. These curvature attributes were calculated by running the Java program *Curvature* (Schmidt, pers. Comm.) in order to detect faults, trends, lineaments or any other features in the potential field data that were not visible or difficult to observe in the Bouguer gravity anomaly field (e.g. Figure 3.3).

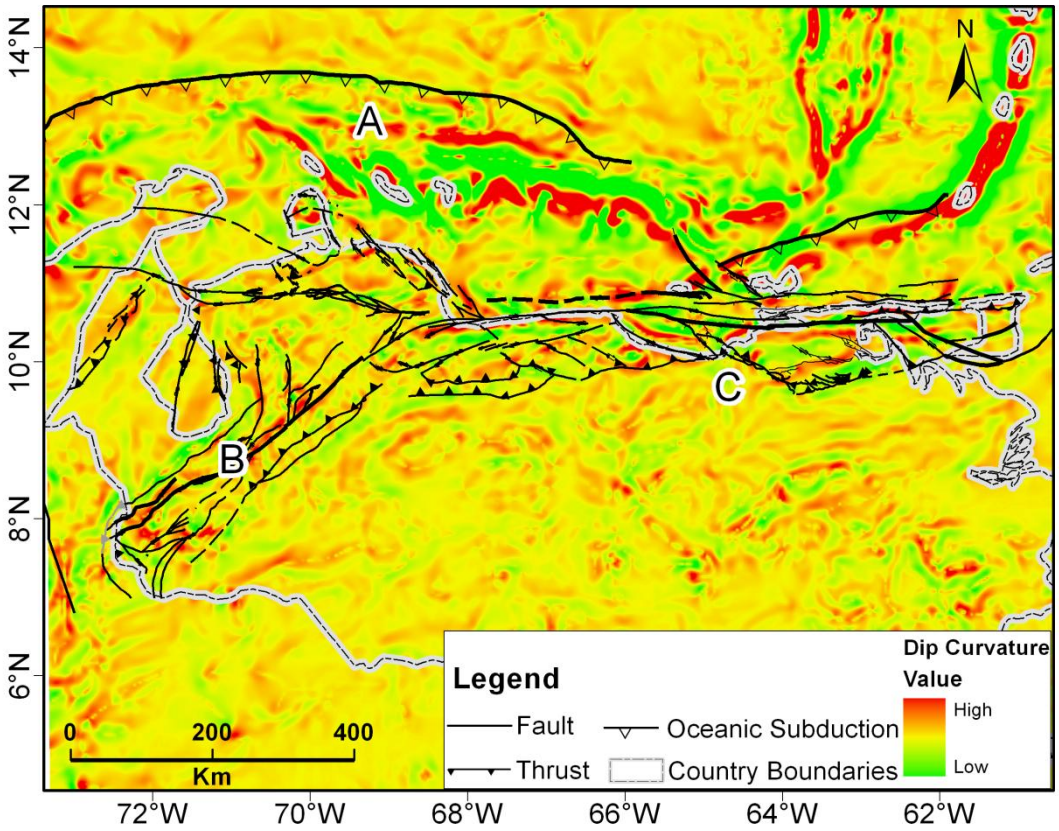

Figure 3.3 Map of dip curvature of the Bouguer anomaly shown in Figure 3.2. The light grey lines represent the coastline. Fault zones are indicated by black lines. A) Shows lineaments in the South Caribbean deformation belt; B) lineaments of the Mérida Andes; C) lineaments of the Serranía del Interior Thrust Belt.

In general, all calculated curvature attributes successfully highlight main features observable in the gravity data. Plausible results were obtained from dip curvature, minimum curvature, and most positive curvature. Here, we present the "dip curvature" (Figure 3.3) which shows the rate of change of dip in the direction of maximum dip. This attribute can be used to improve the detection of linear features (e.g. channels) and the trace of faults which are represented by the juxtaposition of positive and negative curvature values if they separate geological domains with different densities. In the dip curvature map (Figure 3.3) the South American Thrust System is clearly displayed by trend of negative and positive values in the Lesser Antilles arc. Boconó and Oca-Ancon fault systems are also marked by lineaments parallel to the general strike of faulting. Despite their excellent gravity data coverage, very diffuse values were obtained in the Venezuelan basin, Barinas Apure Basin and Eastern Basin. This result suggests low density inhomogeneities in their internal structure and that the main trend direction of the anomalies is dominated by crustal structures with monotonous regional field. Remarkable results were obtained in Eastern Venezuela where maximum and minimum lineaments are observed. These gravity field curvature values highlight the Eastern Venezuela thrust system, which is a structure in the upper crust observed from Eastern Venezuela basin to northern Trinidad, suggesting high density contrasts in its internal structure which dominate the SW-NE strike of the Bouguer Anomaly in this area. These important observations are related to gravity effect which could be caused by the detached oceanic slab underneath continental crust (Russo et al. 1996; VanDecar et al. 2003) and its continuation southward into the South American continent. Taking into account its wavelength, the SW-NE strike of the Bouguer Anomaly seem to be more related to shallow structures and to density contrasts in the Easter Cordillera than to the deep detached slab.

3.4.2. Euler-deconvolution

The Euler-deconvolution of potential fields is widely used as semi-automated method based on the Euler's homogeneity equation. In many cases, it can be used to provide preliminary information of the depth distribution of gravity and magnetic sources by deconvolution of both fields. No further information is necessary. The deconvolution is controlled by a structural index SI which is related to the underlying basic structure (SI=0, indicates thin plate; SI=1, an elongated body and SI=2, a point source) (Thompson 1982; Reid et al. 1990). Resulting source points are always clustered which describe edges or center of

bodies with density contrasts to their surroundings. Strong gradients in the fields lead to clustering in these specific areas often belonging to tectonic structures. The software *Regder* of Pašteka and Richter (2002) use a regularized procedure to obtain stable derivatives in the Euler's homogeneity functions based on Tikhonov's approach (Tikhonov and Arsenin 1977). The amount of clustered source points can be reduced by statistical criteria to obtain the most reliable results. Source points were selected according to three criteria: minimum standard deviation (Thompson 1982), the minimum condition number from the singular value decomposition procedure (FitzGerald et al. 2004), and points with the smallest error from the Euler equation (Cooper 2004).

For the study area we calculated Euler source points with SI = 0, 1, 2 and different window sizes 100, 200, 500 km in order to include long and very long wavelengths in the anomalies. Figure 3.4 and Figure 3.5 show the Euler source points for SI = 2 and window size of 200 km included in the modeling process. These solutions show the centers of bodies with high density contrast. For instance, clusters of points in Western Venezuela from 0 to 50 km depth are consistent with the position of the Caribbean slab. The Euler source points also show an important cluster of solutions situated within the upper crust and mantle below Eastern Basin. This can be a result of a decrease in density contrast (e.g. Figure 3.4 and Figure 3.5) probably associated with subsiding of the basin and/or with lower crustal density inhomogeneities.

3.4.3. 3-Density modeling

The presented model was developed by an interactive forward-modeling procedure using the software IGMAS (Interactive Gravity and Magnetic Application System) (http://www.gravity.uni-kiel.de/igmas). The kernel of the system uses polyhedrons for the approximation of geological bodies with constant density to get the gravity effect of the model. The algorithm transforms the volume integral involved in the vertical attraction of a homogeneous polyhedron into a sum of line integrals by applying the gauss theorem in 3-D and 2-D (Götze 1978; Götze and Lahmeyer 1988; Schmidt and Götze 1998). Then the calculated gravity effect of the modeled structures is compared to the observed gravity.

The three-dimensional model geometry is defined by a series of parallel vertical cross-sections. Our 3-D model is comprised of 27 parallel sections with similar orientations. They

follow the directions of the onshore seismic profiles of BOLIVAR and GEODINOS projects (see Figure 3.1 for location). Here, we present four parallel sections to illustrate the main characteristics of the 3-D model (e.g. Figure 3.4) which are constrained by the results of the wide-angle seismic refraction profiles (Schmitz et al. 2008), Moho depth taken from receiver function studies (Niu et al. 2007) and the location of seismic hypocenters. Additionally, we used depth estimations from Euler deconvolution, mapped surface geology and focal mechanism solutions for modeling constrains. In figures 3.4 and 3.5 we present the planes located at 70°W, 67°W, 65°W and 64°W, which are identical with the location of the velocity models presented by Schmitz (2008). Additional constraining data can be seen in these figures (e.g. Euler's solutions, Seismicity and receiver function Moho depth). Only gravity data within a maximum distance of ±2 km is projected onto the cross-section. For Euler's solutions, seismicity, and receiver function Moho depth, the maximum distance for projection is 10 km.

a)

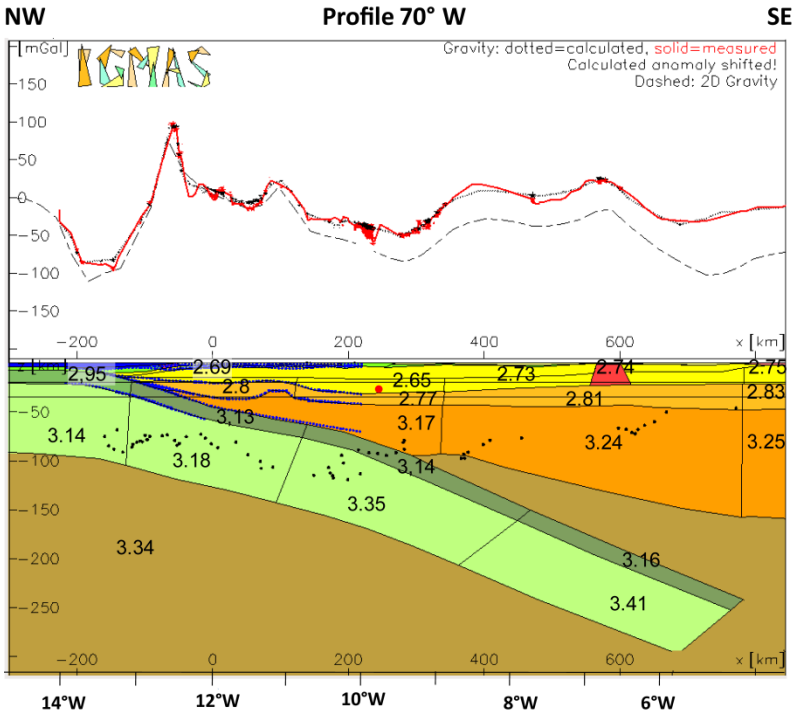

b)

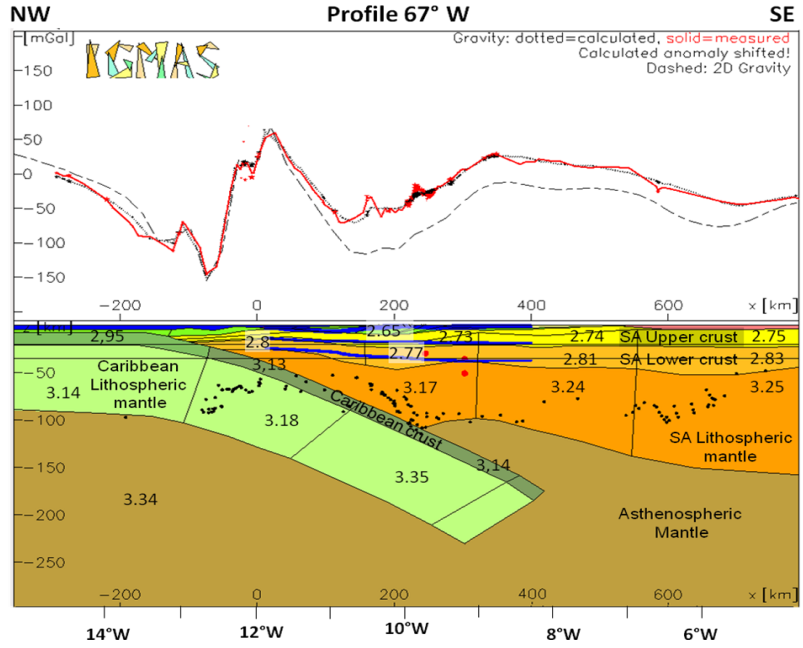

Figure 3.4 Representative vertical cross-sections of the 3D density model. (a) Vertical cross-section along the 2-D velocity profile 70°W. (b) Vertical cross-section along the 2-D velocity profile 67° W. The upper part shows three lines: the measured gravity curve in red, the gravity of the 3-D density model (black dotted line) and the modeled gravity of a 2-D approach (black dashed line). The lower part represents the modeled structures of the lithosphere. Numbers indicate body density in Mg/m3. Also included are the locations of the Euler source points for window size of 200 km and SI = 2 (black dots). Blue lines indicate the findings of the wide-angle seismic experiment. Moho depth for receiver function (red dots).

a)

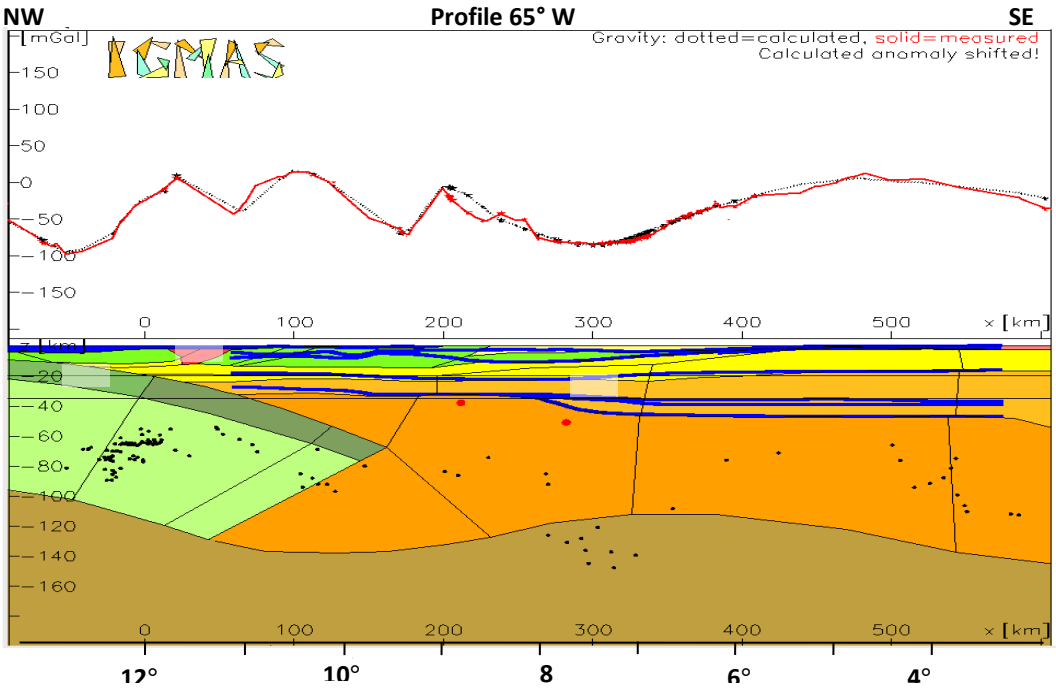

b)

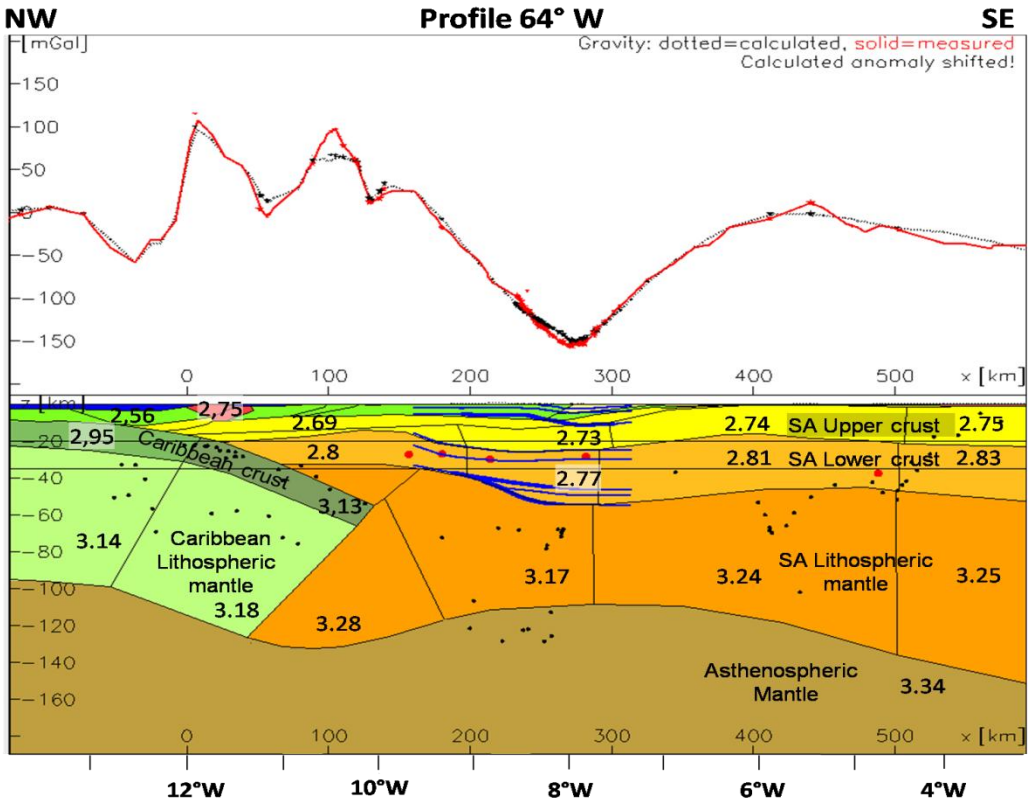

Figure 3.5 Representative vertical cross-sections. (a) Vertical cross-section along the 2-D velocity profile 65°W. (b) Vertical cross-section along the 2-D velocity profile 64° W. Graphical indications as described in the previous figure.

3.5. Density model

3.5.1. Vp - Density conversion

A review of previous density models of the region reveals several inconsistencies among densities and geometries of the proposed model (Rodriguez and Sousa 2003; Schmitz et al. 2005; Bezada et al. 2008; Chacín et al. 2008; Jácome et al. 2008; Magnani et al. 2009). To avoid ambiguities the density values used in the 3-D gravity modeling were initially assigned from predicted values that were calculated from the seismic velocity observations. Specifically, empirical functions from Nafe and Drake (1963), Christensen and Mooney (1995), and the Birch (1960; 1961) were used. They provide empirical relationships between Vp and ρ which were found by reworking and analyzing rocks in boreholes and/or laboratory. We also considered density modifications due to high temperature and larger pressure conditions and changes in the mineralogical and chemical composition of oceanic and continental rocks. These calculations have been performed using the methods described by Hacker and Abers (2004) and Sobolev and Babeyko (1994). This approach determines the equilibrium thermal mineralogical composition of a rock of a given bulk-chemical composition, and then the calculated model proportions and mineral compositions are used to calculate density and the isotropic elastic wave velocities of the rock. P/T conditions used were estimated from heat-flow measurements in South America (Hamza and Muñoz 1996). According to Hamza and Muñoz (1996) heat flow values observed in Venezuela are between 20 and 180 mW/m^2 but, given the characteristics of the data, these values are only a representative estimation of the geothermal regime. Although no detailed information about rock composition is available, a typical basaltic composition for oceanic crust and average composition between diorite and granodiorite for the continental crust was assumed. However, the final density values for each body in the model were fit during the modeling process in order to adjust the observed gravity field.

3.5.2. Model sections

The final density model consists of approx. 50 bodies which represent the main geological units. Table 3.1 shows the estimated mean density values used to assemble the 3-D gravity model. Density ranges of 2.70-2.76 Mg/m^3, 2.78-2.85 and 3.17-3.25 Mg/m^3 were selected for the South America upper crust, lower crust and mantle, respectively. The range of

density values describes lateral variations mainly in NS direction, which appear to be related to characteristic changes in rock composition and possibly to the tectonic age of the continental lithosphere. The Caribbean crust and mantle have been modeled using density values in the range of 2.95-3.18 and 3.14-3.41 Mg/m^3, respectively, these values describe mainly vertical variations of the portions of the plate subducted beneath South America and were calculated by the thermodynamic approach of Hacker and Abers (2004) and Sobolev and Babeyko (1994).

Table 3.1 Mean density values used to assemble the 3-D density model

Model units	Density Mg/m^3
Qt sediments	2.20-2.40
Tertiary sediments	2.45-2.51
Caribbean crust	2.95-3.18
Ocean water	1.03
Caribbean lithospheric mantle	3.14-3.41
Asthenospheric mantle	3.34
South America upper crust	2.70-2.76
South America lower crust	2.77-2.85
Volcanic arc	2.85
Meta Ophiolitic series	2.92
South America lithospheric mantle	3.17-3.25

Figure 3.6 shows the map of residual anomaly (misfit) between the measured and calculated Bouguer anomaly of the model. The histogram of the residuals shows a tight concentration of residual anomaly values around -0.12×10^{-5} m/s^2 (Arith. Mean), resulting in a standard deviation of 15.54×10^{-5} m/s^2 and a correlation factor between measured and calculated anomaly of 0.95. These statistics indicate that the 3-D density model can reproduce the observed Bouguer anomaly at intermediate- to long-wavelength scale. Another justification can be obtained from the visual inspection of the observed and calculated fields along the four 2-D profiles presented. In all these models the amplitudes of the gravity anomalies are satisfied within 5%. Taking into account the available constraining data, the wide range of the gravity anomaly between -205×10^{-5} to $+225\times10^{-5}$ m/s^2, and the accuracy of the gravity data, we considered the observed misfit as not significant and without consequence to the regional discussion.

The four vertical cross-sections, located at 70°W, 67°W, 65°W and 64°W, illustrate characteristic parts of the 3-D gravity model. The cross-section along the 70° W meridian (Figure 3.4) shows the slab of the Caribbean plate with the most northern upper surface of the slab constrained by the seismic profile. The geometry of the slab at depths greater than 250 km is based on the intermediate depth seismicity observed beneath Maracaibo block, Mérida Andes and Eastern Columbia where the position of the slab has been fixed on the seismic cluster of the Bucaramanga nest (Colmenares and Zoback 2003; Corredor 2003). The top of the slab has also been imaged from tomography studies (Van der Hilst and Mann 1994). An important crustal thinning is present in the area of the Falcón basin, where Moho depths are reduced by approximately 10 km (Bezada et al. 2008). The 3-D model shows this feature (Figures 3.4, 3.7, and 3.8) as a semi-elliptical shape with major semi-axis of 100 km in E-W direction. Positions of upper and lower crust, oceanic crust and slab are fully controlled by the 2-D velocity model. In this cross-section the majority of the projected Euler solution points are concentrated into the Caribbean mantle, indicating a strong density contrast.

Figure 3.4b presents a cross-section along 67°W. The final model fits the observed gravity data. Basement, upper and lower crust, and mantle boundaries were modeled in agreement with the findings of the velocity model though a significant difference on the shape of Moho topography is observed between 9° and 12° N with consequent change on Bouguer anomaly. Therefore, a minor modification of Moho topography was necessary in order to adjust the modeled field to the observed one. The upper continental crust is modeled by six layers. Sedimentary rocks are represented by two layers representing Guárico basin infill. Basin basement (Cretaceous) and material attached to Cordillera de la Costa range are also included. The Caribbean slab was modeled with two layers: Caribbean crust and lithospheric Caribbean mantle, respectively. Here, a few clusters of Euler source points, which indicate a weak density contrast in the upper and lower crust, have been used to constrain the location of the down going slab beneath Cordillera de la Costa range.

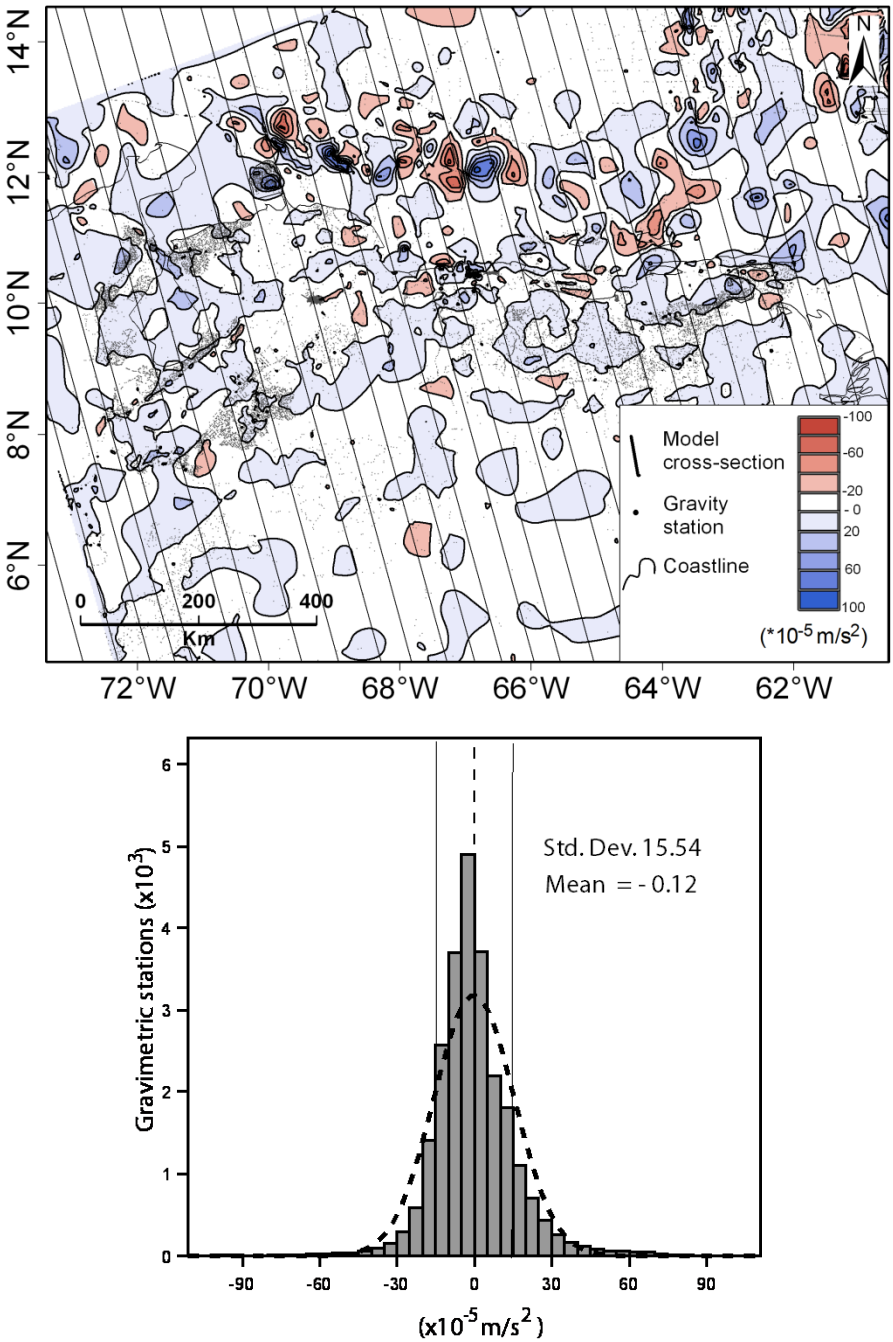

Figure 3.6 a) Residual gravity field of the study area obtained by subtracting the calculated gravity effect of the 3-D model from the observed gravity field (black lines indicate position of the vertical cross-sections used to defined model geometry). Maximum misfits are caused by short-wavelength anomalies; we considered only the regional field and did not attempt to explain this short-wavelength (for further explanation see text). b) Histogram of residual gravity. The histogram shows a tight concentration around the arithmetic mean (Mean = -0.12×10-5 m/s2) with a standard deviation Std. Dev =15.54×10-5 m/s2. The resulting correlation coefficient between the observed and calculated gravity fields is 0.95.

Figure 3.4a and 3.4b also show the 2-D and the 3-D calculated gravity fields. The calculated gravity field using 3-D approach satisfied the observed gravity field within 5% in

all presented cross-sections. On the other hand, the 2-D approach has a good fit near 12° N. However, a misfit between the observed and 2-D modeled gravity fields is observed to the north and to the south which extends for more than 600 km of horizontal offset. If we accept that the finding of the seismic modeling are correct the most plausible cause of the misfit lies in the ambiguity of the density estimation. In this scenario, only unrealistic density values overcome the misfit between the observed and 2-D modeled gravity fields which is more of 50×10^{-5} m/s^2 in some areas of the profile. These observations lead us to the assumption that the misfit is a direct consequence of the three dimensional effect of the cortical structure. Specifically, the Caribbean slab position which changes laterally the shape of the Moho and the lithospheric and asthenospheric mantle boundary.

The cortical structure in eastern Venezuela is represented by the cross-sections along 65° W and 64° W. The 3-D model is in good agreement with the 2-D velocity models and results from receiver function analysis. Here, the crustal thickness reaches ~50 km on the Eastern Venezuela Basin. Many positions of Euler solution points correlate well with the lower crust and Moho topography, most of the source points are located in the lower crust indicating strong internal density contrast. Offshore, a cluster of Euler points at 65° W and 64° W show density contrast or structure dipping southward which is interpreted as the Caribbean slab. During the modeling, an alternative model was tested (Figure 3.9b) including the South American oceanic slab detached underneath Eastern Venezuela Basin (VanDecar et al. 2003). However, the total contribution of such slab position does not represent an important effect on the gravity field. These results are in agreement with our curvature analysis of the gravity field. In this area, most of the prominent curvature lineaments correlate with short-wavelength anomalies located on the north of Eastern Venezuela Basin. We have modeled the slab geometry according to subduction-transform propagation model which involves purely westward subduction with the slab break off along a vertical, dip-slip tear through the lithosphere (Clark et al. 2008).

Another aspect of the 3-D model corresponds to rocks on the Guyana Shield, modeled with a small negative density contrast due to a large amount of meta-sediments. Short wavelength gravity anomalies from igneous and intrusive rocks were ignored. The regional field was adjusted by cortical root.

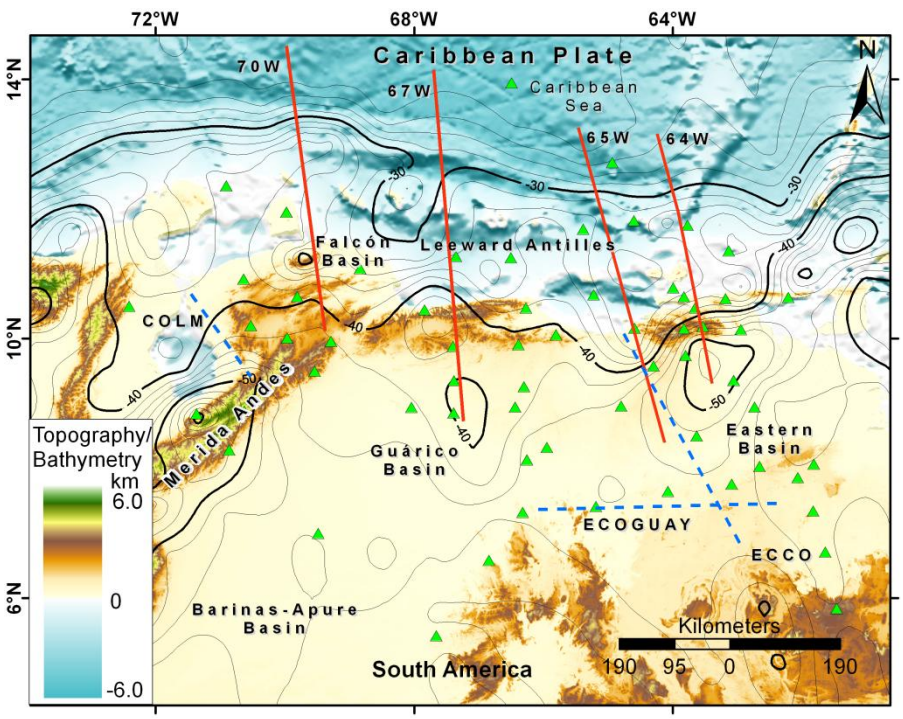

Figure 3.7 Moho relief map for both continental and oceanic crust for the Caribbean-South American plate boundary derived from the 3-D gravity model in the study area (contoured every 2 km). Moho depths estimated from seismic studies have been extended to whole area. Topography/Bathymetry (color bar). The reflection/wide-angle profiles used to derive our reference model are shown as red lines labeled by 70 W, 67 W, 65 W and 64 W (Schmitz et al. 2008). Locations of the active source refraction profiles of Schmitz et al. (2002) are indicated by dashed blue lines labeled as ECOGUAY, ECCO and COLM profiles. The location of the Moho observations of Niu et al. (2007) shown as green triangles.

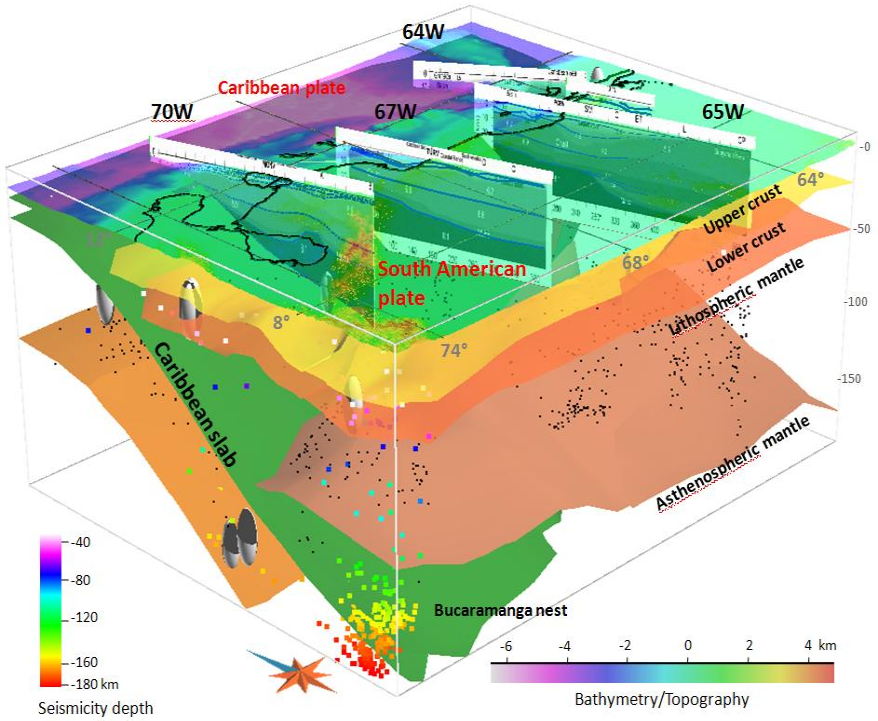

Figure 3.8 A perspective view of the final 3-D density model for the Caribbean-South American plate boundary. Each surface represents a major layer boundary. The coastline is shown as a black line. Black and red letters describe boundary names and additional information. Thin blue lines represent findings of 2D velocity models. It is also included the 2-D velocity models, Topography/Bathymetry (color bar), Euler's source points (black points), seismicity (rainbow color points) and focal mechanic solutions (FUNVISIS 2007).

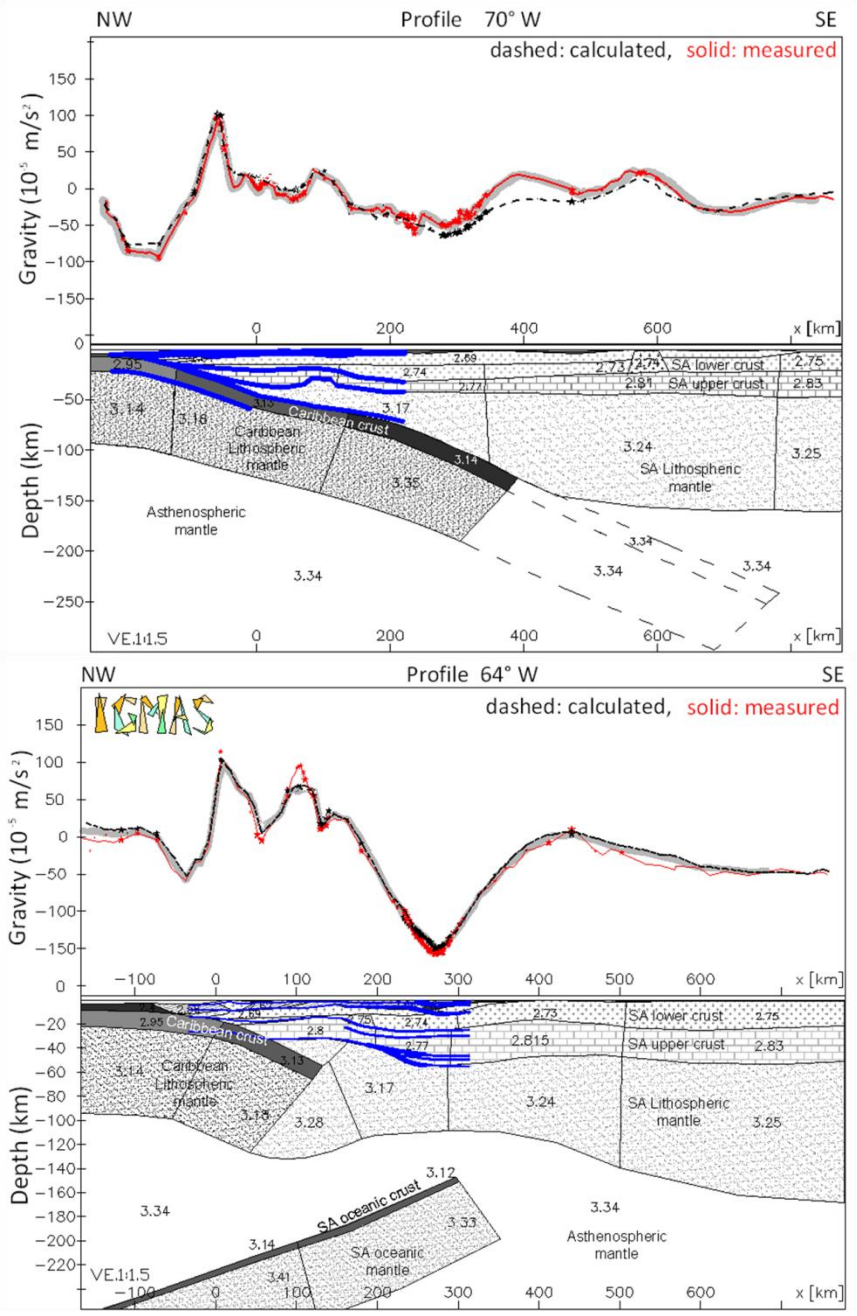

Figure 3.9 Model alternatives and trials. a) Representative vertical cross-section along profile 70° W. It bases on the assumption of a short slab (position of the slab in our final model is shown as dashed line). b) Vertical cross-section along profile 64° W based on hypothetic slab detached beneath Eastern Venezuela Basin. The upper part shows three lines: the measured gravity (red line), the gravity of the 3-D alternative density model (black dashed line) and the modeled gravity from our final model (gray line). The lower part represents the modeled structures of the lithospheric densities. Blue lines indicate the findings of the wide-angle seismic experiment.

3.5.3. Model variability

Here, we present test calculations which can prove the sensibility of de 3-D gravity modeling on different geometries of lithospheric gross structure. For alternative models we assumed that the density distribution equals exactly the densities in the base model. In particular, we were interested in Eastern and Western Venezuela, where two different alternative models are used to explain the structure and geodynamic in these regions of the Caribbean-South American eastern boundary. In Western Venezuela we tested how the gravity field changes in response to the continuous slab (Van der Hilst and Mann 1994) or tear fault structure (Taboada et al. 2000). The easternmost part of the slab in our 3-D model is based on the crustal structure derived from the seismic profile 70° W. The tear fault structure's model fits the crustal structure reasonably well. However, the shorter slab results in a decreased gravity response for model offsets between 300 and 600 km in the profile (Figure 3.9a), caused by the lacking slab and the adjusted lithospheric and asthenospheric mantle boundary. Observed misfit is far bigger than the errors associated with the whole gravity data. This implies that a long slab provides a more realistic explanation and better fit to the gravity signal in this area, and is more consistent with the intermediate and deep seismicity observed in the slab in Northeast Colombia. Eastern Venezuela structure was modeled constrained by seismic cross-sections along 65° W and 64° W and receiver function analysis. Here, two alternative models concerning slab break-off for the South American oceanic slab is tested: A detached slab underneath Eastern Venezuela Basin (VanDecar et al. 2003) and vertical dip-slip tearing of the slab (Clark et al. 2008). Modeling results show that contribution in the gravity field of detached slab does not represent an important effect in the gravity signal of Eastern Venezuela Basin (Figure 3.9b). The most possible reason is the low density contrast estimated for the slab in that position. Besides, a bigger effect can be achieved with higher density contrast, but this assumption is not in agreement with our density estimation. In the final model, we have modeled the slab according to the subduction-transform propagation model, which involves purely westward subduction with the slab break off along a vertical, dip-slip tear through the lithosphere, proposed by Clack et al. (2008), whose results are in agreement with our curvature analysis of the gravity field and Euler source points.

3.5.4. Moho variations

A general finding of our modeling was that those parts of the modeled Moho which are constrained by the four seismic profiles did not need much modifications of the model geometry to obtain a good fit between the modeled and observed gravity fields. However, a more detailed inspection of the entire modeling area reveals some important differences in Moho depth (Figure 3.7).

The Guayana Shield is regionally underlain by crust thicker than 45 km, northwards beneath Eastern Venezuela, Guárico and Barinas-Apure Basin crustal thickness reaches ~40 km along the coastline. Regarding the Caribbean Mountain System the derived crustal thickness oscillates around 30 km and decreases slightly toward the Leeward Antilles (Figure 3.7).

The oceanic plateau in the Venezuelan basin is underlain by crustal thickness of about 20 km. A pronounced crustal thickness of about 35 km is observed beneath Aves Ridge and Lesser Antilles Volcanic Arc.

Compared to the thick crust of Venezuelan continental basins, the Mérida Andes shows a relatively thin crustal root up to 55 km thickness, this estimation is well constrained by receiver function analyses on the southwest but with some discrepancies on the northeast. Maracaibo block seems to have a crustal thickness of 35-40 km. The high topography of the Santa Marta-Perijá cordilleras is compensated by thick crust that reaches more than 40 km thickness.

The anomalous crustal thickness zone in the Falcón Basin (27 km) shows a semi-elliptical shape in the 3-D model with major semi-axis of 100 km in E-W direction extending eastwards into the Bonaire Basin (Schmitz et al. 2008).

The crustal thickness on the Eastern Venezuela Basin gradually decreases from 50 to 40 km near the Venezuelan Atlantic coast. Northeast of this feature a maximum crustal thickness of ~50 km has been identified beneath the Tobago trough.

Other minor variations in the Moho relief are included at the Leeward Antilles arc. For instance, Aruba, Curacao, and Bonaire blocks. Strong E-W variations in density and thickness are observed. Our preferred model also includes the Bonaire, Cariaco, Granada, and Tobago basins; all filled with considerate amounts of sediments, and each modeled with a typical individual crustal thickness.

3.6. Conclusions and outlook

A recompilation of gravity data in Venezuela and adjacent areas has been done for 3-D modeling of the gravity field. Standard errors of the new database are approx. 0.5×10^{-5} m/s^2 for observed measurement and in the range of $\pm$ (5–15)$\times10^{-5}$m/s^2 for the calculated Bouguer anomaly. However, maximum errors which are higher than expected were found. For purposes of a continental to regional scale density modeling the database is good enough.

The new Bouguer anomaly map of Venezuela was interpreted by applying curvature analysis, and Euler deconvolution. The performed curvature analysis and Euler source points of the gravity field show density contrasts of the major features mainly from shallow structures (e.g. attached material in the Coastal Cordillera Thrust Belt). Locations of Euler source points were interpreted as derived from slab positions in western and eastern Venezuela. This result supports the thesis of slab underneath Maracaibo and Mérida Andes and does not corroborate the interpretation of detached oceanic slab underneath Maturin Basin.

The presented 3-D density model represents a realistic distribution of densities constrained by available geophysical and geological data, including velocity models, results from receiver function analysis and seismicity. With regard to former 2-D gravity models it was demonstrated that these approaches always under or over-estimate the gravity effect as consequence of three-dimensionality of structures in the region. This may explain discrepancies and ambiguity in previous models. Despite the good fit between the calculated gravity effects of our final 3-D model with the observed gravity field, further advances, for example 3-D magnetic modeling, will provide more information especially in areas like Mérida Andes where no deep seismic data is available.

Discussion of the geometry of the major tectonic features within the model leads to the following main conclusions:

In Western Venezuela, the Caribbean slab extends from Northern Colombia to the area of the Bucaramanga “nest” seismic cluster, beneath Maracaibo block. Here, the slab inclines with approx. 15° and the dip angle increases up to 32° in depths greater than 100 km. The dip direction is about N150°E ± 5 increasing slightly eastward.

In Eastern Venezuela, modeling results support the hypothesis of subduction-transform propagation model mechanism which involves purely westward subduction with the slab break off along a vertical, dip-slip tear through the lithosphere. Rather small contributions on the gravity field have been found from alternative slab position underneath Eastern Venezuela Basin.

Results suggest that Northern South American lower crust is relatively light and the density of the Caribbean crust, despite of its anomalous thickness, is typical for an oceanic crust.

4. Crustal density structure in northwestern South America derived from analysis and 3-D modeling of gravity and seismicity data

This paper presents a three-dimensional (3-D) interpretation of new gravity and seismicity data sets for northern South America. A 3-D forward density model was constructed on the basis of deep wide-angle seismic refraction sections, Moho depth from receiver functions, and surface geology. Density values were estimated from published borehole data for sediments by using empirical velocity–density functions and considering mineralogical–chemical composition variations under typical pressure–temperature conditions for upper and lower crustal rocks. The modeled 3-D density structure was kept as simple as possible. The continental and oceanic plates were formed by two sedimentary bodies, one crustal body, and one mantle lithosphere body overlying a sub-lithospheric mantle. The Caribbean plate was modeled with an atypical crustal thickness of ~18 km (including sediments). The geometry of the Caribbean plate was modeled using a combination of gravity modeling and analyses of the seismicity and focal-mechanism solutions. Intermediate seismicity and the orientation of the T-axes appeared aligned along the predicted position of the slab. As a result, the estimated slab dip angle under Maracaibo and the Mérida Andes was ~15° and increases up to ~20° after 100 km depth. The model showed two orientations in the slab strike: ~N150°E ± 5 in western Colombia and southward underneath the Maracaibo block. The modeling results suggest that the northern South American upper and lower crusts are relatively light and the density of the Caribbean crust is typical for an oceanic crust.

4.1. Introduction

The regional tectonics of the northern South American area has been under controversy for more than three decades. These debates have focused on the origin and evolution of the Caribbean plate and its actual boundaries among the plates that interact in this area.

In general terms, several studies have attempted determination of the crustal structure in northern South America. For instance, the regional tectonics has been explained primarily by

using relocated earthquakes and their focal mechanisms. These studies have nevertheless identified segments of the subducted lithosphere of the Caribbean and Nazca plates beneath northwestern South America (Dewey 1972; Pennington 1981; Perez and Aggarwal 1981; Van der Hilst and Mann 1994; Malavé and Suárez 1995; Perez et al. 1997; Taboada et al. 2000) by means of seismic tomography and earthquake location. Although seismicity is shallow and diffuse in this region; earthquakes with hypocenters below 70 km depth are not located in well-defined seismic zones. As a result, precise delineation of the subducted slabs and their tectonics has not been achieved.

A few wide-angle seismic studies provide information on the crustal structure of the Caribbean plate (thickness and internal structure) and their associated foreland basins (i.e. sediments infill) (Edgar et al. 1971; Ocola et al. 1976; Bowland and Rosencrantz 1988), but still details are vague, consequently, the crustal structure is still poorly resolved.

Likewise, in terms of density distribution, a few two-dimensional (2-D) gravity models have been used to explain the main anomalies observed in the regional gravity field (Bonini et al. 1977; Bonini et al. 1980; Bosch and Rodriguez 1992; Chacín et al. 2008; Mantilla-Pimiento et al. 2009). These investigations were focused on either 2-D forward modeling or some particular local features (e.g. Mérida Andes). Since the influence of density distribution is a parameter of first order importance for understanding the present-day structure and tectonic evolution of this area, having available a realistic density distribution of the three-dimensional (3-D) gravity response is desirable for studying the whole region. The main aim of this study was to establish and describe a 3-D density model of northern South America between 5° to 15°N and 70° to 78°W (Figure 4.1) encompassing parts of Colombia, Venezuela, the Caribbean Sea, and the Pacific Ocean. This goal was achieved using up-to-date published geophysical and geological data including topography, bathymetry, wide-angle

seismic studies, seismicity distribution, deep boreholes, and surface geology. Small details present in the regional structure were omitted during the modeling process. Furthermore, we analyzed the Bouguer anomaly data by means of spectral analysis and Euler deconvolution techniques. Results from these analyses provided constraints for some structures in the uppermost crust. Additionally, we calculated the isostatic crustal root using local and regional isostatic compensation models. These calculations of compensation level provided constraints for the top of the mantle lithosphere in the density model. We also used seismic hypocenters to constrain the geometry and position of the Caribbean and Nazca slabs. We examined the focal mechanism solutions and the correlation of the density model with the tectonics and geodynamics of this region. The results of our work represent new, independent information to provide verification and constraints for future structural models.

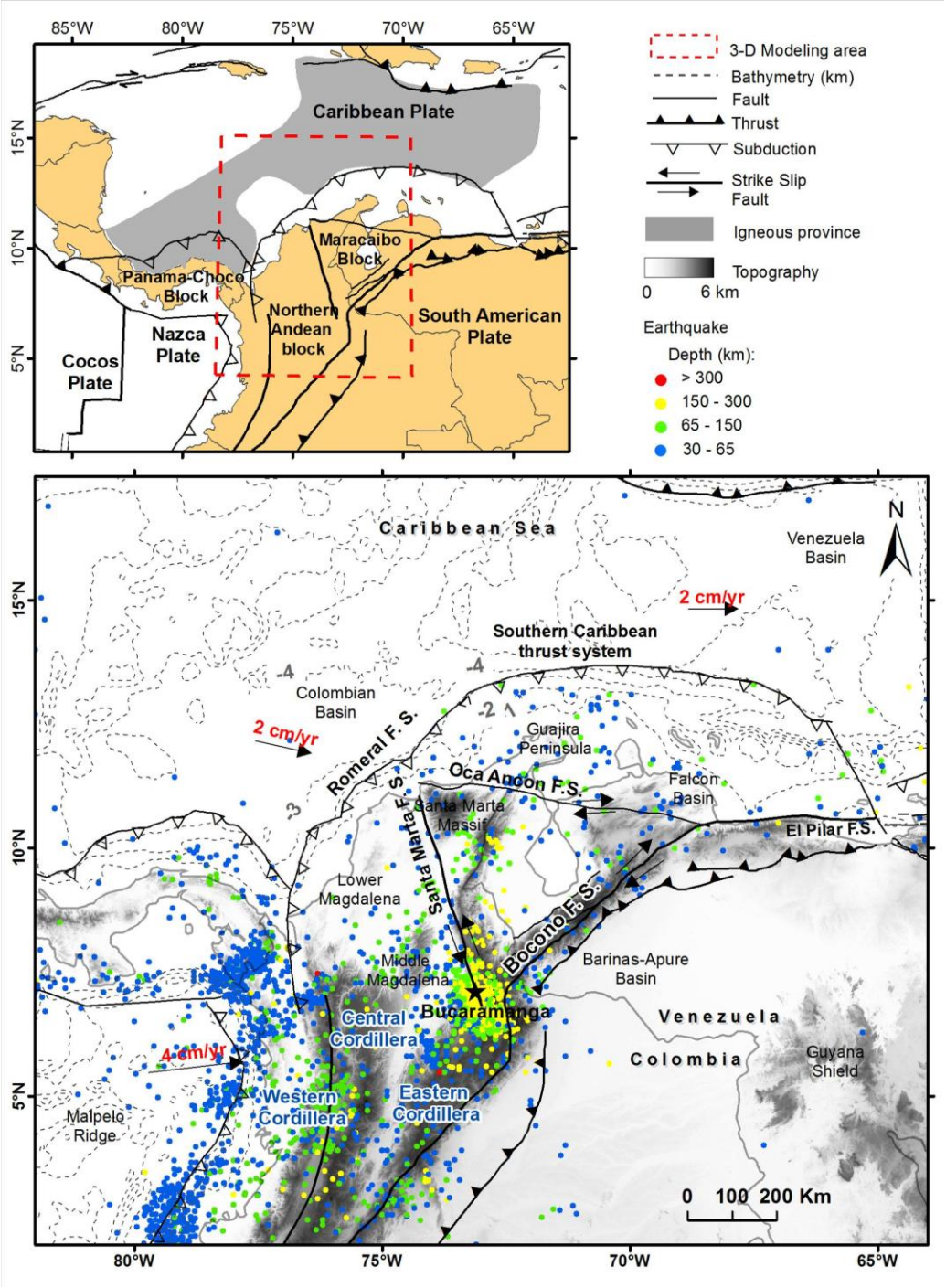

Figure 4.1 Neotectonic plate setting and kinematics of the northern South American and Caribbean regions, indicating the main active fault systems. Red box marks the study area. Arrows with red numbers indicate relative regional motions. Gray colors indicate topography. Dashed lines show bathymetry. Seismicity (1900 to December 2010) from the National Seismological Network of Venezuela (FUNVISIS 2007) and Harvard (http://www.seismology.harvard.edu) catalogues (Mw > 3.5).

4.2. Geological setting

It is commonly accepted that the present shape of northwestern South America is the result of interactions between the South American, Nazca, and Caribbean plates (Figure 4.1), which began during the Late Jurassic–Early Cretaceous with the separation of the Americas and the formation of the proto-Caribbean ocean basin (Pindell 1994; Meschede and Frisch 1998). The origin, tectonic structure, and the geodynamics of the Caribbean plate have remained controversial over the last few decades and are still open questions. The Caribbean plate has been recognized as a large igneous province (LIP) formed by widespread flood basalt volcanism during the Late Cretaceous (Donnelly et al. 1990). However, Hoernle et al. (2004) have proposed that the Caribbean large igneous province (CLIP) does not represent a single oceanic plateau, but instead consists of remnants of multiple smaller igneous structures (e.g. oceanic plateaus and paleo–hotspot tracks) formed over at least 56 Ma, possibly overprinted by later in situ magmatism. The complex interaction between the Caribbean and South American plates resulted in a large proportion of its margins tectonically uplifted and sub-aerially exposed. Large proportions of its margins have been accreted along the northwestern margin of South America.

Early models of the tectonic evolution of the Nazca plate were established by means of reconstruction of magnetic anomalies and bathymetric data (Hey 1977; Lonsdale and Klitgord 1978). These models suggest that major plate reorganization took place in the region around 25 Ma, breaking the ancient Farallon plate into the Cocos–Nazca plate and the Juan de Fuca plate. Differential stresses between the Cocos segment and the Nazca segment near the Galapagos hot spot later evolved into N–S seafloor spreading (Cocos–Nazca Spreading Center) along the two segments and originating from both Nazca and Cocos plates.

According to recent GPS data, the present–day motion of the Caribbean plate is toward the east–southeast at about 10–20 mm/a (5°) with respect to the stable South American craton, while the Nazca plate is accommodated by the Pacific subduction zone almost perpendicularly (88°) beneath South America at 58 mm/a. (Freymueller et al. 1993; Kellogg and Vega 1995; Perez et al. 2001; Trenkamp et al. 2002).

The oceanic Nazca plate in the study area (Figure 4.1) has an age of less than 26 Ma (Lonsdale 2005) and carries the Malpelo Volcanic Ridge, a block of thickened oceanic crust. This structure is believed to be the result of the interaction between the Galapagos hot spot and the Nazca Spreading Center during the last 20 Ma. (Sallarès et al. 2003). The subduction of the Nazca plate beneath the most northern portion of South America is poorly imaged though Gutscher et al. (1999) have defined a region from 6º N to 2.5º N of steep ESE-dipping with a narrow volcanic arc. The motion of the Nazca plate has been accommodated along the southern Panama Fault Zone since 9 Ma. (Molnar and Sykes 1969; Van Andel et al. 1971; Jordan 1975). In this area, the forearc and volcanic arc systems along the western coast of Costa Rica and Panama were created as a result of the subduction of the Cocos and Nazca plates under the Caribbean plate. The Benioff zone is poorly imaged, but is documented to dip to the northeast by about 33° (Muñoz 1988).

The hypothetical geometry and kinematics of the subducted Caribbean plate in the northeast region of Colombia has been characterized mainly by seismicity. Seismicity in this region (Figure 4.1) is strongly characterized by shallow earthquakes of moderate and low magnitude. However, some events associated with subduction processes have been recorded for depths greater than 150 km (McCann and Pennington 1990; Malavé and Suárez 1995; Colmenares and Zoback 2003; Corredor 2003). In southwest Venezuela, seismicity is characterized by the Bucaramanga nest composed of intermediate and deep events clustering

in small volume. Eastward, the seismicity is mainly focused on the Boconó and Oca–Ancón fault systems with several shallow depth events but with some intermediate depth seismicity. Over the years, several authors have postulated about the direction and dip of the Caribbean slab. Dewey (1972) concluded that these seismic events occurred a continuous slab from a portion of the Caribbean lithosphere subducting beneath northern Colombia, which has a strike of N10°E dipping eastward; Pennington (1981) reported N109°E dipping 25°–30°; and Kellog and Bonini (1982; 1995) postulated a zone dipping ~30° which ends at a 200 km depth. Similarly, Schneider et al. (1987) defined a Wadati-Benioff zone up to 190 km in depth, striking N10°E and dipping ~30°. The 3-D tomography model of Van der Hilst and Mann (1994) revealed a slab of ~300 km length extending along the entire width of the Venezuelan Andes, and estimates the dip angle and dip direction of the slab of 17° ± 3° and 50° ± 20°, respectively. In their interpretation, Malavé and Suárez (1995) extended the slab eastward showing a slab of 180 km depth with an angle of 25°–32°. In addition, a tear fault along the Oca Ancon–El Pilar fault system has also been proposed by Taboada et al. (2000) whose concluded that the Bucaramanga nest may correspond to an inflexion zone or hinge in the slab. More recently, Zarifi et al. (2007) proposed a scenario of collision between the Nazca and the Caribbean slabs. They explain the variation in the focal mechanism of micro-earthquakes and the complexity in the source of the moderate size earthquakes in the Bucaramanga nest as a consequence of an active process of dehydration embrittlement and the concentrated stress field in the collision zone.

The tectonics of northern South America has been explained by the interaction of a set of different blocks that move independently among the larger plates (e.g. the Maracaibo and Panama–Choco blocks). These blocks are bounded by major strike-slip faults and thrust systems that extend over the area. In the study area, the Caribbean and South American plate

boundary have been described as a wide area, 600 km wide and 800 km long, limited by oppositely verging fold, thrust belts, and foreland basins that are traversed in the middle by the Boconó and El Pilar dextral strike-slip fault systems (Audemard and Audemard 2002).

The northern termination of the Andes separates into three main mountain ranges—Eastern, Central, and Western cordilleras (Figure 4.1). Each range is characterized by several isolated massifs (e.g. Santa Marta massif) and accreted oceanic terranes associated with transpressive tectonics. Consequently, the northern Venezuela orogeny consists of a thrust belt made up of several first-order imbricated oceanic and continental tectonic units accreted with general south-vergence since the Late Cretaceous (Beck 1985; Bellizzia 1986; Ostos 1990).

4.3. Gravity data

4.3.1. Gravity database

The gravity data used in the density modeling have been presented in several publications (Izarra et al. 2005; Sanchez et al. 2010; Sanchez-Rojas 2011). The data were collected from different institutions, e.g. Simón Bolívar University, the National Geophysical Data Center (NGDC), and the Venezuelan Foundation for Seismological Research (FUNVISIS). In order to extend the data coverage of the above referred publications, new data from the Marine Geoscience Data System (MGDS) (Carbotte et al. 2004) and from the Absolute Gravity Database (AGrav) (Wilmes et al. 2009) were included. Here we present a brief review of the accuracy and reliability of these data, since these affect the accuracy of the results obtained by the 3-D gravity modeling.

According to Sanchez-Rojas (2011) taking into account all the different sources of errors in the databases, the accuracy of the computed Bouguer anomaly of the Venezuelan gravity

database was estimated to be 1×10^{-5} m/s^2 or less (1×10^{-5} m/s^2= 1 mGal). In order to check coordinate errors after including the MGDS, NGDC, and AGrav, datasets to the Sanchez-Rojas (2011) data we compared the station heights with those obtained by interpolating a high resolution digital terrain model (90 m spacing). Stations with height differences higher than 50 m were removed. The resulting maxima variation of the no-topography-corrected Bouguer gravity data in the study area is 14.03×10^{-5} m/s^2. Using the standard deviation of the height differences (12.35 m) the resolution and accuracy of this gravity data is 6.6×10^{-5} m/s^2.

Therefore, the maximum tolerance between observed and calculated gravity accepted as maximum misfit was the maxima variation of the no-topography-corrected Bouguer gravity value (14.03×10^{-5} m/s^2). This is due to the fact that most of the new added data correspond to rugged mountainous terrains with limited accessibility which, in some cases, the stations coordinates and heights were derived by reading from topographic maps. In areas of large spacing of the gravity cross sections and far from the location of the available constraints, only the regional field was modeled.

4.3.2. Bouguer anomaly map

The final gravity compilation contained about 40,000 observations onshore and more than 20,000 offshore. All data were reprocessed according to standard procedures using the 1980 Geodetic Reference System and a reference density of 2.67 Mg/m^3. Topographic corrections were calculated up to 167 km (Hayford zone O2) using a digital terrain model based on the Shuttle Radar Topography Mission (SRTM) with a grid spacing of 90 m.

The calculated anomaly map consists of Bouguer anomalies (BA) onshore (correction density of 2.67 Mg/m^3) and Free Air anomaly (FAA) offshore (Figure 4.2). The overall magnitude of the anomaly ranges from –225 to 200 × 10^{-5} m/s^2. Gravity anomalies have

negative high amplitudes along the strike of Mérida Andes. Here, the Bouguer anomaly decreases to -120 × 10^{-5} m/s^2 over igneous and meta-igneous rock of continental crust origin. Over the surrounding sedimentary basins, the anomalies are close to zero. Specifically, the Barinas–Apure Foreland Basin shows BA values near 20 × 10^{-5} m/s^2 and the Maracaibo basin -40 × 10^{-5} m/s^2. Bouguer anomalies with high amplitudes are located in the Santa Marta area and Guajira Peninsula. Here, BA rises to +130 × 10^{-5} m/s^2 over the predominantly crystalline rocks of the uplifted region of the Santa Marta massif and +100 × 10^{-5} m/s^2 over the Cretaceous low-grade volcano sedimentary metamorphic rocks with intercalated mafic and ultramafic plutonic rocks in the Guajira Peninsula. Over the adjacent Cenozoic basins, they decrease down to –80 × 10^{-5} m/s^2 over the Lower Magdalena basin and to –65 × 10^{-5} m/s^2 over the Guajira Basin. Steep gravity gradients characterize the Santa Marta and Oca-Ancón fault systems on the west and north sides of the massif, respectively. Offshore, the free air anomaly is characterized by a broad gravity low with a trend along the South Caribbean accretionary prism. Over the Venezuelan basin, FAA reaches zero values. In the area of the Colombian basin, gravity values decrease down to -20 × 10^{-5} m/s^2.

Also in the FAA, a broad gravity low with WNW–ESE trend is caused by the subduction zone in northern Venezuela. The anomaly in the area of the Leeward Antilles appears as elongated local highs separated by gravity lows that are caused by sedimentary basins located between the islands and the positive topography onshore (i.e. Aruba, Bonaire, and Curacao).

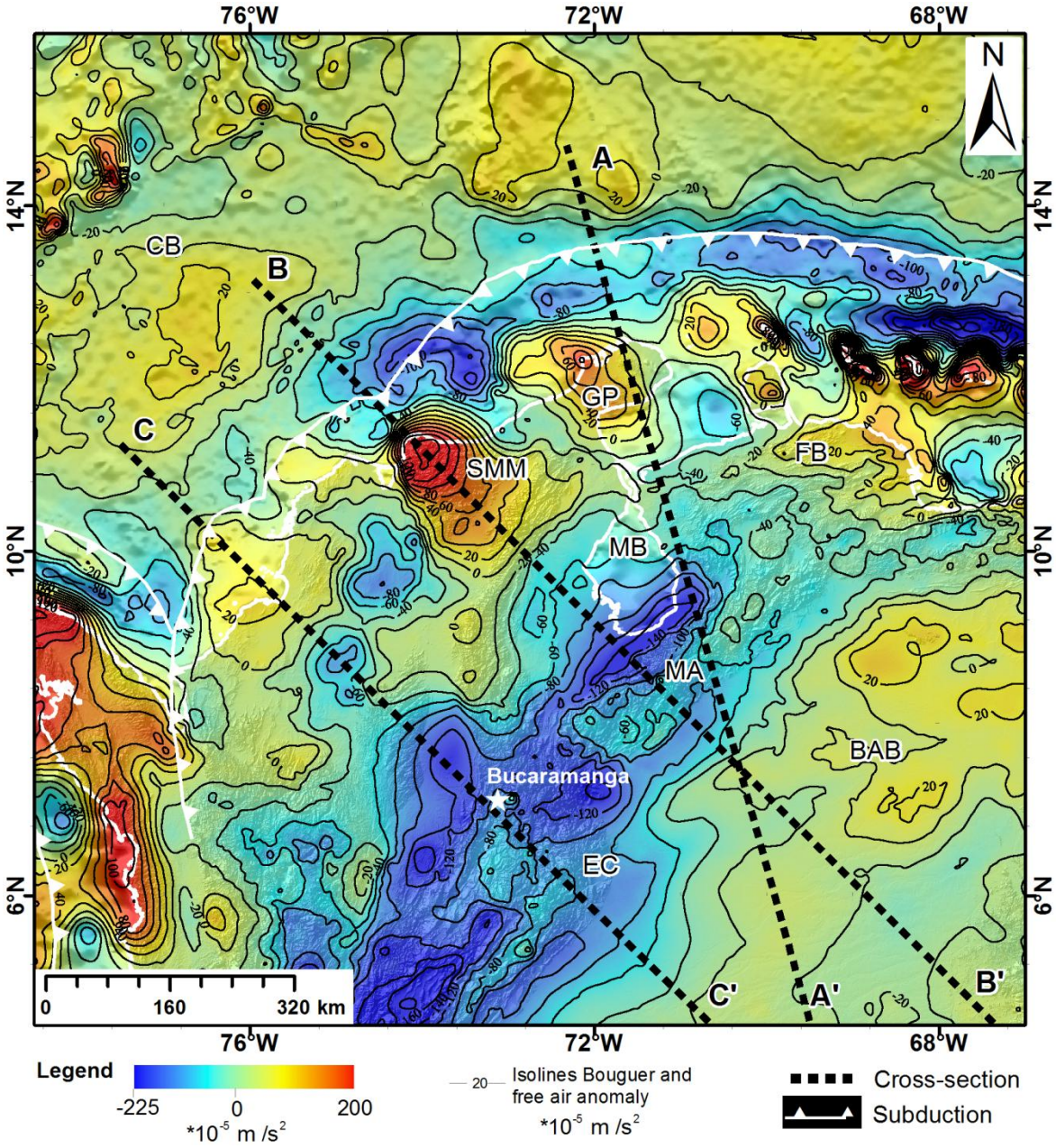

Figure 4.2 Gravity anomaly map of northwestern South America. It includes shaded digital topography illuminated from the NW. The black dashed lines mark the locations of the vertical cross sections AA′, BB′, and CC′. Equivalence of used acronyms is as follows: Santa Marta Massif (SMM), Colombian Basin (CB), Mérida Andes (MA), Falcón Basin (FB), Barinas–Apure Basin (BAB), Guajira Peninsula (GP), and Maracaibo Block (MB). Contour lines 10×10^{-5} m/s^2 spacing. Coastlines (white lines).

4.3.3. Isostatic analysis

Based on the gravity anomaly data and topography heights, two maps of the isostatic crustal continental root were calculated. The Airy–Heiskanen and Vening–Meinesz approaches were used for these calculations. In general, calculation of the isostatic balance by the Airy–Heiskanen model assumes that the crustal density is constant and isostatic compensation is determined by local variations of the crustal thickness. The crust is assumed to be in static equilibrium and the topographic load is compensated by buoyancy forces acting on the surface of equilibrium without any lateral strength. In the Vening–Meinesz isostasy model, the regional lithosphere is able to sustain the horizontal pressure gradient that arises between two lithospheric columns of different weight. In other words, the lithosphere is capable of flexing under its own weight and shields the underlying asthenosphere from pressure gradients that may originate within the lithosphere.

We analysed a series of surfaces of isostatic equilibrium using several physical parameters and crustal thicknesses. For instance, crustal and mantle densities were established based on the initial 3-D gravity model. To consider the effect of the Colombian land crust variations, average crustal thicknesses of T = 30, 35 and 40 km were used. For the Vening–Meinesz isostasy model, surfaces of isostatic equilibrium were calculated for rigidity values of 1×10^{21}, 1×10^{22}, and 1×10^{23} Nm. Final surfaces of isostatic equilibrium were selected according to the smallest root-mean-square misfit of surface with seismic determinations of the shape of the Moho. The smallest misfit was found for an average crustal thickness of 40 km and crustal and mantle densities of 2.67 and 3.25 Mg/m^3. For the Vening–Meinesz isostasy model, the selected rigidity value was 1×10^{21} Nm.

The main differences found between seismically-constrained surfaces calculated by the Airy–Heiskanen and Vening–Meinesz approaches were approximately 3 km in the continental

area. Our main purpose here is not to study the isostatic state of the lithosphere in this region, but rather to constraints on the shape of the Moho. The results of these computations are shown in figure 4.3.

The strong positive anomaly (up to 200 × 10^{-5} m/s^2 at the Santa Marta massif) and its high relief (5,776 m) suggest a lack of isostatic equilibrium and recent uplift with uncompensated heavy material within the massif at a relatively shallow depth. Unfortunately, there are no velocity models or other geophysical constraints available in this area to verify this observation. The strong negative gravity anomalies over the Mérida Andes and the Western and Eastern Cordilleras ranging from 40 to 200 × 10^{-5} m/s^2 are characterized by relative positive values within the more regional negative anomaly. These relative positive anomalies suggest that these areas are out of isostatic equilibrium with an excess of mass. The estimated isostatic thickness (regional and local) was used to constrain the Moho or the base of the mantle lithosphere in the gravity model only in continental areas.

For oceanic crustal areas (Venezuelan and Colombian basins), the assumed values of crustal thickness (40 km) and the crustal and mantle densities (2.67 and 3.25 Mg/m^3) do not comply with the crustal characteristics. Although the values of gravity anomalies near zero in the Venezuelan and Colombian Basins suggest isostatic equilibrium with an isostatic root between 21 and 25 km depth, its further implications are not discussed within this work.

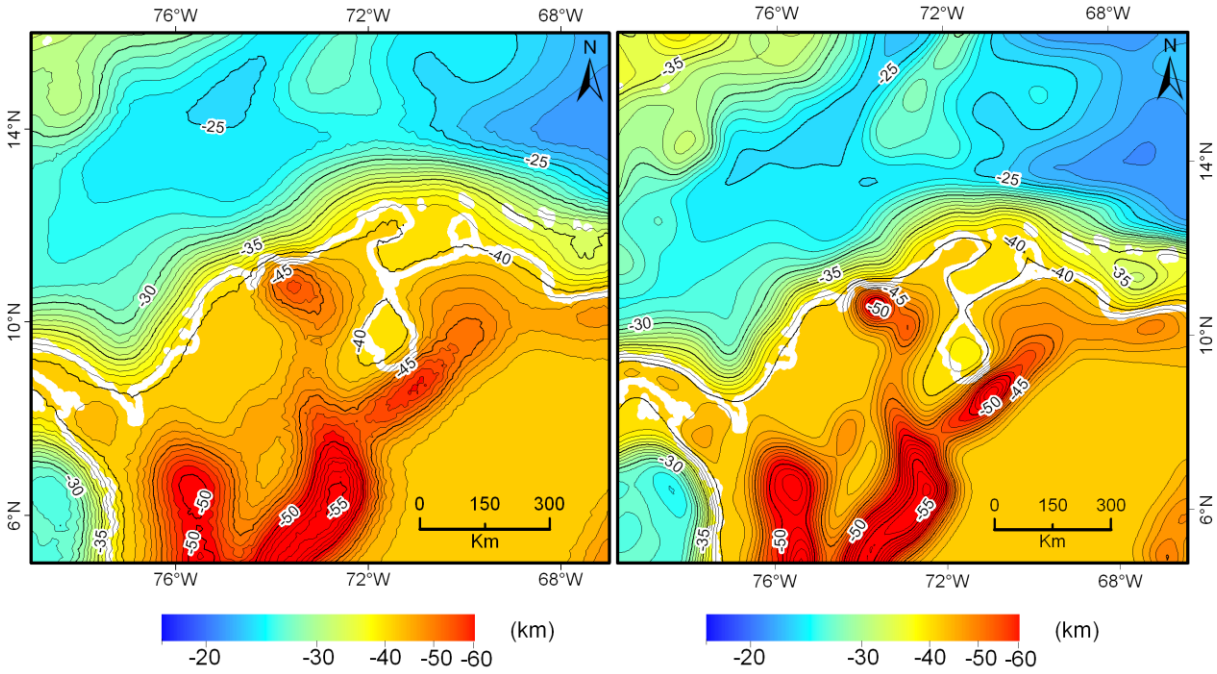

Figure 4.3 Isostatic crustal thickness maps of the study area. Left) Airy–Heiskanen modeled Moho. Right) Vening–Meinesz modeled Moho. Parameters used for calculations: T = 40 km, ρ_{mantle} and ρ_{upper} crust = 3.35 and 2.75 g/cm^3, respectively, rigidity = 1 × 10^{21} N m. Coastlines (white lines). Contour lines (black) every 5 km. For more detailed information, refer to the corresponding text.

4.3.4. Euler-deconvolution

The Euler-deconvolution of potential fields is widely used as a semi-automated method based on Euler's homogeneity equation. In many cases, it can be used to provide preliminary information about the depth distribution of gravity and magnetic sources by deconvolution of both fields. Aside from the potential field, no further information is necessary to use this method. The deconvolution is controlled by a structural index (SI) which is related to the underlying basic structure (SI = 0 indicates the assumption of a thin plate; SI = 1, an elongated body; and SI = 2, a point source) (Thompson 1982; Reid et al. 1990). Resulting source points are always clustered, which describe edges of a body with density contrasts to their surroundings. Strong gradients in the fields lead to clustering in these specific areas that

often belong to tectonic structures. The applied Regder software of Pašteka and Richter (2002) uses a regularized procedure to obtain stable derivatives in Euler's homogeneity functions based on Tikhonov's approach (Tikhonov and Arsenin 1977). The amount of clustered source points can be reduced by statistical criteria, e.g. solutions with the minimum standard deviation (Thompson 1982), solutions with the minimum condition number from the singular value decomposition procedure that is used to solve the equation system (FitzGerald et al. 2004), and solution points with the smallest error from the Euler equation (Cooper 2004).

For the study area, the gravity data was interpolated to produce a grid with a node spacing of ~6 km. Window sizes of 48, 102, 150 km were used to calculate Euler source points with SI = 0, 1, 2. Large window sizes were used in order to detect very deep sources. The large numbers of solutions were drastically reduced after selecting solutions with estimated depth with minimum standard deviation of 3 km. Solutions for window sizes of 102 and 150 km showed poor statistic. The most likely explanations for this result are that the 102 and 150 km window sizes include gravity gradients arising from several sources. The selected source points calculated for SI = 0 and 2 are shown in figure 4.4. These points are also included and shown in the selected cross sections to constrain the geometry of particular bodies during the modeling process.

In general, as shown in figure 4.4a, the depths of Euler source points for SI = 0 image mainly shallow structures (30 km or less). Clusters have good correlation with the Santa Marta massif, Mérida Andes, and Caribbean islands to the north of Falcón Basin. The clusters of source points are localized in the northern and southern flank of the Mérida Andes. These clusters follow the main strike of this structure (N ~45° E). The deepest clusters of source points (15–30 km depth) are localized north and southwest of the Santa Marta massif. Depths

of Euler source points using SI = 2 (Figure 4.4b) vary from ~10 km at the Colombian basin, Mérida Andes and northern Santa Marta massif to 120 km beneath Mérida Andes and northern Santa Marta massif. Around of the Santa Marta massif area the depths of mass centers are located between 20 and 60 km. The presence of these clusters correlated with the location of longitudinal and transversal fault lines and suggests high density contrast of the massif respect the rocks of the surrounding areas.

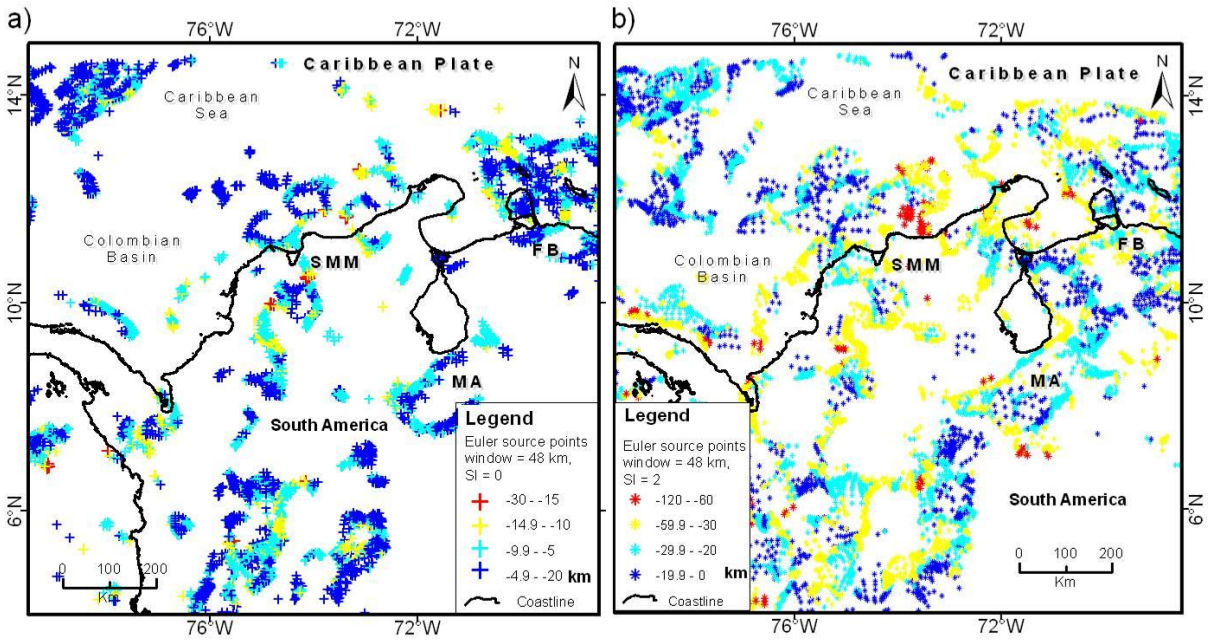

Figure 4.4 Euler source points (depths of source points) derived for a window size of 300 km. a) SI = 0. b) SI = 2. Colors indicate depth (blue = shallow and red = greater depths). Equivalence of used acronyms is as follows: Santa Marta Massif (SMM), Mérida Andes (MA), and Falcón Basin (FB).

4.3.5. Power spectrum analysis

For analyzing potential field data, spectral methods are common for obtaining a regional/residual field separation. Here, the complete Bouguer gravity anomaly was used to get a first estimate of the source depths. The methodology assumes that, for large samples, in a plot of the logarithm of the power spectrum (E) versus the wave number (radial/distance),

the depth to the causative sources can be approximated by straight lines and therefore can be used to separate sources at different depths of the gravity signal. Due to the two-dimensional character of the data set, radial averaging of the power spectrum was performed to obtain a one-dimensional representation (Mishra and Naidu 1974; Dimitriadis et al. 1987; Tselentis et al. 1988). Confidence limits for the depth estimations were calculated from the standard errors of the slopes of the best fitting lines for the linear segments.

The gravity data of the study area, covering a surface of 900 × 900 km^2, was interpolated to produce a grid with a node spacing of 5 km. Results of the power spectrum analysis for this dataset showed three tendencies for the correlation between energy (E) and wavenumber (radial/distance) (Figure 4.5a). The most regional part of the spectrum appoints to depths of about 101 km. The local part of the spectrum resulted in depths of ~15 km. The main aim of the spectral analysis was focused on the intermediate depths of about 44 km because this depth could correspond to the crust–mantle boundary (Moho). In order to perform the same analysis for specific anomalies in the study area, a window size of 300 km was used, which correspond to six times the expected source-depth to assure a depth-estimation error of <10% according to Regan and Hinze (1976). Results over the anomalies observed in the Santa Marta massif, Colombia Basin, Middle Magdalena Basin, and Mérida Andes indicated that Moho depth has a wide variability between 23 and 57 km (Figure 4.5b–e).

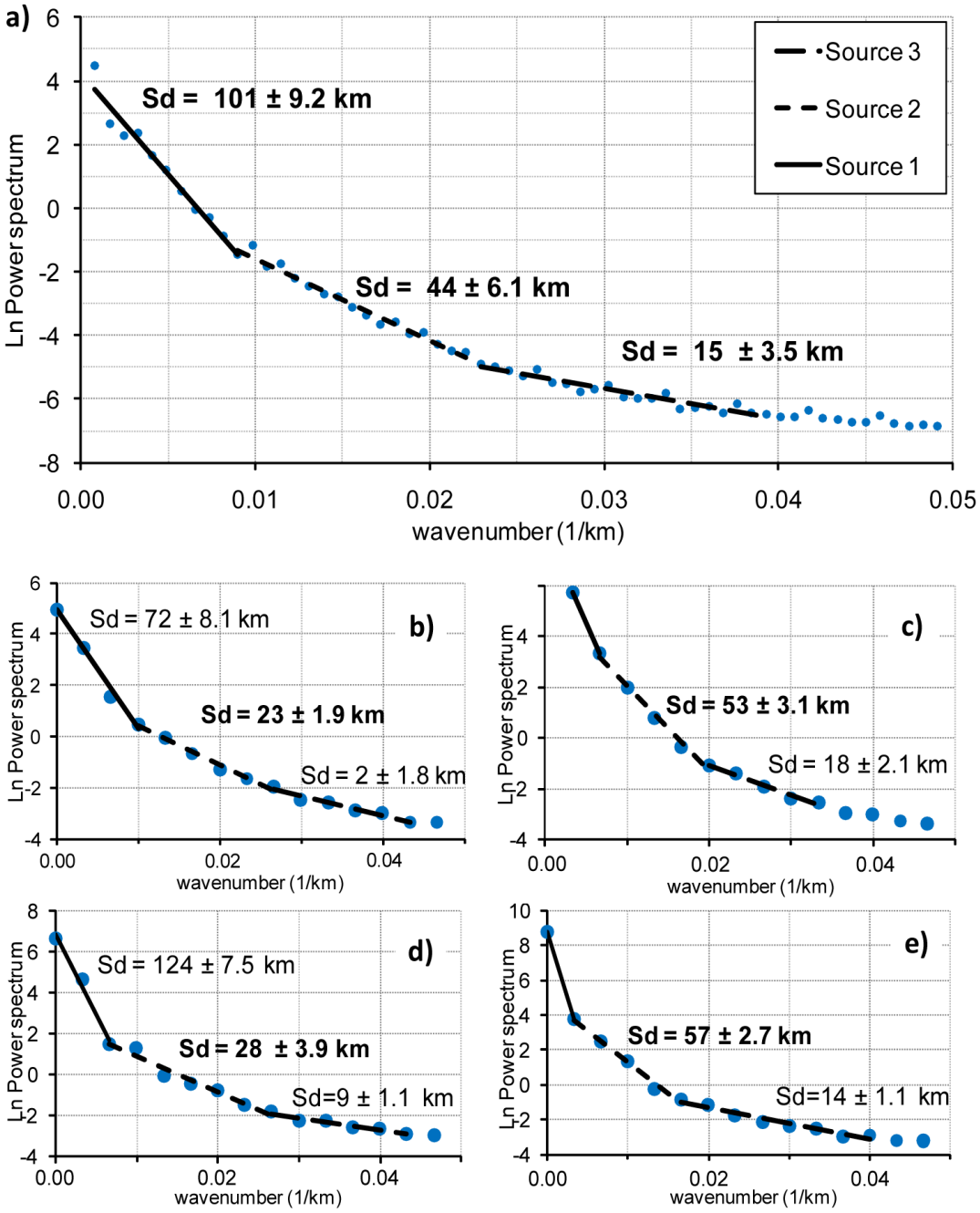

Figure 4.5 a) Graph representing the natural logarithm of the radial gravity power spectrum versus the frequency for the whole Bouguer anomaly map. Three domains have been recognized that denote the maximum depth of the attracting source in depths (SD) of 15, 44, and 101 km below the surface. For comparison (b), (c), (d), and (e) show the power spectrum of the Colombian Basin, Santa Marta Massif, Lower Magdalena Basin, and Mérida Andes, respectively.

4.4. 3-D gravity modeling

The gravity response of our model was calculated using the Interactive Gravity and Magnetic Application System (IGMAS). It is based on an interactive forward-modeling procedure where the calculated gravity effect of the modeled structures is compared to the observed gravity. The algorithm uses polyhedrons for the approximation of geological bodies with constant density/susceptibility. The surface of the polyhedron is triangulated, and the integral is solved by applying the Gauss theorem in 3-D and 2-D (Götze 1978; Götze and Lahmeyer 1988; Schmidt and Götze 1998).

4.4.1. Initial model

The 3-D density model extends from 0 to 300 km in depth. It was first developed along 18 parallel north–south cross sections and was later extended to 34 planes. In order to avoid edge effects, the model was extended more than 1000 km in each horizontal direction. The first and last cross sections are located close to longitudes ~86°W and ~62°W. The first and the last five cross sections are located in an area with no gravity stations, but they control the 3-D geometry variations of the model outside of the study area. The typical distances between consecutive cross sections are between 40 and 100 km. In this work, we present three vertical cross sections to illustrate the main characteristics of the 3-D model. The positions of the vertical sections shown herein were chosen to be perpendicular to the strike direction of the Caribbean slab at particular geographical features such as the Mérida Andes, the Santa Marta massif, or areas with strong response with the seismogenic layer (i.e. Bucaramanga seismic nest).

4.4.2. Reference density model

In order to overcome the difference between the observed and modeled gravity caused by the use of the absolute densities and not by including the mass of the entire earth in the model (Kirchner 1997), a three layer reference model was imposed on the 3-D model. The reference model represents the structure of the "normal Earth," and it extends to the same depth as the 3-D model.

The reference model has an intracrustal density discontinuity at 20 km that separates upper and lower crust with mean densities of 2.67 and 2.9 Mg/m^3, respectively. The upper mantle has a density of 3.34 Mg/m^3, and it is separated from the lower crust by a discontinuity at a depth of 40 km. These values are consistent with the 1-D IASP91 crustal model (Kennett and Engdahl 1991), as well as with global velocity–density databases (Christensen and Mooney 1995).

4.4.3. Density values for modeled bodies and geometry constraints

The final density model consisted of approximately 50 bodies that represented the main geological units observed in northern South America. Simplified geologic maps of Colombia (Gómez et al. 2007) and Venezuela (Hackley et al. 2006) were used to constrain the geometry and location of the most significant geologic units in the model region.

The earth structure in northern South America was represented by a layered model composed (from top to bottom) of upper and lower crust above the lithospheric and asthenospheric mantle. Each layer was also composed of a series of blocks allowing lateral and vertical density variations within the layer. A more complex structure was modeled in the upper crust in order to take into account the lateral and vertical variations observed in the surface geology and seismic profiles. The depth to the boundary between the upper and lower

crust was used to establish an intracrustal density discontinuity as a proxy for the shallow and deep density structure. Following the same criteria, the Caribbean oceanic plate and the subducted slab were formed from four layers (sediments, meta-sediments, the Caribbean crust, and the lithospheric mantle) overlying a body representing the asthenospheric mantle. Figure 4.6 shows the distribution and references of the information incorporated into the 3-D density model to constrain the geometry and density of the bodies (simplified geological map, local seismic networks, borehole records, refraction seismic profiles, and receiver functions results).

The preliminary density values for each of the bodies forming the 3-D model were selected after studying the dependency of this physical parameter with the seismic velocity, rock composition, and pressure–temperature conditions (P/T) of crustal and mantle materials that were appropriate for the northern South America setting. Measured density values were also considered. Final density values were adjusted to fit the observed gravity and the calculated gravity of the density model. Table 4.1 and figure 4.7 show the final density values assigned and modeled in our preferred 3-D gravity model. The following subsections describe in more detail the data and procedures used to establish these values.

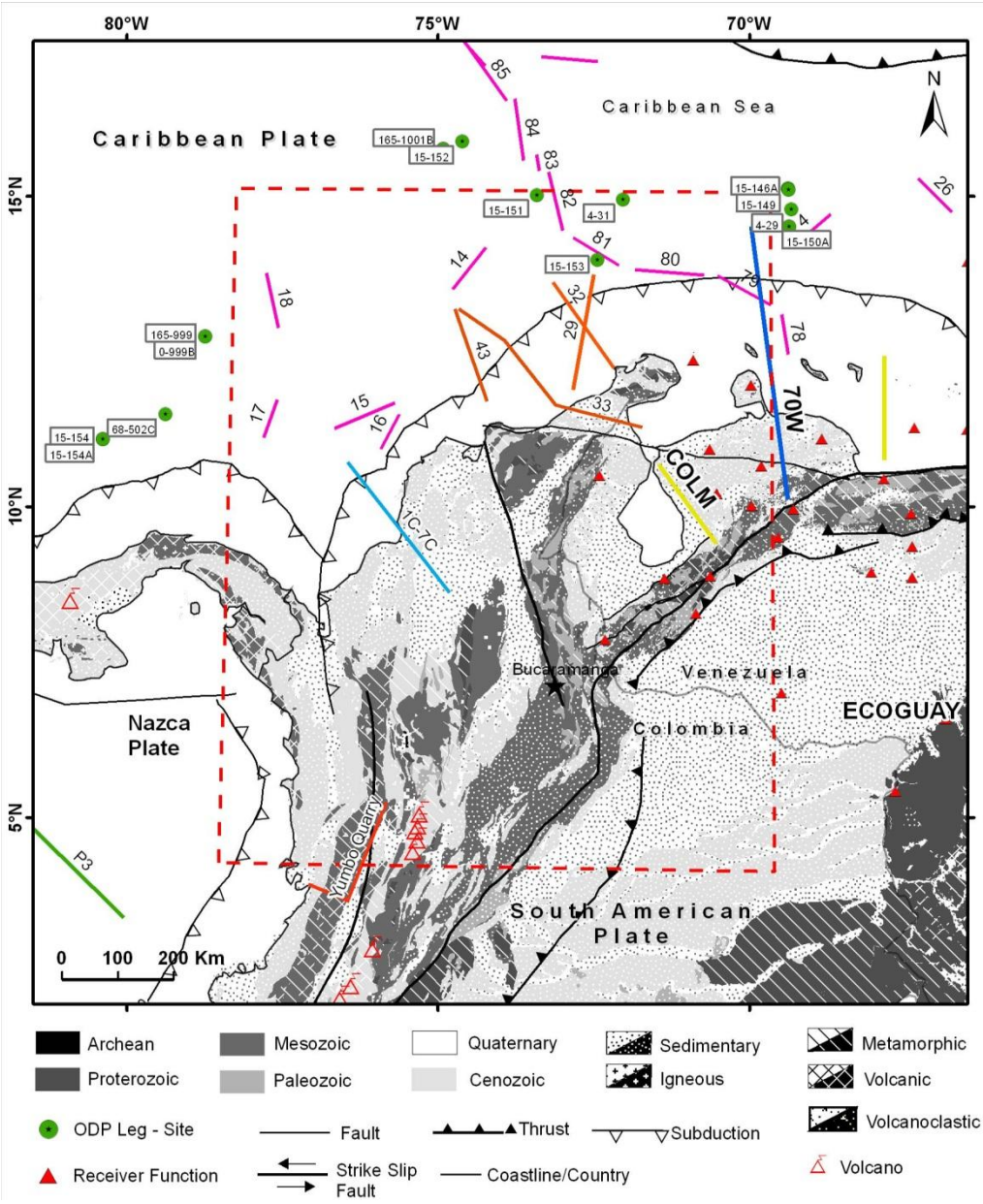

Figure 4.6 Distribution and references of the information incorporated into the 3-D density model to constrain the geometry and density of the bodies. Simplified geology map, borehole records of the Deep Sea Drilling Project sites from Leg 4 and 15 (Fox and Schreiber 1978), receiver functions results, and 2-D velocity models. Sources of the 2-D velocity models are Edgar et al. (1971) (purple lines), Mooney et al. (1979) (red lines), Schmitz et al. (2008) and Schmitz et al. (2002) (blue lines), Guédez (2003) (yellow lines), and Mantilla-Pimiento et al. (2009) (light blue). Text indicates the name of the seismic profiles.

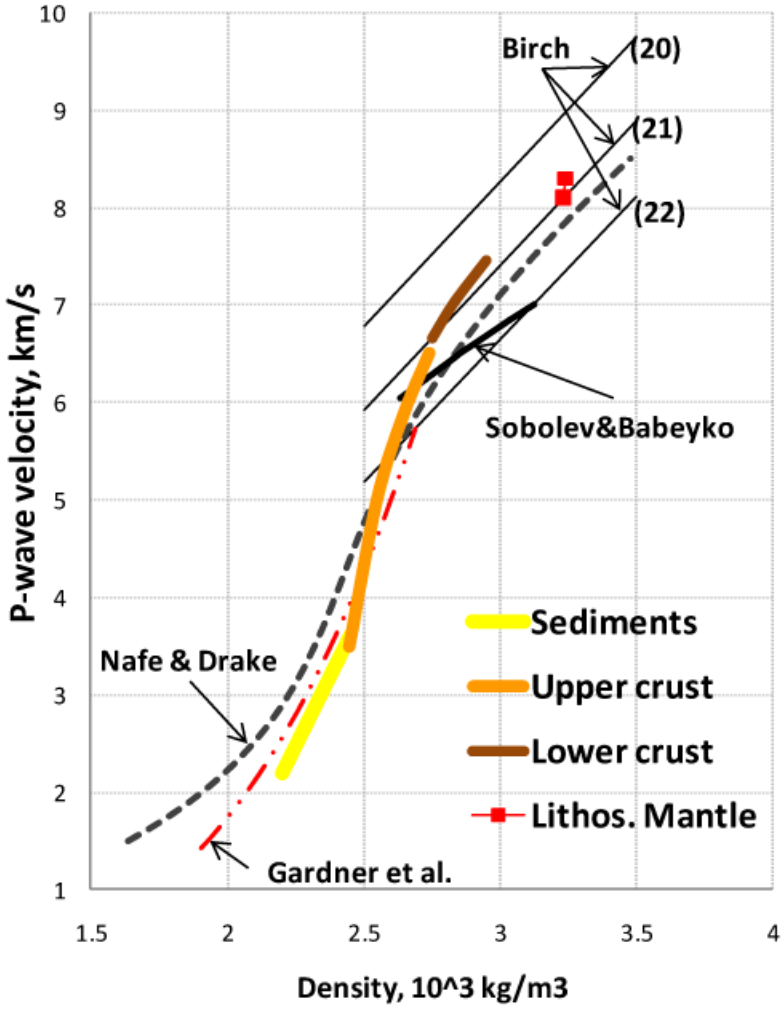

Figure 4.7 Diagram of the density/velocity relationship for sediments, crystalline crust, and uppermost mantle rocks used in the gravity model. The velocity values were taken from the seismic observations along profiles COLM and 70°W (Figure 4.1). The density values were constrained by these velocity observations and estimated from Gardner et al. (1974), Sobolev and Babeyko (1994), Nafe and Drake (1963) (dashed line), and Birch (1960; 1961) (solid lines, shown for atomic mass 20, 21, and 22) conversion functions.

Table 4.1 assigned and modeled in the final 3-D gravity model

Model units	Density Mg/m^3
Qt sediments	2.20-2.4
Tertiary sediments	2.45-2.51
Caribbean crust	2.95-3.18
Nazca crust	2.85-3.1-
Ocean water	1.03
Caribbean lithospheric mantle	3.14-3.41
Nazca lithospheric mantle	3.25-3.40
South America upper crust	2.70-2.76
South America lower crust	2.78-2.85
Volcanic arc	2.85
Meta Ophiolitic series	2.92
South America lithospheric mantle	3.17-3.25

4.4.3.1. South American plate (Continental margin)

Crustal densities for the continental margin were estimated based on the empirical P-wave velocity–density relationships (Nafe and Drake 1963; Christensen and Mooney 1995) and the available seismic models. A determination of densities based solely on this approach is simplistic and may carry significant uncertainties. However, it is a fair approximation for large-scale lithospheric models. In addition, preliminary densities were calculated using the methods described by Sobolev and Babeyko (1994). This approach estimates densities of anhydrous magmatic rocks from seismic velocities at in situ pressure and temperature (P/T) conditions. The in situ P/T conditions were estimated from surface heat flow measurement data in South America (Hamza and Muñoz 1996) and Colombia (INGEOMINAS 1999; Vargas et al. 2007) using the heat conduction equation and the lithostatic pressure equation. Surface heat flow of the continental margin shows values between 30 and 180 mW/m^2. The lowest values were observed in the southern and northeastern parts of the study area at the Barinas-Apure Basin (Venezuela) and the Magdalena basin (Colombia), 40 and 60 mW/m^2, respectively. The highest values, observed in Venezuela, seem to be representative of the

geothermal regime of the coastal regions. In northern Colombia, the geothermal anomalies map (INGEOMINAS 1999) which includes more details and representative information for this area, shows multiple areas with high and low values of the geothermal gradient, which is representative of the complexity of this region. At the Caribbean coast, mainly a flat area, the heat flow values are between 60–90 mW/m^2. The Santa Marta massif (pyramidal structure in the north with topography reaching heights up to 5700 m) is characterized by a heat flow higher than 100 mW/m^2. In the nearby central and northern Cordillera regions, the occurrence of a large number of thermal springs and volcanoes along a narrow belt extending from northern Ecuador to the northeastern border with Venezuela indicate the existence of significant regional geothermal anomalies (>150 mW/m^2).

4.4.3.2. Continental Moho

Special care was taken to model the Moho discontinuity in order to avoid or minimize the ambiguity due to non-uniqueness solution. We compiled an updated database containing results from Moho depth estimations. The majority of the data was produced during experiments carried out by the BOLIVAR and GEODINOS projects (Levander et al. 2006; Schmitz et al. 2008). Two deep seismic wide-angle profiles (Figure 4.6) were included in the model (Guédez 2003; Bezada et al. 2008; Schmitz et al. 2008). The first profile is located close to the longitude 70°W and extending roughly from latitudes 14°N to about 10°N. The second profile (COLM) is located in the Maracaibo block. In addition, several short seismic profiles from Edgar et al. (1971) and Mooney et al. (1979) were digitized and used to constrain the model. Results from these 2-D velocity models show a layered structure which represents the upper crust, the lower crust, and the lithospheric mantle with mean velocities of 5.9–6.0, 6.5–7.4, and 8.1 km/s, respectively. In their interpretation, Bezada et al. (2008) found

evidence of a significantly thinned crust (27 km) and positioning of the top of the Caribbean slab beneath the Falcón Basin. Underneath the COLM profile, Guédez (2003) showed a crust thickness between 41 and 42 km for the Maracaibo block. The geometries defined by the COLM and 70°W profiles in the model were not modified. Only areas that were not constrained by these profiles were modified.

Moho depth estimations from receiver function studies in Venezuela (Niu et al. 2007) were also included as modeling constraints. Results of receiver functions analysis indicated a typical crustal thickness value in the Guayana Shield of around 38 km. Beneath the Mérida Andes Moho, the depth is 55 km. Toward the plate boundary, the receiver function interface steps upward to 30 km beneath the Serranía del Interior and shallows more gradually to 26 km beneath the strike-slip system (Niu et al. 2007).

Spectral analysis results were used to constrain depths corresponding to the density contrasts of the upper crust and the lithospheric mantle in the gravity model. Confidence limits for the calculated depth estimations (not shown here) had a standard deviation of ~3 km. Errors in depth are greater for the deeper regions of this interface because of the inclusion of multiples wavelengths in the analyses anomaly (i.e. deeper sources).

Due to the lack of independent constraints obtained from geophysical, geological, and tectonic interpretations, for most of study area, the Vening-Meinesz isostatic crustal thickness map was included as a constraint in the model. The Moho was shaped following the general trend of the isostatic surface under the assumption that the orogenic topography was primarily compensated by a crustal root. Regions within the model that were characterized by the Moho constrained to isostatic crustal thickness were the Lower–Middle Magdalena and the Colombian cordilleras.

4.4.3.3. Continental lithosphere–asthenosphere boundary

Geometry of the continental lithosphere–asthenosphere boundary (LAB) was modeled mostly by fitting the intermediate-to-long-wavelength Bouguer anomaly, but also by maintaining consistency with continental-scale seismic tomography models in the region (e.g. Van der Hilst and Mann 1994; Taboada et al. 2000; Heintz et al. 2005). However, the LAB from these tomography models was poorly resolved as a consequence of different factors (e.g. scarce seismic stations distribution).

The composition of the asthenosphere mantle body was assumed to be an average of the values expected for a fertile lherzolite and harzburgite. Final density values for the lower lithosphere and for the lithospheric mantle range between 2.78–2.85 and 3.17–3.25 Mg/m^3, respectively. The asthenospheric mantle density was kept constant (3.34 Mg/m^3).

4.4.3.4. Caribbean plate

The density values of the Caribbean plate used in the 3-D gravity modeling were assigned based on recovered samples of the Deep Sea Drilling Project (DSDP) sites from Leg 4 and 15 (Fox and Schreiber 1978). Recovered samples of basalts and dolerites with different degrees of alteration (slightly to severely altered) from these sites had average densities of 2.695 and 2.832 Mg/m^3 for basalts and dolerites, respectively. The mean density for all samples was 2.78 Mg/m^3.

Moreover, the preliminary density of the Caribbean plate was constrained with estimated values calculated considering pressure conditions and changes in the mineralogical and chemical composition using the method described by Hacker et al. (2003). P/T conditions were estimated from heat flow measurement data from the International Heat Flow Commission (http://www.heatflow.und.edu/index2.html). In situ crustal temperatures were

calculated using the heat conduction equation and the lithostatic pressure equation. Chemical compositions were based upon the values published by Sinton et al. (1998) and Spadea et al. (1989).

Seismic velocities converted to density were also used as proxies for density values. For the Caribbean plate, seismic refraction results in the Grenada Trough, Aves Ridge, Venezuelan Basin, and part of the Colombian Basin have shown seismic velocities in the range of 6.0 to 6.3 km/s (Ewing et al. 1960; Edgar et al. 1971; Schmitz et al. 2008). Initial crustal density estimations were made by directly converting velocity into density using the velocity–density relationships of Nafe–Drake (1963), Christensen and Mooney (1995), and the Birch empirical functions (Birch 1960; 1961). Densities for sedimentary layers were calculated using Gardner's equation (Gardner et al. 1974), assuming sedimentary layers with seismic velocities in the range of 2.3–2.45 km/s (Ewing et al. 1960; Edgar et al. 1971; Schmitz et al. 2008). Density curves for the velocity–density relationships are shown in figure 9 together with the density values of our final model.

Density values of the bodies representing the subducted Caribbean crust in the 3-D gravity modeling were assigned following the method described by Hacker et al. (2003). The rock density database of Hacker et al. (2003) were used to establish changes in the density of the subducted Caribbean crust with depth due to high temperature, higher pressure conditions, and changes in the mineralogical and chemical composition. Final model densities for the Caribbean crust and lithospheric Mantle were in the range of 2.95–3.18 and 3.14–3.41 Mg/m^3, respectively (Table 4.1).

Geometry of the slab was controlled by means of the seismic refraction profiles presented by Edgar et al. (1971) and with the profile 70°W (Bezada et al. 2008; Schmitz et al. 2008).

Additionally, we used depth estimations from Euler deconvolution to constrain the location of the down-going slab.

For instance, clusters of Euler deconvolution points for SI = 0 located at depths between 0 and 50 km in the northern region of the model (Colombian basin) suggest the existence of a high-density bodies or density heterogeneities in the oceanic crust. These cluster appeared to be following the dip of the slab. Furthermore, several sets of these clusters were used to estimate the bottom of the sedimentary infill, and the geometry of some bodies in the upper crust that were also observed in the geologic map (Figure 4.4).

4.4.3.5. Nazca plate

The density values of the Nazca plate were modeled based on the result of a 2-D gravity–velocity model along a wide-angle profile acquired across the Malpelo Ridge (Sallarès et al. 2003). This velocity model was determined using a joint refraction/reflection travel time inversion method. The gravity modeling was performed by converting the velocity models to density models using empirical velocity–density relations. In terms of seismic velocities, Sallarès et al. (2003) showed that the Nazca plate consist of two different layers. The upper layer is characterized by large vertical velocity gradients with velocities typically ranging from 3.0–3.5 km/s at the top of the layer to ~6.5 km/s at the bottom. In the long-wavelength structure, the thickness of the layer (3.5 ± 0.5 km) is quite uniform regardless of total crustal thickness. The layer lying below this boundary down to the Moho interface has a highly variable thickness ranging from 4 km in the oceanic basins to 15 km in the thickest crustal segments. It is characterized by a nearly uniform velocity with velocities rarely exceeding 7.2–7.3 km/s. Additionally, Sallarès et al. (2003) observed that at the end of the profile in the

Malpelo ridges and other nearby profiles, the oceanic crust was 7–8 km thick, similar to that of a normal oceanic crust. Furthermore, oceanic layers have densities between 2.40–2.70 and 2.70–3.10 Mg/m^3. Mantle density was kept constant (3.3 Mg/m^3).

4.5. Seismotectonic model

The purpose of this section is to point out the main characteristics and peculiarities of the earthquake distribution and to analyze the kinematics of the subducting slabs (Caribbean and Nazca) in northwestern South American in order to improve the final 3-D model. For this purpose, seismic hypocenters distribution and the focal mechanism solutions for earthquakes with magnitude >3.5 were collected from different sources; earthquakes and focal mechanism solutions from Harvard (http://www.seismology.harvard.edu) and FUNVISIS (FUNVISIS 2007) catalogues. The datasets presented by Malavé and Suárez (1995) for the northeast region of Colombia and new data from Palma et al. (2010) for Venezuela were also included. In this work, the whole collected data was reinterpreted by mainly considering its relationship with the position of the downgoing Caribbean plate. The new data in the compilation of Palma et al. (2010) were recorded by the Venezuelan seismological network with support of the Colombian network (Red Sismológica Nacional de Colombia - RSNC). Both networks have been upgraded (enlarged and modernized) with new three-component broadband stations installed during the last decade.

4.5.1. Earthquake focal mechanism solutions

New focal-mechanism solutions (FMS) in Palma et al. (2010) were obtained by reading the polarity of the first P-wave arrivals at seismic stations that were evenly distributed in azimuth and distance around the earthquake epicenter. Table 4.2 shows focal mechanism solutions and hypocentral parameters of events reported by Palma et al. (2010) that apparently

lie within the subducted Caribbean slab beneath the southern Caribbean coast. They were selected after removing from the datasets FMS that correspond to shallow distributed continental seismicity that occurs and are related to the complex pattern of deformation in the northern Andes (i.e. Colombian cordilleras and Mérida Andes). These focal solutions were added to the datasets of Malavé and Suárez (1995) and Harvard's seismology group (http://www.seismology.harvard.edu). Figure 4.8 shows the locations of the focal-mechanism solutions used in this study.

The spatial distribution of the hypocenters shows that there is a close relationship between intermediate depth earthquakes and the subducted Caribbean lithosphere in the region. The new focal mechanism solutions show that these events apparently lie within a lithospheric slab. Based on the results of FMS from the analysis, earthquakes with depths ranging from 40 km to 190 km (Figure 4.8) were used to image the strike and dip of the slab. Specifically, events 4, 7, 43, and 51 show similar strike direction for the modeled slab. Coincidentally, FMS for events 43 and 51, located beneath the Sierra de Perijá, are similar to results presented by Malavé and Suárez (1995) for two events that occurred on November 17, 1968 and December 14, 1970 (M-2, M-3). On the contrary, T-axes for events 9, 10, 54, and 56, located beneath Bucaramanga nest, have different orientations, these observation correlate well with the assumption of a collision zone of Caribbean slab with the top of Nazca. Three cross sections (Figures 4.8b-d) were selected to show the correlation of the dip of the slab with the observed seismicity and focal mechanisms. These vertical cross sections show intermediate seismicity within the subducted slab, and the orientation of the T-axes (side-looking projection on the cross sections) aligned quite well along the predicted position of the slab. These observations are more clearly visible in the western part of Bucaramanga nest, which is viewed as the culmination of the Caribbean plate slab underneath the Mérida Andes where the angle of subduction is steeper.

Although seismicity and FMS for northwestern South America cannot be used to determine the exact position of the Caribbean slab, the new seismic data recorded in the last two decades reveal new insights into the position of the slab. Thus, the 3-D model is the result of interpreting the new seismicity data and gravity modeling. Taking into account all data limitations, this model compiles the regional knowledge of the lithospheric structure for this area.

Table 4.2 Parameters of focal mechanism solutions for earthquakes within the study area in northwestern South America (Palma et al. 2010).

TimeEvent	Longitude	Latitude	Magnitude	Depth	Nodal plane A			Nodal plane B			T axis		P axis		Id
(dd/mm/yyyy)	N (°)	W (°)	Mw	(km)	Azi	Dip	Rake	Azi	Dip	Rake	Azi	Dip	Azi	Dip	-----
10/22/2005 05:41:21	-71.236	11.33	3.8	136.4	270	46	-164.4	169	78.8	-45.1	226.7	20.7	118.9	38.9	4
01/01/2006 09:43:12	-71.327	12.088	5	92.5	110	63	-128.2	350	45.5	-39.5	226.4	10	330.8	54.7	7
01/06/2006 19:04:22	-73.207	6.813	4.7	167.6	29	88	-97.4	284	7.7	-15.1	126.1	42.5	291.4	46.5	9
01/10/2006 03:14:42	-73.071	6.815	5.4	167.2	245	10	-23.3	358	86.1	-99.2	96.5	40.4	258.2	48.2	10
05/06/2007 04:47:14	-73.097	6.814	5.3	164.5	21	45	146.6	136	67.1	50.1	0.2	50.8	253.7	13	39
07/06/2007 19:08:20	-72.573	10.115	4.2	158.3	358	74	-62.6	116	31.4	-148.1	67.1	24.1	300.7	53	43
11/20/2007 05:56:22	-73.072	6.823	4.4	158.8	37	84	-111.3	292	22.1	-16.1	145.4	35.5	284.9	46.8	47
01/16/2008 23:47:31	-72.627	9.709	4.7	171	166	31	174.2	261	87	59.1	142.7	40	17.2	34.7	51
02/17/2008 21:15:03	-73.069	6.801	5.5	161.7	19	51	-143.5	264	62.4	-45.2	323.9	6.8	225.6	50.5	54
03/28/2008 16:35:59	-72.989	6.912	5.2	160.9	41	37	-16.1	144	80.4	-125.9	261.6	26.5	19.4	43.1	56

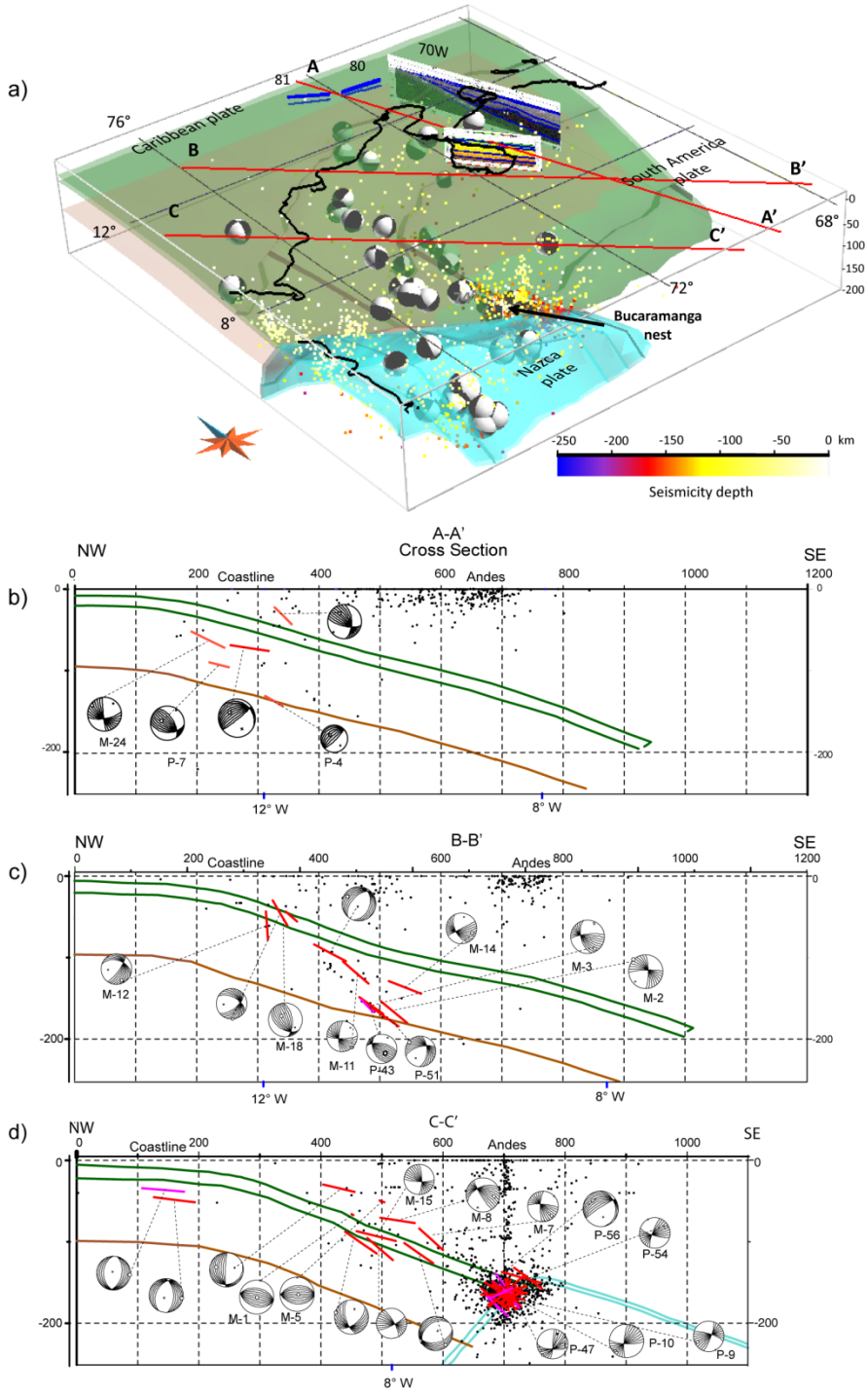

Figure 4.8 a) 3-D perspective view of seismic hypocenters and focal mechanism solutions in northwestern South America. b) Cross section A–A′, across the Paraguana Peninsula and Mérida Andes. c) Cross section B–B′ across the Santa Marta massif. d) Cross section C–C′ across central Colombia and above the Bucaramanga nest. CMT solutions plotted as 3-D spheres where black and white shaded regions correspond to compressional and dilatational arrival quadrants, respectively. Red lines are the projection of the T-axis on the A, B, and C profiles. Focal mechanism solution data have been taken from the Harvard and FUNVISIS catalogues (FUNVISIS 2007). Also included is the 2-D velocity model labeled 70W. Green and blue lines are the top and bottom of the Caribbean and Nazca crust, respectively. Brown line is the lithosphere–asthenosphere boundary. The coastline is shown as a black line. Seismicity (color points).

4.6. Results and discussion

This section describes the results obtained from our analysis of the gravity field, forward modeling, and the data constraints used. We focus our description and discussion on the geometry of the lithospheric structure for the more significant first-order features evident in the model.

4.6.1. Model accuracy and limitations

Like many geophysical methods, gravity modeling (forward or inversion) generates non-unique results. The primary limitation on this method is that gravity data carry no inherent depth information. Additionally, inaccuracies in the seismic constraints may result in errors. Also, erroneous density values may be of some significance. Under these conditions, for testing the accuracy of the final model a statistical analysis of the residual (misfit) between the measured and calculated Bouguer was performed. Figure 4.9 shows the residual (misfit) between the measured and calculated Bouguer anomaly of the model. 95% of the residual anomalies lie in the range $\pm 25 \times 10^{-5}$ m/s^2. The histogram in figure 4.9b shows a tight concentration of residual anomaly values around -1.6×10^{-5} m/s^2 (arithmetic mean). Computed statistics show a standard deviation of 12.36×10^{-5} m/s^2 and a correlation factor of 0.96 between the measured and calculated anomaly.

The greatest differences in the residual anomaly map (Figure 4.9) are found between cross sections where the geometry of the geological bodies is interpolated. Typical separation of the cross sections of the gravity model is around 50 km. Geological structures smaller than this magnitude were not modeled. Specifically, Central Cordillera and Mérida Andes regions show high residual values, higher than the standard deviation. These differences are caused by local anomalies corresponding to geological bodies with high and low density contrasts.

However, some of the misfits could be correlated with tectonic features. For instance, positive and negative residual anomalies can be observed over the Santa Marta massif, suggesting that intrusions within the massif have a higher or lighter density than the value assigned to the whole structure. Negative residual anomalies can be observed along the trench axis of the North Panama Deformed Belt, indicating that the material should have a local density considerably lower than the value selected for the whole structure (e.g. accretionary prism and trench sediments).

Despite the previous-mentioned local misfits, statistical analysis indicated that the 3-D density model reproduces the observed Bouguer anomaly at an intermediate-to-long scale. The 3-D model we present in this work is one of several possible models. Although considering the accuracy of the gravity data and the applied constraints, this model satisfies the regional tectonics and geodynamics of the study area.

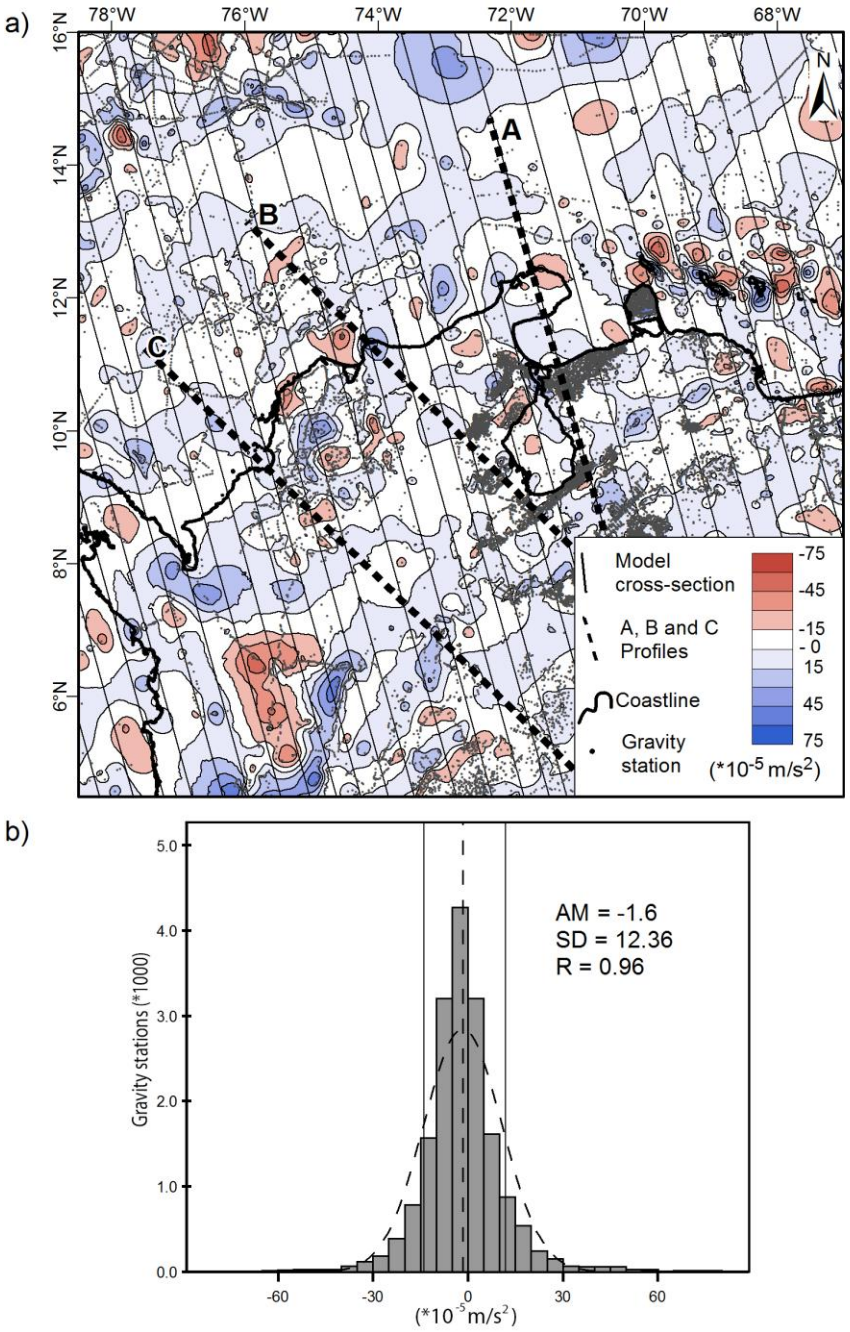

Figure 4.9 a) Residual gravity field of the study area obtained by subtracting the calculated gravity effect of the 3-D model from the observed gravity field (black lines indicate position of the vertical cross sections used to define the model geometry). Maximum misfits are caused by short-wavelength anomalies, and we considered only the regional field and did not attempt to explain these short-wavelength anomalies (for further explanation, see text). b) Histogram of residual gravity, arithmetic mean (AM), standard deviation (SD), and correlation coefficient (R).

4.6.2. Model sections

Figures 4.10 and 4.11 show the selected vertical sections as well as additional constraining data (e.g. Euler's solutions, seismicity, and receiver function Moho depth). Only gravity data within a maximum distance of ±2 km was projected onto the cross section. For Euler's solutions, seismicity, and receiver function Moho depth, the maximum distance for projection was 20 km.

In general, the three vertical cross sections illustrate the characteristic parts of the 3-D gravity model and its consistency or misfit with the constraining data (Figure 4.6). Also, these cross sections show the combination of 3-D forward modeling with inverse modeling techniques (i.e. spectral analysis and Euler deconvolution).

The cross section AA′ crosses roughly N–S the main elements of the Southeast Caribbean–South America boundary (Figure 4.2) from the Venezuela Basin to the Barinas–Apure Foreland Basin in southwestern Venezuela, crossing metamorphic and igneous rocks of the Guajira peninsula and Mérida Andes. Figure 4.11 shows the slab of the Caribbean plate with the most northern upper surface of the slab constrained by the seismic profiles from Edgar et al. (1971) (Profile 81). Layer boundaries in this seismic profile have general misfit of less than ~5 km with the gravity model. The continental structure in the gravity model is in agreement with the seismic profile COLM (Guédez 2003; Schmitz et al. 2008). The Moho and the intermediate depth discontinuity between COLM and this cross section have less than 3 km misfit. By means of 2-D forward modeling, Guédez (2003) proposed seismic-derived densities for the lower crust and mantle of 2.9 and 3.3 Mg/m^3, respectively, but due to the 3-D variations of the Caribbean slab and the upper crust, these value were adjusted to fit the calculated and the measured field of our final model. Adjusted densities of the lower crust and

lithospheric mantle in the area of the COLM profile are 2.85 and 3.17 Mg/m^3. The 3-D modeling makes clear that even if the 2-D refraction horizons are taken into account, the 3-D gravity effect has to be considered to fit the measured field.

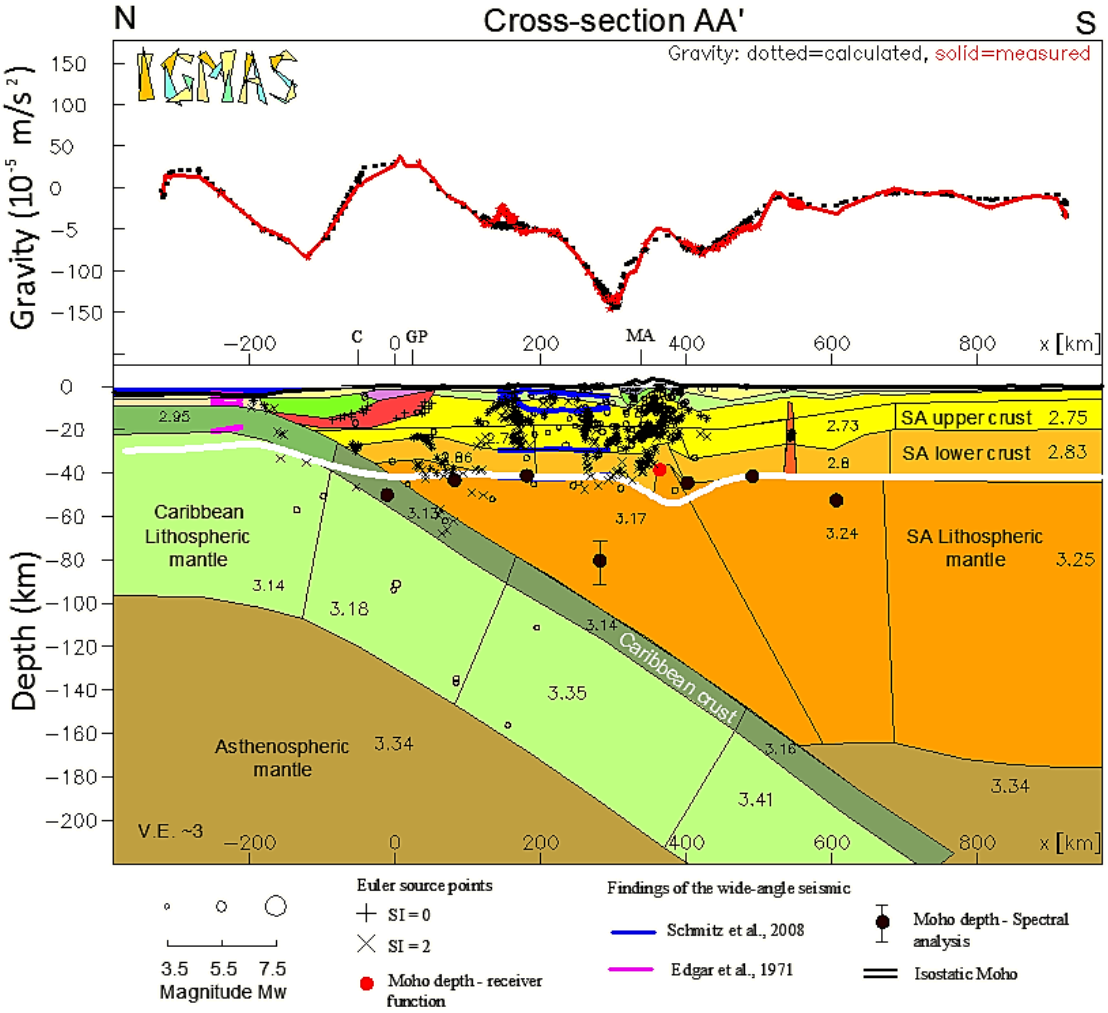

Figure 4.10 Vertical cross section AA′ (for location see Figure 4.2). This profile corresponds to the vertical cross section used to build the 3-D model which overlaps the 2-D velocity profile COLM. The upper part shows two lines: the measured gravity curve in red and the gravity of the 3-D density model (black dotted line). The lower part represents the modeled structures of the lithosphere. Numbers indicate body density in Mg/m^3. Also included are the locations of the Euler source points (black stars and crosses), seismicity (black circles), findings of wide-angle seismic (blue and purple lines), and results from receiver functions and spectral analysis. The white line is the Vening–Meinesz isostatic depth to Moho (see Figure 4.6 for references).

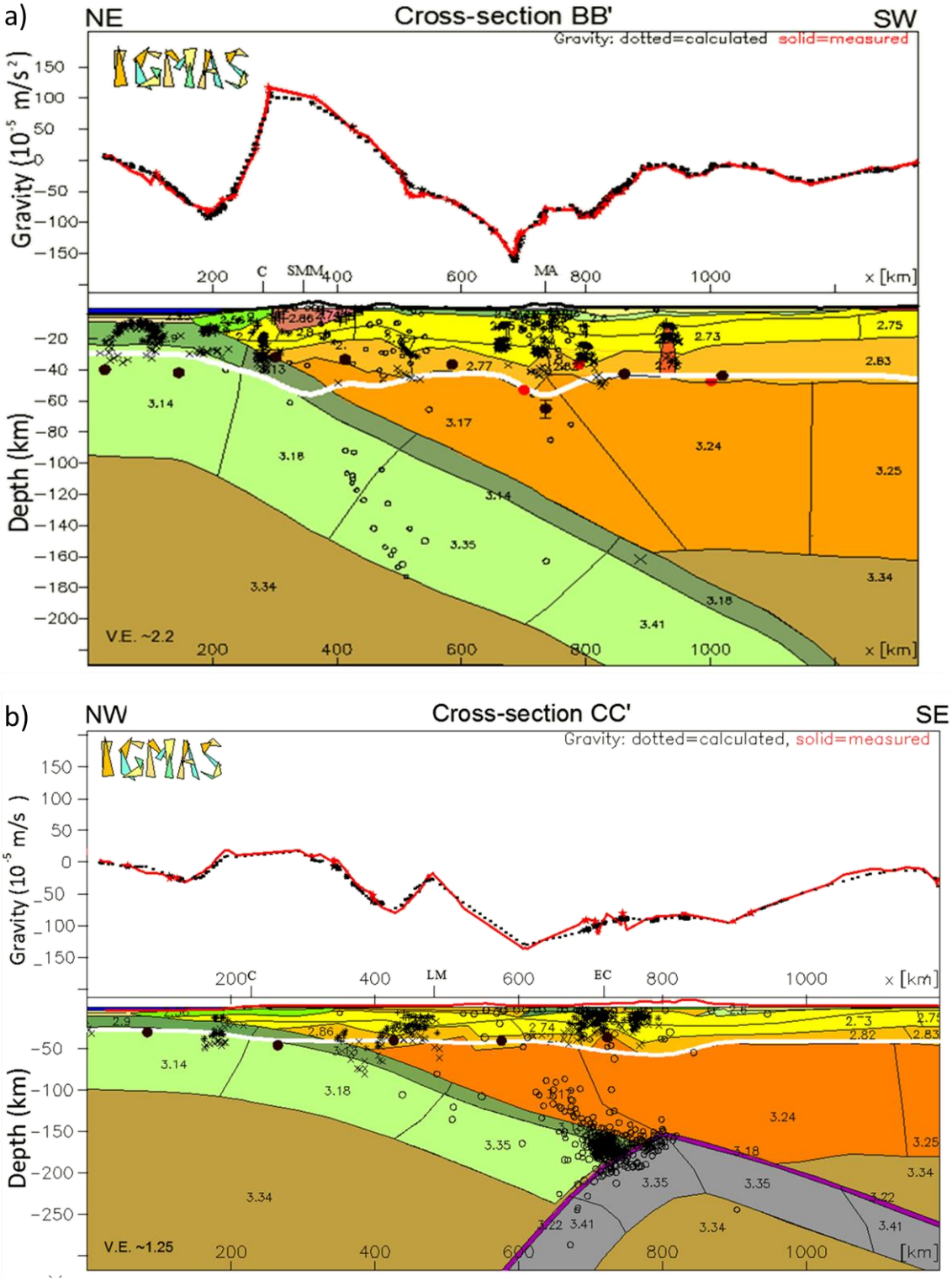

Figure 4.11 a) Vertical cross section BB′ along the Santa Marta massif and Mérida Andes. b) Vertical cross section CC′ along the Lower Magdalena and Bucaramanga nest. Graphical indications as described in figure 4.10.

In addition, cross section AA′ shows the effectiveness of spectral analysis and Euler deconvolution (inverse modeling). Estimations of the Moho from spectral analysis show good fit with the 2-D refraction horizons of the COLM profile (Guédez 2003). Standard errors for the depth estimations provide confidence limits for these values. For instance, values with low standard errors have good correlation with the seismic model. On the other hand, a value with a high standard error beneath the Mérida Andes estimated a structure at 80 ±10 km depth that had no correlation with any geological feature. Dense clusters of Euler's source points mark strong density contrasts beneath the Mérida Andes and surroundings areas. These clusters were interpreted as the edges and centers of several bodies, which were afterwards modeled to fit the observed gravity. For instance, a high density body was included to fit observed gravity and rocks that crop out in the Guajira peninsula. Likewise, a needle-like intrusive body south of the Mérida Andes was modeled. The proposed geometry for these bodies was achieved by constraining them at depth with the Euler's source points. Very small bodies were not modeled. This was because the wavelengths of the anomalies caused by these bodies are too short. Another method that provided insight into the structures in this area was isostatic analysis, which provided the isostatic compensation level for the continental area. Figure 7 shows that the isostatic compensation level is in good agreement with the Moho estimated with seismic modeling and receiver function techniques. For the oceanic areas, the compensation level is not representative because the isostatic calculations assumed a typical continental crust.

Cross section BB′ cuts the 3-D model roughly along NW–SE from the Colombian Basin to the Barinas–Apure Basin. BB′ crosses the Santa Marta massif, which has a higher positive BA in the study area (Figure 4.2). In the central portion, BB′ crosses the Mérida Andes and ends near the Guyana shield at its southeastern tip. Figure 4.11a shows that the Euler

deconvolution, receiver functions and the isostatic compensation surface level are the primary data constraining the geometry of the continental Moho. Seismic hypocenters at depths down to 150 km seismicity are scarce and do not define a clear slab. Due to the lack of better constraining data, the top of the slab was finely fitted accordingly to the long wavelength of the observed gravity field and according to the seismotectonic model presented in the previous section.

In this cross section the depths of mass centers vary from 10 km in Colombian basin near the Southern Caribbean thrust system to 40 km at the northern edge of Santa Marta massif. In Colombian basin, the location of the points in the Colombian basin clearly marks density contrasts within the Caribbean plate. This has led to the assumption that the slab gradually sags towards the continent. This behavior is also observed in sections AA' and CC'. The Euler points calculated using SI = 0 and 2 yielded mass centers at an approximate location of the Santa Marta massif. The Santa Marta massif is an uplifted region formed of predominantly crystalline rocks accreted to South America during Cretaceous times. The geometry of this rock body was modeled following the edge of the density contrast by Euler points (SI = 0). According to the gravity anomaly, this massif has very high density compared with the Caribbean slab and the surroundings continental rocks. Due to the Euler points, the short wavelength of the observed gravity high and the lack of other constraining data, we explain the observed anomaly as being caused by the high-density crustal body, rather than the thinner crust.

Cross section CC′ is roughly parallel to cross section BB′ (Figure 4.2). It runs through the Colombian and Low Magdalena Basins and crossed the Colombian Eastern cordillera and the Bucaramanga seismic nest. At the northwestern end of the Low Magdalena Basin this section crosses a positive BA attributed to a basement high. Due to the lack of other constraining data,

the Moho and the intermediate depth discontinuity modeled in this cross follows the isostatic compensation surface, assuming that the regional isostatic compensation occurs primarily in the mantle.

Major crustal bodies modeled in figure 4.11b represent the subducted Caribbean slab and a portion of the Nazca slab, which extend from southwest Colombia. In spite of no crossing those profiles the northern upper surface of the Caribbean slab largely follows the seismic structure of the seismic profiles 15, 16 and 17 given by Edgar et al. (1971). The position of the Caribbean slab was adjusted as predicted by the Focal mechanics solutions (previous section) and thus might be expected that solutions from the Bucaramanga seismic nest have sources in the slab. In spite of different alternatives model that have been proposed to explain the Bucaramanga seismic nest. We favor, probably the more convincing interpretation, is that seismic events in the Bucaramanga nest occurred a continuous slab from a portion of the Caribbean lithosphere subducting beneath northern Colombia. Such a hypothesis has been originally postulated by Dewey (1972) and used by Pennington (1981), Kellog and Bonini, Schneider et al. (1987), Van der Hilst and Mann (1994), Malavé and Suárez (1995), Taboada et al. (2000) and Zarifi et al. (2007) to describe the subduction, overlap and/or collision of the Caribbean and Nazca plates. Zarifi et al. (2007) proposed a scenario of collision between the edges of the Nazca and the Caribbean slabs, but there is no obvious reason as to why this would occur, especially because this assumption contradict the tomographic model of Van der Hilst and Mann (1994), which show a portion of the Nazca slab north of Bucaramanga.

In the area, the present gravity modeling propose a structure with an overlap area between the Nazca and Caribbean slabs as was proposed by Van der Hilst and Mann (1994), and include a collision zone as suggested by Zarifi et al. (2007), since this geometry explain the complexity in the source of earthquakes inside the nest. The main difference, as illustrated in

figure 4.11d, is that the observed seismicity result from the collision of the southern segment of the Caribbean slab with the top of the Nazca plate.

4.6.3. Moho

The depth to the Moho discontinuity (i.e. crust-mantle boundary) was used to estimate the crustal thickness of both oceanic and continental crust. The crustal thickness of the continental plate was assumed to be the depth to the Moho discontinuity, and for the offshore areas was calculated by subtracting the modeled Moho depth from the bathymetry. The thickness of the oceanic and continental crust obtained from the 3D density model is shown in figure 4.12. The Caribbean plate seemed to have a heterogeneous crustal thickness. Typical thickness in the Venezuelan and Colombian basins is 18 km. This thickness is observed in approximately 75% of the study area. The thickest oceanic crust is observed in the southern Colombian Basin. Its low FAA values suggest that the crustal thickness in this area is caused by more than 10 km of light density deformed sediments and metamorphic rocks of the accretionary prism developed by the Neogene convergence between the Caribbean and South American plates. Regions with a greater crust thickness than 18 km correlate with bathymetric features, e.g. the South Nicaraguan Rise, and the Beata and Aves Ridges. The Beata Ridge was compensated for by a crustal root that exceeded 20 km. The Beata ridge represents the western edge of the Venezuelan Basin and is mainly limited by horsts and grabens. Seismic refraction profiles presented by Edgar et al. (1971) and reinterpreted by Donnelly (1994), showed that in the southwestern area of the Beata ridge is about 20 km deep and 10 km in the northeastern area. In contrast, according to our interpretation based on a gravity model that matches the Bouguer field in this area, the Beata ridge has an average thickness of approximately 20 km with a slightly increase in the southwestern area. Similar results were

observed below the Nicaragua Rise that shows a crustal root exceeding 25 km, which is also larger than the previously inferred 20 km (Edgar et al. 1971). Differences in deep of the root of the Caribbean crust in these areas are probably caused by the low resolution of the seismic data available and/or under estimation of the seismic velocities.

Thickness of the continental crust reaches values between 28 and ~64 km (Figure 4.12). The thickest crust was modeled underneath the Colombian Central and Eastern Cordilleras (~64 km). Beneath the Mérida Andes a maximum of ~65 km is reached, and this value gradually decreases toward the south and north of the main strike of this feature. The maximum crustal thickness of ~60 km is partially constrained by receiver function analysis (Niu et al. 2007) with Moho depths of 58 and 55 km around this maximum (Figures 4.10 and 4.11a). Moho depth estimations of 42 and 38 km beneath the Mérida Andes from receiver function analysis correlate well with the intracrustal density discontinuity in this area and with uplifted blocks along the strike of the structure. The geometry and position of these blocks are partially constrained by dense clusters of Euler's source points (Figures 4.10 and 4.11a).

Beneath Falcón Basin and the Maracaibo block, the crustal thickness values extracted from the gravity model are consistent with the crustal thickness modeled along the 70°W (Bezada et al. 2008) and COLM (Guédez 2003) profiles. For instance, crust thickness shows values of approximately 27 and 35 km, which was consistent with the crustal thickness of ~27 km modeled along the 70°W and COLM profiles. The regional extension of this anomalous crustal thickness of 27 km was limited to the area of Falcón Basin.

Underneath Lower Magdalena Basin, the crust is 35 km thick and thickens to 40 km in the Middle Magdalena area. These values gradually decrease to 25 km to the north along the Colombian coast. The gravimetric high in the middle Magdalena Basin was modeled with a Moho depth of 30 km, covering an area of 150 × 150 km^2. This area has the shallowest crustal

thickness onshore. The high topography of the Western, Central, and Eastern cordilleras is compensated by thick crust that reaches more than 50, 55, and 65 km, respectively.

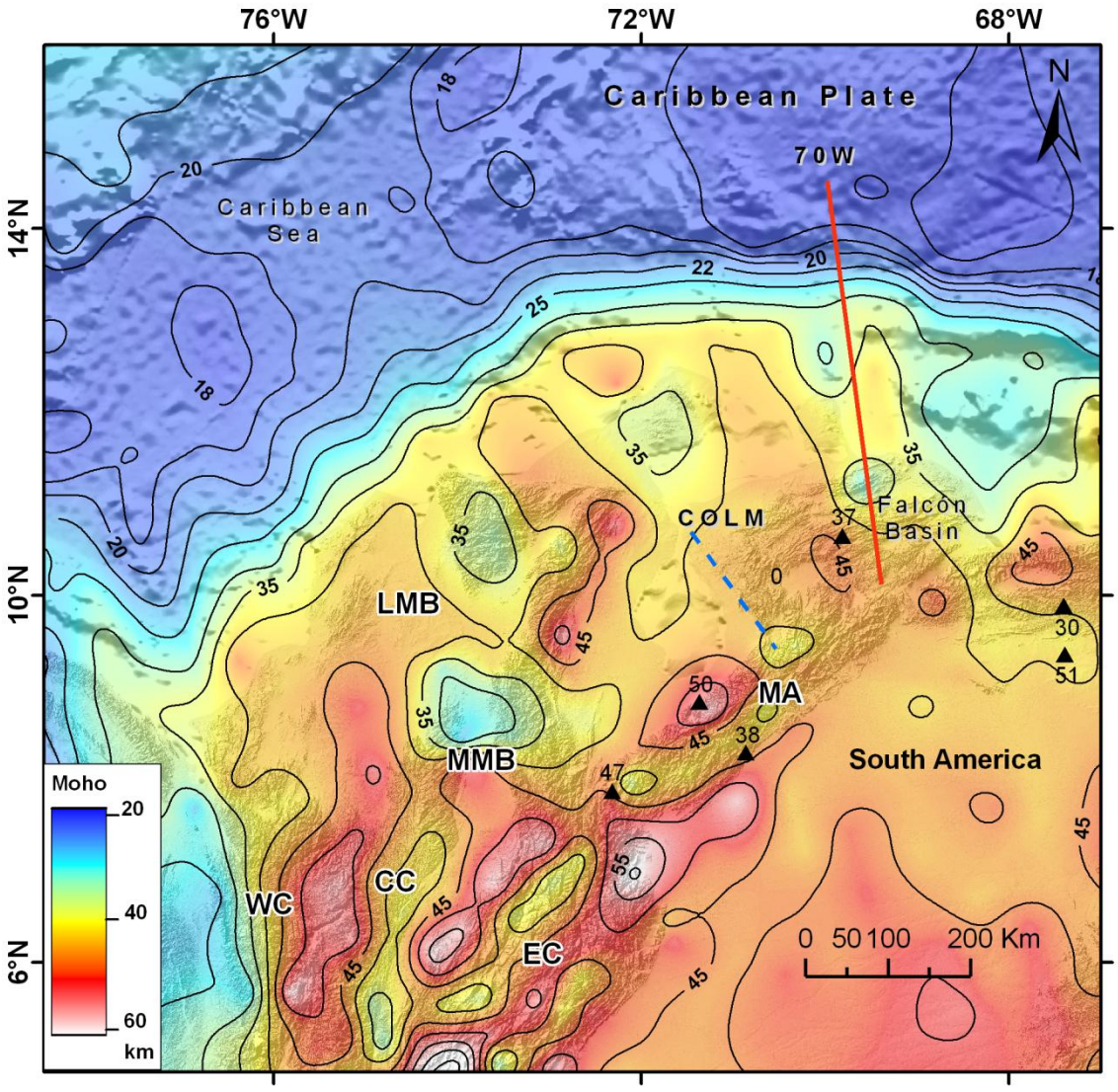

Figure 4.12 Crustal thickness resulting from the model (includes shaded digital topography and bathymetry illuminated from the NW). Variable contour lines (black lines). The reflection/wide-angle profiles used to derive our reference model are shown as red, purple, and blue lines labeled as 70W, 81, and COLM.

4.6.4. Lithosphere–asthenosphere boundary

The lithospheric mantle resulting from our best-fitting model in the continental margin reaches depths between 90 and 170 km. In particular, the depth to the LAB beneath the Mérida Andes is ~120 km. This value increases to 145 km below the Barinas–Apure and Guárico Basins. Underneath the Colombian cordilleras, the lithospheric crust is also thicker than 120 km, but gradually decreases northward. There, it is substituted by Caribbean oceanic crust. Lower densities with respect to the surroundings were assigned below volcanic zones in Colombia, which reflect the effect on the densities of its thermal conditions, whereas the LAB underneath the Guyana Shield, which corresponds to a cool and low-density body, reaches values higher than 170 km. These results have to be considered as a rough approximation because there were not additional data available to constrain these values. Moreover, this deep boundary could be shifted approximately 10 km without affecting the fit of the final model, which was a magnitude higher than the standard errors found in the gravity dataset.

4.6.5. Caribbean plate

The density of 2.95 Mg/m^3 selected for the Caribbean plate body is an average of the values expected for oceanic crust lithology characterized by the presence of basalts and dolerite. This value is higher than the mean density of 2.78 Mg/m^3 calculated from the results of the Deep Sea Drilling Project sites from Leg 4 and 15 (Figure 4.6) (Fox and Schreiber 1978), but within the ranges of normal oceanic crust (Christensen and Mooney 1995). Moreover, this relatively high density is adequate for most of the basalt-dolerite rocks forming nearly all oceanic crust, and it is relatively lower than the density values calculated by Hacker et al. [2003] for metamorphosed and fresh basalts with heat fluxes higher than 60 mW/m^2. At near-seafloor conditions, fresh oceanic crust would have a density of 3.05 Mg/m^3. Therefore,

a density of 2.95 Mg/m^3 selected for the oceanic crust of the Caribbean plate implies a mixture of fresh basalts and metamorphosed basalts that is consistent with seismic findings. Furthermore, an increase in the estimated average basalt-dolerite rock density is necessary for achieving a fit with the observed FA anomaly.

Figure 4.13 shows the depth of the subducted Caribbean slab resulting of our final model. This map was obtained by interpolation of the top of the slab and shows contour lines every 10 km up to 190 km depth and includes a topography–bathymetry shaded map. Figure 4.13 shows the Caribbean slab as a continuous feature. This implies that the region was characterized by a continuous, SE trending shallow subduction zone. The depths for the top of the slab are from 20 km at the Colombian Basin to 190 km toward the southeast of the Mérida Andes. The culmination of the Caribbean slab at this location offers a possible explanation for the cluster of seismicity in northern Colombia (Corredor 2003). The dip direction of the slab measured near the cross section CC′ is ~N150°E ± 5 (western Colombia), increasing eastward to near South direction (measured near the cross section AA′). The more abrupt changes in the strike of the slab occur beneath the Santa Marta massif and following the strike of the Santa Marta fault system. The dip angle in the gravity model based on the seismicity ranges between 12° and 20°. In addition, the interpreted 3-D geometry of the Caribbean slab is consistent with the results of Malavé and Suárez (1995) on the basis of the examination of the focal depths. Based upon the new focal depths and gravity modeling, our interpretation is that the slab continues underneath the Maracaibo block.

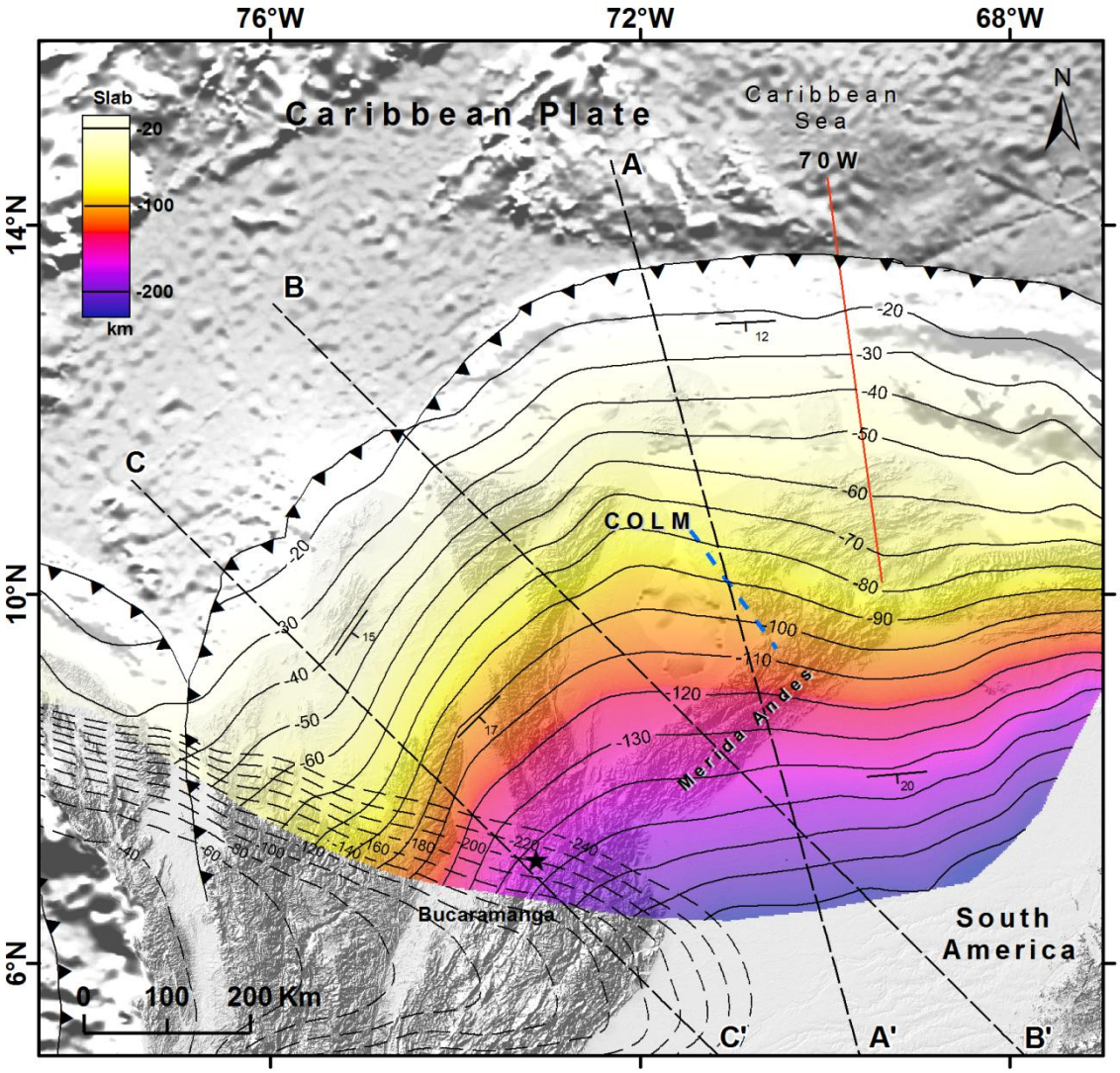

Figure 4.13 Geometry of the Caribbean slab underneath the continental margin resulting from the model (includes shaded digital topography and bathymetry illuminated from the NW). Segmented lines are contours of the top of the Nazca slab. Contour lines every 10 km Blue and red lines show locations of the seismic profiles.

4.7. Conclusions

Gravity data analysis and forward gravity modeling were used to construct a 3-D lithospheric density model of northeastern South America. 3-D gravity modeling allowed the

available results from 2-D seismic models to be extended in a realistic 3-D distribution of densities constrained by results from seismic refraction, receiver function analysis, seismicity, focal mechanism solutions, and surface geology.

Analysis of the Bouguer anomaly generated by the final 3-D density model revealed that this model reproduced the observed Bouguer anomaly at a regional scale. The final average misfit between the observed and modeled Bouguer anomalies had a standard deviation of $\pm 12.36 \times 10^{-5}$ m/s^2, which lies within the maximum error of the measured Bouguer anomaly ($\pm 14.03 \times 10^{-5}$ m/s^2). A discussion of the geometry of the major density discontinuities within the model lead to the following main conclusions:

1. The Caribbean slab extends from northern Colombia to the area of the Bucaramanga nest, which is a seismic cluster located beneath the southern edge of the Maracaibo block. Here, the slab inclines approximately 15°, and the dip angle increases up to 20° at depths greater than 100 km. The dip direction of the slab changes from N~150°E ± 5 in western Colombia to south direction in eastern Venezuela. This change occurs mainly underneath the Maracaibo block.
2. The results suggest that the continental crust at this region is relatively light and the average density of the Caribbean crust, despite its anomalous thickness and heterogeneity, is typical for an oceanic crust. Density variation within the continental lithospheric crust is mainly dominated by tectonic and thermal age, and the density values of the bodies used for modeling the Guyana shield are slightly higher than the densities of the continental crust near the Caribbean–South American boundary. In addition to this regional behavior, the lithospheric mantle in the volcanic zones in Colombia was modeled with a lower density to reflect the effects of its thermal conditions, which also include a thinner lithosphere.
3. Focal mechanism solutions and 3-D distribution of the recent seismicity in the region,

analyzed by means of P arrivals, showed good correlation with the regional tectonics of northern Colombia and western Venezuela and supported the thesis of oblique subduction underneath the Maracaibo block proposed by Malavé and Suárez (1995).

Despite the current data limitations the results presented here represents a uniquely detailed and well-constrained representation of the lithospheric density distribution and give useful hints for the evaluation and construction of dynamic models of northwestern South America. Finally, we suggest that a detailed study of the continental lithosphere base on teleseismic and regional seismology (e. g. Finite frequency P-wave tomography and/or imaging of scattered waves in receiver functions), which might provide a better determination of the Caribbean slab position. We also suggest that a new study of the micro seismicity might improve the presented 3D lithospheric model.

5. Summary and outlook

5.1. Conclusions

A new Bouguer gravity map of Venezuela was developed based on an up-to-date dataset available in the country. All data were reprocessed and homogenized according to gravity processing standards, and the effects of the topography were corrected with digital topographic maps. The final dataset was comprised of more than ~80,000 observation points. Standard errors of the new database are approx. 0.5×10^{-5} m/s^2 for observed measurement and in the range of $\pm$ (5–15)$\times10^{-5}$m/s^2 for the calculated Bouguer anomaly. However, maximum errors which are higher than expected were found. For purposes of a continental to regional scale density modeling the database is good enough.

The new Bouguer anomaly map of Venezuela was interpreted by applying different inverse and forward techniques. For instance, curvature analysis, and Euler deconvolution. The performed curvature analysis and Euler source points of the gravity field show density contrasts of the major features mainly from shallow structures (e.g. attached material in the Coastal Cordillera Thrust Belt). Locations of Euler source points were interpreted as derived from slab positions in western and eastern Venezuela. This result supports the thesis of slab underneath Maracaibo and Mérida Andes and does not corroborate the interpretation of detached oceanic slab underneath Maturin Basin.

The Free-Air gravity and topography were used to performed admittance analysis of the data windows over the Mérida Andes provided elastic thicknesses in the range of 30–35 km. *Te* values presented in this work using the admittance method were found to be lower than *Te* calculations carried out in previous studies on the scale of South America and surrounding plates. These differences in the Te calculation could be caused by tectonical heterogeneities and problems associated with the admittance technique (window size, data coverage and presence of noise), but these arguments are still in discussion. It is possible that satisfactory results for this area that has a very complicated structure could only be obtained by a more sophisticated approach.

Gravity data analysis and forward gravity modeling were used to construct a 3-D lithospheric density model of northern South America. This 3-D gravity modeling allowed the

visualization of interpreted horizon in 2-D seismic models over the whole area, extended in a realistic 3-D distribution of densities. The final model was constrained by results from seismic refraction as well as receiver function analysis, seismicity, focal mechanism solutions, and surface geology.

Analysis of the Bouguer anomaly generated by the final 3-D density model revealed that this model reproduced the observed Bouguer anomaly at a regional scale. The final average misfit between the observed and modeled Bouguer anomalies had a standard deviation of $\pm 12.36 \times 10^{-5}$ m/s^2, which lies within the maximums error expected of the calculated Bouguer anomaly ($\pm 14.03 \times 10^{-5}$ m/s^2).

Main conclusions derived from the discussion of the major tectonic features in the 3-D model were:

In Northwestern South America, the Caribbean slab extends from northern Colombia to the area of the Bucaramanga nest, which is a seismic cluster located beneath the southern edge of the Maracaibo block. Here, the slab inclines approximately 15°, and the dip angle increases up to 20° at depths greater than 100 km. The dip direction of the slab changes from N~150°E ± 5 in western Colombia to South direction in western Venezuela. This change occurs mainly underneath the Maracaibo block.

The results suggest that the continental crust at this region is relatively light and the average density of the Caribbean crust, despite its anomalous thickness and heterogeneity, is typical for an oceanic crust. Density variation within the continental lithospheric crust is mainly dominated by tectonic and thermal age, and the density values of the bodies used for modeling the Guyana shield are slightly higher than the densities of the continental crust near the Caribbean–South American boundary. In addition to this regional behavior, the lithospheric mantle in the volcanic zones in Colombia was modeled with a lower density to reflect the effects of its thermal conditions, which also include a thinner lithosphere.

Focal mechanism solutions and 3-D distribution of the recent seismicity in the region, analyzed by means of P arrivals, showed good correlation with the regional tectonics of northern Colombia and western Venezuela and supported the thesis of oblique subduction underneath the Maracaibo block proposed in seismological studies in this area.

In Eastern Venezuela, modeling results support the hypothesis of subduction-transform propagation model mechanism which involves purely westward subduction with the slab

break off along a vertical, dip-slip tear through the lithosphere. Rather small contributions on the gravity field have been found from alternative slab position underneath Eastern Venezuela Basin.

5.2. Outlook

Apart from the gravity modeling to resolve the open questions related to the position of the Caribbean slab and the continental crustal structures overlying the slab. I suggest that a detailed study of the micro seismicity of the continental lithosphere is necessary, which might provide a better determination of the Caribbean slab position and hence, improve the presented 3D lithospheric model.

The Bouguer gravity map presented in this work can be greatly improved by adding more gravity data in areas with scarce and poor quality data (e.g. Mérida Andes and Guyana shield). The gravity database can be combined with satellite-derived gravity models making possible the analysis of the density structure for those low-coverage regions of the South American continent.

Considering the new projects in this area and the amount of new data that have been collected the structure of the 3-D model could be improved to generate a more detailed structure. This model could be combined with another potential field modeling, such as, magnetic to constrain further the main geometries of first-order density discontinuities. A possible extension of the model to nearby areas might produce new results where geo-information produced by geophysical experiments conducted along the Caribbean margin could be compiled in one model to generate an integrated image of the entire continental lithosphere structure.

Apart from the continental cortical structure to resolve the open questions related to the low density and low velocity material in central and eastern Venezuela new geophysical methods and/or measurements (active or passive seismic measurements) are necessary. A more detailed model could answer the question of the existence of serpentinized mantle, milonization or intructions under the Coastal cordilleras in the northern of Venezuela, which is also relevant for understanding seismic activity, and provide new keys of the geodynamic of this region.

After recognizing, the differences in the values of elastic thickness presented in this dissertation, that probably are caused by the simple model used to estimate the elastic thickness. This study was based on one-dimensional inverse techniques applied along selected profiles. In the near future, I attempt to produce a new map of elastic thickness for the Northern South American plate (work in progress). I pretend to use the effective elastic thickness for constraining factors and processes affecting the geodynamics of the continental lithosphere (temperature, crustal and lithospheric thickness, and compositional crustal structure, deformation and stress fields) and compare new results with previous authors. This will involve characterize the rigidity structure that exists along the Caribbean margin. I am using the fan wavelet method for flexural isostatic analysis developed by Kirby and Swain (2009), that is able to recover a value of T_e for each single point in a geographical grid inverting the coherence between topography and Bouguer anomaly. Due to the existence of the gaps areas and noise in the land gravity database available for the continent, the new analysis may be computed from gravity derived from satellite missions.

Also, this new data represent an improvement for the further gravity modeling, because gravity missions like GOCE (Gravity Field and Steady-State Ocean Circulation Explorer) provide Earth's gravity field and high-accuracy gravity gradients, which can be modeled simultaneously, allowing a better control of the modeled structures. Also, the GOCE mission aims at an accuracy of the gravity anomaly in the range of 1×10^{-5}m/s^2 that is better than the accuracy estimated for the gravity database presented in chapter 2.

6. References

Alfonso, M. (2004). *Interpretación Geofísica Integrada de transectas Norte-Sur y Oeste-Este en la Plataforma deltana de Venezuela*. Bsc. Thesis, Universidad Simón Bolívar.

Aubouin, J., *et al.* (1982). The Central American Trench as an example of a subduction zone. *Tectonophysics* **86**(1-3): 113-132.

Audemard, F. A. (1993). *Néotectonique, sismotectonique et aléa sismique du nord-ouest du Vénézuela (système de failles d'Oca-Ancón)*. PhD Thesis, University of Montpellier II.

Audemard, F. A. (1998). *Evolution géodynamique de la facade nord Sud-américaine: nouveaux apports de l'histoire geéologique du Bassin de Falcón, Vénézuéla*. XIV Caribbean Geological Conference, Trinidad.

Audemard, F. E. (1991). *Tectonics of Western Venezuela*. PhD Thesis, Rice University.

Audemard, F. E. and F. A. Audemard (2002). Structure of the Mérida Andes, Venezuela; relations with the South America-Caribbean geodynamic interaction. *Tectonophysics* **345**(1-4): 299-327.

Avé Lallemant, H. G. (1997). Transpression, displacement partitioning, and exhumation in the eastern Caribbean/South American plate boundary zone. *Tectonics* **16**: 272-289.

Ávila, M. (2005). *Modelado Bidimensional de la Corteza en la Zona de Colisión Caribe-Suamérica, Región Oriental de Venezuela (Estado Anzoátegui)*. BSc. Thesis, Universidad Simón Bolívar.

B.Sc.Ughi, A. (2002). *Modelaje geofísico integrado de la región central de Venezuela por medio del análisis de flexión de placas en la sección 67° 00' 00'' W*. B.Sc. Thesis, Universidad Central de Venezuela.

Ball, M. M. and C. G. A. Harrison (1969). *Origin of the Gulf and Caribbean and implications regarding ocean ridge extension, migration, and shear*. Transcripts Gulf Coast Association Geological Society**:** 287- 294.

Beck, C. (1985). *La chaine Caraïbe au méridien de Caracas: géologie, tectogenese, place dans l'évolution géodynamique Mesozoique-Cenozoique des Caraïbes Méridionales*. PhD. Thesis, L'Universite des Sciences et Techniques de Lille.

Bellizzia, A. B. (1986). *Sistema Montañoso del Caribe, una cordillera alóctona en la parte Norte de América del Sur*. Sociedad Venezolana de Geólogos, Memorias VI Congreso Geológico Venezolano. **10:** 6657-6836.

Bellizzia, M. (1961). *Geología del Macizo de El Baúl, Estado Cojedes*. III Congreso Geológico Venezolano, Ministerio de energía y minas. **4:** 1453-1530.

Bezada, M. J., *et al.* (2008). Crustal structure in the Falcón Basin area, northwestern Venezuela, from seismic and gravimetric evidence. *Journal of Geodynamics* **45**(4-5): 191-200.

Bhattacharyya, B. K. and L.-K. Leu (1977). Spectral Analysis of Gravity and Magnetic Anomalies due to Rectangular Prismatic Bodies. *Geophysics* **42**(1): 41-50.

Birch, F. (1960). The Velocity of Compressional Waves in Rocks to 10 Kilobars, Part 1. *J Geophys Res* **65**(4): 1083-1102.

Birch, F. (1961). The Velocity of Compressional Waves in Rocks to 10 Kilobars, Part 2. *J Geophys Res* **66**(7): 2199-2224.

Bonini, W. E., *et al.* (1977). *Gravity studies across the western Caribbean Mountains*. V Congreso Latinoamericano de Geología. Caracas, Venezuela. **I:** 2299-2311.

Bonini, W. E., *et al.* (1980). *Late Cenozoic uplifts of the Maracaibo - Santa Marta Block, slow subduction of the Caribbean plate and results*
from a gravity study. 9th Trans. Caribbean Geol**:** 99 - 105.
Bosch, M. and I. Rodriguez (1992). North Venezuelan collisional crustal block: The boundary between the Caribbean and South American plates. *Journal of South American Earth Sciences* **6**(3): 133-143.
Bowland, C. L. and E. Rosencrantz (1988). Upper crustal structure of the western Colombian Basin, Caribbean Sea. *Geological Society of America Bulletin* **100**(4): 534-546.
Burke, K. (1988). Tectonic evolution of the Caribbean. *Annual Review Earth Planetary Sciences* **16**: 201-230.
Burke K, *et al.* (1978). Bouyant ocean floor and the evolution of the Caribbean. *Journal of Geophysical Research* **83**: 3949-3945.
Carballo, A. (2004). *Modelo Geodinámico Integrado de la Subcuenca de Guárico y la Cordillera Central Venezolana en el Estado Guárico*. Thesis, Universidad Simón Bolívar.
Carbotte, S. M., *et al.* (2004). New Integrated Data Management System for Ridge2000 and MARGINS Research. *Eos Trans. AGU* **85**(51): 533.
Castillo, E. (2005). *Modelado 2D Gravimétrico y Magnético de un transecto O-E en la Cuenca Oriental de Venezuela*. Bsc. Thesis, Universidad Simón Bolívar.
Ceron, J. (2008). *Crustal structure of the Colombian Caribbean basin and margins*. PhD. Thesis, University of South Carolina.
Chacín, L., *et al.* (2008). Flexural and gravity modelling of the Mérida Andes and Barinas-Apure Basin, Western Venezuela. *Tectonophysics* **405**(1-4): 155-167.
Chacín, L. F. (2003). *Modelo geodinámico integrado de la Cuenca Barinas - Apure y los Andes de Mérida en el estado Táchira*. Thesis, Universidad Simón Bolívar.
Christensen, N. I. and W. D. Mooney (1995). Seismic velocity structure and composition of the continental crust: A global view. *J. Geophys. Res.* **100**(B6): 9761-9788.
Clark, S. A., *et al.* (2008). Identification and tectonic implications of a tear in the South American plate at the southern end of the Lesser Antilles. *Geochem. Geophys. Geosyst.* **9**.
Colletta, B., *et al.* (1997). Tectonic inheritance, crustal architecture, and contrasting structural styles in the Venezuela Andes. *Tectonics* **16**(5): 777-794.
Colmenares, L. and M. D. Zoback (2003). Stress field and seismotectonics of northern South America. *Geology* **31**(8): 721-724.
Cooper, G. R. J. (2004). Euler deconvolution applied to potential field gradients. *Exploration Geophysics* **35**(3): 165-170.
Corredor, F. (2003). Seismic strain rates and distributed continental deformation in the northern Andes and three-dimensional seismotectonics of northwestern South America. *Tectonophysics* **372**(3-4): 147-166.
DeMets, C., *et al.* (1994). Effect of Recent Revisions to the Geomagnetic Reversal Time Scale on Estimates of Current Plate Motions. *Geophys Res Lett* **21**(20): 2191–2194.
Dewey, J. (1972). Seismicity and tectonics of western Venezuela. *Bulletin of the Seismological Society of America* **62**(6): 1711 -1751.
Dimitriadis, K., *et al.* (1987). A BASIC program for 2-D spectral analysis of gravity data and source-depth estimation. *Computers & Geosciences* **13**(5): 549-560.
Donnelly, T. W. (1985). Mesozoic and Cenozoic plate evolution of the Caribbean region. F. G. Stehli and S. D. Webb**:** 89-121.
Donnelly, T. W. (1994). The Caribbean sea floor. *Caribbean geology: an introduction*. D. SK and J. TA, Assoc, Kingston**:** 41-64.

Donnelly, T. W., *et al.* (1990). History and tectonic setting of Caribbean magmatism. *The Caribbean Region (The Geology of North America)*. G. Dengo and J. E. Case, Geol. Soc. Am. **H:** 339-374.

Drewes, H., *et al.* (1991). Absolute and relative gravimetric surveys of national and geodynamic networks in Venezuela. *Journal of South American Earth Sciences* **4**(4): 273-286.

Edgar, N. T., *et al.* (1971). Seismic refraction and reflection in Caribbean sea. *AAPG Bulletin* **55**(6): 833-870.

Ewing, J., *et al.* (1960). Geophysical Measurements in the Western Caribbean Sea and in the Gulf of Mexico. *J. Geophys. Res.* **65**(12).

Feo-Codecido, G., *et al.* (1984). *Basement and Paleozoic rocks of the Venezuelan Llanos basins*. The Caribbean-South American Plate Boundary and Regional Tectonics. R. B. Hargrave, Geol. Soc. of Am. **Boulder:** 175-187.

FitzGerald, D., *et al.* (2004). New discrimination techniques for Euler deconvolution. *Computers & Geosciences* **30**(5): 461-469.

Forsyth, D. W. (1985). Subsurface Loading and Estimates of the Flexural Rigidity of Continental Lithosphere. *J. Geophys. Res.* **90**(B14): 12623-12632.

Fox, P. J. and E. Schreiber (1978). Compressional Wave Velocities in Basalt and Dolerite Samples Recovered during Leg 15. *DSDP Initial Reports*. **15:** 1013-1016.

Freymueller, J. T., *et al.* (1993). Plate Motions in the North Andean Region. *J Geophys Res* **98**.

Frisch, W., *et al.* (1992). Origin of the Central American ophiolites: Evidence from paleomagnetic results. *GSA Bulletin* **104**(10): 1301-1314.

FUNVISIS (2007). *Digital seismological database, Earthquakes data from 1910 to 1997*. Caracas,Venezuela, Fundacion Venezolana de Investigaciones Sismologicas.

Gardner, G. H. F., *et al.* (1974). Formation velocity and density---the diagnostic basics for stratigraphic traps. *Geophysics* **39**(6): 770-780.

Giunta, G., *et al.* (2002). The southern margin of the Caribbean Plate in Venezuela: tectono-magmatic setting of the ophiolitic units and kinematic evolution. *Lithos* **63**(1-2): 19-40.

Gómez, J., *et al.* (2007). *Mapa Geológico de Colombia*. Bogotá, INGEOMINAS.

González de Juana, C., *et al.* (1980). *Geología de Venezuela y de sus Cuencas Petrolíferas* Caracas, Ediciones Foninves.

Götze, H. J. (1978). Ein numerisches Verfahren zur Berechnung der gravimetrischen Feldgrößen dreidimensionaler Modellkörper. *Meteorology and Atmospheric Physics* **27**(2): 195-215.

Götze, H. J. and B. Lahmeyer (1988). Application of three-dimensional interactive modeling in gravity and magnetics. *Geophysics* **53**(8): 1096-1108.

Graterol, V. R. (1988). *Mapa de anomalía de Bouguer de la Republica de Venezuela*. Caracas, Universidad Simón Bolívar; Dirección de Cartografía Nacional de Venezuela; Energy, Mines and Resources Canada; Defense mapping agency, Inter American geodetic survey**:** Mapa de anomalía de Bouguer de la Republica de Venezuela (P=2.67 g/cc).

Guédez, R. (2003). *Estudio cortical en el área centro-norte y noroccidental de Venezuela a partir de datos de sísmica de refracción*. B.Sc. Bsc Thesis, Universidad Central de Venezuela.

Gutscher, M. A., *et al.* (1999). Tectonic segmentation of the North Andean margin: impact of the Carnegie Ridge collision. *Earth and Planetary Science Letters* **168**(3-4): 255-270.

Hacker, B. R. and G. A. Abers (2004). Subduction Factory 3: An Excel worksheet and macro for calculating the densities, seismic wave speeds, and H2O contents of minerals and rocks at pressure and temperature. *Geochem. Geophys. Geosyst.* **5**.

Hacker, B. R., *et al.* (2003). Subduction factory 1. Theoretical mineralogy, densities, seismic wave speeds, and H2O contents. *J. Geophys. Res.* **108**(B1): 2029.

Hackley, P. C., *et al.* (2006). *Mapa Geológico de Venezuela a Escala 1:750,000: U.S. Geological Survey Open-File Report 2006-1109*, U.S. Geological Survey.

Hamza, V. M. and M. Muñoz (1996). Heat flow map of South America. *Geothermics* **25**(6): 599-621.

Heintz, M., *et al.* (2005). Upper mantle structure of the South American continent and neighboring oceans from surface wave tomography. *Tectonophysics* **406**(1-2): 115-139.

Heiskanen, W. and H. Moritz (1967). Physical geodesy. *Bulletin Géodésique (1946 - 1975)* **86**(1): 491-492.

Henriques, L. (2004). *Modelado geodinámico integrado de la Cuenca Barinas-Apure y los Andes de Mérida, Edo. Barinas*. B.Sc. Thesis, Universidad Simón Bolívar.

Hey, R. (1977). Tectonic evolution of the Cocos-Nazca spreading center. *Geological Society of America Bulletin* **88**(10): 1404-1420.

Hoernle, K., *et al.* (2004). 70 m.y. history (139-69 Ma) for the Caribbean large igneous province. *Geology* **32**(8): 697-700.

INGEOMINAS (1999). *Mapa Geotérmico de Colombia*. Informe Interno. Santafé de Bogotá, INGEOMINAS.

Izarra, C., *et al.* (2005). *Analyzing gravity anomalies over the Caribbean and northern Venezuela tectonic plate boundary*. 6th ISAG. Barcelona, Spain**:** 394-396.

Jácome, M. I., *et al.* (2003). Formation of the Maturin Foreland Basin, eastern Venezuela: Thrust sheet loading or subduction dynamic topography. *Tectonics* **22**.

Jácome, M. I., *et al.* (2008). Integrated seismic, flexural and gravimetric modelling of the Coastal Cordillera Thrust Belt and the Guárico Basin, North-Central Region, Venezuela. *Tectonophysics* **459**(1-4): 27-37.

Jaspe, J. (2004). *Generación de modelos de basamento de los arcos de Arauca y Mérida en la cuenca Barinas-Apure a través de integración de datos geofísicos*. B.Sc. Thesis, Universidad Central de Venezuela.

Jordan, T. H. (1975). The Present-Day Motions of the Caribbean Plate. *J. Geophys. Res.* **80**.

Karl, J. H. (1971). The Bouguer correction for the spherical earth. *Geophysics* **36**(4): 761-762.

Kellogg, J. N. and W. E. Bonini (1982). Subduction of the Caribbean plate and basement uplifts in the overriding South American plate. *Tectonics* **1**(3): 251-276.

Kellogg, J. N. and V. Vega (1995). Tectonic development of Panama, Costa Rica, and the Colombian Andes: constraints from global positioning system geodetic studies and gravity. *Special Paper-Geological Society of America* **V**(295): 75- 90.

Kennett, B. L. N. and E. R. Engdahl (1991). Traveltimes for global earthquake location and phase identification. *Geophysical Journal International* **105**(2): 429-465.

Kirby, J. F. and C. J. Swain (2009). A reassessment of spectral Te estimation in continental interiors: The case of North America. *J. Geophys. Res.* **114**(B8): B08401.

Kirchner, A. (1997). *3D-Dichtemodellierung zur Anpassung des Schwere-und des Schwerepotentialfeldes der zentralen Anden*. PhD. Thesis, Freie Universität Berlin.

Klitgord KD, a. S. H. (1986). Plate kinematics of the central Atlantic. *The Geology of North America. The Western North Atlantic Region* **M**: 351-378.

Kohn, B. P., *et al.* (1984). Mesozoic-Pleistocene fission-track ages on rocks of the Venezuelan Andes and their tectonic implications. *The Caribbean South American*

PIate Boundary and Regional Tectonics. W. E. Bonini, R. B. Hargraves and R. Shagam, Geological Society ofAmerica Memoir. **162:** 365-384.

Kwang-Sun, C., *et al.* (2007). Precise Terrain Torrection for Gravity Measurement Considering the Earth's Curvature. *Journal of the Korean Earth Science Society* **28**(7): 825-837.

Levander, A., *et al.* (2006). Evolution of the Southern Caribbean Plate Boundary. *Eos Trans. AGU* **87**(9).

Lonsdale, P. (2005). Creation of the Cocos and Nazca plates by fission of the Farallon plate. *Tectonophysics* **404**(3-4): 237-264.

Lonsdale, P. and K. D. Klitgord (1978). Structure and tectonic history of the eastern Panama Basin. *Geological Society of America Bulletin* **89**(7): 981-999.

Magnani, M. B., *et al.* (2009). Crustal structure of the South American-Caribbean plate boundary at 67W from controlled source seismic data. *J Geophys Res* **114**.

Malavé, G. and G. Suárez (1995). Intermediate-depth seismicity in northern Colombia and western Venezuela and its relationship to Caribbean plate subduction. *Tectonics* **14**: 617-628.

Malfait, B. T. and M. G. Dinkelman (1972). Circum-Caribbean Tectonic and Igneous Activity and the Evolution of the Caribbean Plate. *Geological Society of America Bulletin* **83**(2): 251-271.

Mantilla-Pimiento, A. M., *et al.* (2009). Configuration of the Colombian Caribbean Margin: Constraints from 2D seismic reflection data and potencial fields interpretation. *Subduction zone geodynamic*. Dubai, Springer**:** 247-271.

Mauffret, A. and S. Leroy (1997). Seismic stratigraphy and structure of the Caribbean igneous province. *Tectonophysics* **283**(1-4): 61-104.

McCann, W. R. and W. D. Pennington (1990). Seismicity, large earthquakes, and the margin of the Caribbean Plate. *The Caribbean region. The Geology of North America. Boulder*. G. Dengo and J. E. Case. **H**.

McConnell, R. K., *et al.* (1979). *Latin American Gravity Standardization Network 1977 (LAGSN77)*. Panama, Earth Physics Branch, Canada, and Servicio Geodesico Interamericano.

McKenzie, D. and C. Bowin (1976). The Relationship Between Bathymetry and Gravity in the Atlantic Ocean. *J. Geophys. Res.* **81**(11): 1903-1915.

McKenzie, D. and D. Fairhead (1997). Estimates of the effective elastic thickness of the continental lithosphere from Bouguer and free air gravity anomalies. *J. Geophys. Res.* **102**(B12): 27523-27552.

Meschede, M. (1998). The impossible Galapagos connection: Geometric constraints for a near-American origin of the Caribbean plate. *Geologische Rundschau* **87**(2): 200-205.

Meschede, M. and W. Frisch (1998). A plate-tectonic model for the Mesozoic and Early Cenozoic history of the Caribbean plate. *Tectonophysics* **296**(3-4): 269-291.

Mishra, D. C. and P. S. Naidu (1974). Two-Dimensional power spectral analysis of aeromagnetic fields. *Geophysical Prospecting* **22**(2): 345-353.

Molnar, P. and L. R. Sykes (1969). Tectonics of the Caribbean and middle America regions from focal mechanisms and seismicity. *Geological Society of America Bulletin* **80**: 1639– 1684.

Mooney, W. D., *et al.* (1979). Seismic refraction studies of the Western Cordillera, Colombia. *Bulletin of the Seismological Society of America* **69**(6): 1745-1761.

Moritz, H. (1980). Geodetic Reference System 1980. *Bulletin Géodésique* **54**: 395±405.

Muñoz, A. V. (1988). Tectonic patterns of the Panama Block deduced from seismicity, gravitational data and earthquake mechanisms: implications to the seismic hazard. *Tectonophysics* **154**(3-4): 253-267.

Nafe, J. and C. Drake (1963). Physical properties of marine sediments.The Sea. *Interscience* **3**.

Navarro, E., *et al.* (1988). Revisión y redefinición de unidades litoestratigráficas y síntesis de un modelo tectónico para la evolución de la parte Norte-Central de Venezuela durante el Jurásico Medio-Paleógeno. *Acta Cient Venez* **39**: 427-436.

Niu, F., *et al.* (2007). Receiver function study of the crustal structure of the southeastern Caribbean plate boundary and Venezuela. *J Geophys Res* **112**(112): 1-15.

Núñez, D. (2005). *Modelado gravimétrico y magnético de un perfil Oeste – Este a lo largo del paralelo 9°N en la cuenca Barinas-Apure*. B.Sc. Thesis, Universidad Simón Bolívar.

Ocola, L. C., *et al.* (1976). Project Nariño: crustal structure under southern Colombian-northern Ecuador Andes from seismic refraction data. *Bulletin of the Seismological Society of America* **65**(6): 1681-1695.

Ostos, M. (1990). Tectonic evolution of the south-central margin of the Caribbean based on geochemical dates (Evolución tectónica del margen Sur-Central del Caribe basado en dates geoquímicos). *GEOS* **30**: 1-294.

Ostos, M., *et al.* (2005). Overview of the southeast Caribbean–South American plate boundary zone. *Geological Society of America Special Papers* **394**: 53-89.

Palma, M., *et al.* (2010). New focal mechanism solutions for Venezuela and neighbouring areas 2005-2008: importance of the National Seismological Network's density and distribution. *Rev. Téc. Ing. Univ. Zulia* **33**(2): 1 - 14.

Passalacqua, H., *et al.* (1995). Crustal Architecture and Strain Partitioning in the Eastern Venezuelan Ranges. *Petroleum basins of South America*. R. S. A. Tankard and y. H. Welsink, Memorias de la AAPG. **62:** 667 - 679.

Pašteka, R. and P. Richter (2002). *A simple approach to regularised gradients calculation in gravimetry and magnetometry*. EAGE 64th Firenze, Italy

Pennington, W. D. (1981). Subduction of the Eastern Panama Basin and Seismotectonics of Northwestern South America. *J Geophys Res* **86**.

Pérez-Gussinyé, M., *et al.* (2004). On the recovery of effective elastic thickness using spectral methods: Examples from synthetic data and from the Fennoscandian Shield. *J. Geophys. Res.* **109**(B10): B10409.

Perez, O. J. and Y. P. Aggarwal (1981). Present-day tectonics of the southeastern Caribbean and northeastern Venezuela. *Journal of Geophysical Research* **86**(B11): 10791-10804.

Perez, O. J., *et al.* (2001). Velocity Field Across the Southern Caribbean Plate Boundary and Estimates of Caribbean/South-American Plate Motion Using GPS Geodesy 1994-2000. *Geophys Res Lett* **28**.

Perez, O. J., *et al.* (1997). Microseismicity evidence for subduction of the Caribbean plate beneath the South American plate in northwestern Venezuela. *Journal of Geophysical Research* **102**(B8): 17875- 17882.

Pimiento, M. (2007). *Crustal structure of the southwestern Colombian Caribbean margin*. PhD. Thesis, Universität Jena.

Pindell, J. L. (1994). Evolution of the Gulf of Mexico and the Caribbean. *Caribbean Geology, an Introduction*. S. K. Donovan. Kingston, Jamaica, University of the West Indies**:** 13-39.

Pindell, J. L. and S. Barrett (1990). Geologic evolution of the Caribbean: A plate-tectonic perspective. *The Geology of North America. Vol, The Caribbean Region*. G. Dengo and J. E. Case, Geological Society of America. **H:** 405-432.

Pindell, J. L.*, et al.* (1988). A plate-kinematic framework for models of Caribbean evolution. *Tectonophysics* **155**(1-4): 121-138.

Pindell, J. L. and J. F. Dewey (1982). Permo-Triassic reconstruction of western Pangea and the evolution of the Gulf of Mexico/Caribbeanregion. *Tectonics* **1**.

Pindell, J. L.*, et al.* (2005). Plate kinematics and crustal dynamics of circum-Caribbean arc-continent interactions: Tectonic controls on basin development in proto-Caribbean margins. *Caribbean-South American plate interactions, Venezuela, GSA Special Paper 394*. H. G. A. L. a. V. B. Sisson. Boulder, CO, Geological Society of America**:** 7-52.

Regan, R. D. and W. J. Hinze (1976). The effect of finite data length in the spectral analysis of ideal gravity anomalies. *Geophysics* **41**(1): 44-55.

Reid, A. B.*, et al.* (1990). Magnetic interpretation in three dimensions using Euler deconvolution. *Geophysics* **55**(1): 80-91.

Reyes, J. (2002). *Modelaje geofísico integrado de la región central de Venezuela por medio del análisis de flexión de placas en la sección 66° 00' 00'' W*. B.Sc. Thesis, Universidad Central de Venezuela.

Roberts, A. (2001). Curvature attributes and their application to 3D interpreted horizons. *First Break* **19**(2): 85-100.

Rodríguez, I. (1986). *La Cuenca Oriental de Venezuela: Necesidad de imponer una carga adicional para producir la flexión observada de la litosfera*. Primeras Jornadas de Investigación en Ingeniería, Caracas, Universidad Central de Venezuela.

Rodriguez, J. and J. Sousa (2003). *Estudio geologico-estructural y geofisico de la seccion cabo San Roman-Barquisimeto, estados Falcon y Lara*. Bsc. Thesis, Universidad Central de Venezuela.

Rondon, K. (2004). *Modelo Geodinamico lntegrado de la Subcuenca de Guarico y la Cordillera de la Costa en el Estado Anzoategui*. B.Sc. Thesis, Universidad Simón Bolívar.

Ross, M. and C. Scotese (1988). A hierarchical tectonic model of the Gulf of Mexico and Caribbean region. *Tectonophysics* **155**: 139- 168.

Roure, F.*, et al.* (1994). Geometry and kinematics of the North Monagas thrust belt (Venezuela). *Marine and Petroleum Geology* **11**(3): 347-362.

Russo, R. M.*, et al.* (1996). Shear-wave splitting in northeast Venezuela, Trinidad, and the eastern Caribbean. *Physics of the Earth and Planetary Interior* **95**: 251-275.

Russo, R. M. and R. C. Speed (1992). Oblique collision and tectonic wedging of the South American continent and Caribbean terranes. *Geology* **20**(5): 447-450.

Russo, R. M.*, et al.* (1992). Seismicity and Tectonics of the Southeastern Caribbean. *J Geophys Res* **98**.

Sallarès, V.*, et al.* (2003). Seismic structure of Cocos and Malpelo Volcanic Ridges and implications for hot spot-ridge interaction. *J. Geophys. Res.* **108**.

Sanchez-Rojas, J. (2011). New Bouguer gravity maps of Venezuela: Representation and analysis of free-air and Bouguer anomalies with emphasis on spectral analyses and elastic thickness. *International Journal of Geophysics* **2012**: 1-19.

Sanchez, J.*, et al.* (2010). A 3-D lithospheric model of the Caribbean-South American plate boundary. *International Journal of Earth Sciences* **100**(7): 1697-1712.

Schmidt, S. and H. J. Götze (1998). Interactive visualization and modification of 3D-models using GIS-functions. *Physics and Chemistry of The Earth* **23**(3): 289-295.

Schmitz, M., *et al.* (2008). Crustal thickness variations in Venezuela from deep seismic observations. *Tectonophysics* **459**(1-4): 14-26.

Schmitz, M., *et al.* (2002). The crustal structure of the Guayana Shield, Venezuela, from seismic refraction and gravity data. *Tectonophysics* **345**(1-4): 103-118.

Schmitz, M., *et al.* (2005). The major features of the crustal structure in north-eastern Venezuela from deep wide-angle seismic observations and gravity modelling. *Tectonophysics* **399**(1-4): 109-124.

Schneider, J. F., *et al.* (1987). Microseismicity and Focal Mechanisms of the Intermediate-Depth Bucaramanga Nest, Colombia. *J Geophys Res* **92**(B13): 13,913-913,926.

Schubert, C. (1984). Basin formation along the Bocono-Moron-El Pilar Fault System, Venezuela. *J. Geophys. Res.* **89**(B7): 5711-5718.

Sinton, C. W., *et al.* (1998). An oceanic flood basalt province within the Caribbean plate. *Earth and Planetary Science Letters* **155**(3-4): 221-235.

Sobolev, S. V. and A. Y. Babeyko (1994). Modeling of mineralogical composition, density and elastic wave velocities in anhydrous magmatic rocks. *Surveys in Geophysics* **15**(5): 515-544.

Sousa, J., *et al.* (2005). *An integrated geological-geophysical profile across northwestern Venezuela*. 6th International Symposium on Andean Geodynamics. Barcelona**:** 689-692.

Spadea, P., *et al.* (1989). High-Mg extrusive rocks from the Romeral Zone ophiolites in the southewestern Colombian Andes. *Chemical Geology* **77**(3-4): 303-321.

Spector, A. and F. S. Grant (1970). Statistical Models for Interpreting Aeromagnetic Data. *Geophysics* **35**(2): 293-302.

Stephan, J.-F. (1982). *Evolution geodinamique du domaine Caraibe, Andes et chaine Caraibe sur la transversale de Barquisimeto (Venezuela)*. PhD. Thesis.

Stephan, J., *et al.* (1990). Paleogeodynamic maps of the Caribbean: 14 steps from Lias to Present. *Bulletin de La Societe Geologique de France* **8**: 915-919.

Sykes, L. R., *et al.* (1982). Motion of Caribbean Plate during last 7 million years and implications for earlier Cenozoic movements. *J Geophys Res* **87**(B13): 10,656-610,676.

Taboada, A., *et al.* (2000). Geodynamics of the northern Andes: Subductions and intracontinental deformation (Colombia). *Tectonics* **19**: 787-813.

Tapias, F. (2002). *Modelo geológico – estructural, local y regional del subsuelo de Isla de Aves, empleando datos gravimétricos*. B.Sc. Thesis, Universidad Central de Venezuela.

Tassara, A., *et al.* (2007). Elastic thickness structure of South America estimated using wavelets and satellite-derived gravity data. *Earth and Planetary Science Letters* **253**(1-2): 17-36.

Thompson, D. T. (1982). EULDPH: A new technique for making computer-assisted depth estimates from magnetic data. *Geophysics* **47**(1): 31-37.

Tikhonov, A. N. and V. Y. Arsenin (1977). *Solutions of ill posed problems*. New York, Wiley.

Trenkamp, R., *et al.* (2002). Wide plate margin deformation, southern Central America and northwestern South America, CASA GPS observations. *Journal of South American Earth Sciences* **15**(2): 157-171.

Tselentis, G.-A., *et al.* (1988). A spectral approach to moho depths estimation from gravity measurements in Epirus (NW Greece). *Journal of Physics of the Earth* **36**(6): 255-266.

Van Andel, T. H., *et al.* (1971). Tectonics of the Panama Basin, Eastern Equatorial Pacific. *Geological Society of America Bulletin* **82**(6): 1489-1508.

Van der Hilst, R. (1990). *Tomography with P, PP, and pP delay-time data and the three-dimensional mantle structure below the Caribbean region*. PhD. Thesis, University of Utrecht.

Van der Hilst, R. and P. Mann (1994). Tectonic implications of tomographic images of subducted lithosphere beneath northwestern South America. *Geology* **22**(5): 451-454.

VanDecar, J. C., *et al.* (2003). Aseismic continuation of the Lesser Antilles slab beneath continental South America. *J Geophys Res* **108**.

Vargas, C. A., *et al.* (2007). Seismic structure of South-Central Andes of Colombia by tomographic inversion. *Geofísica Internacional* **46**(2): 117-127.

Vieira, E. (2005). *Modelado Bidimensional de la Corteza en la zona de colisión Caribe-Suramérica, Región Central de Venezuela (Edo. Guárico)*. B.Sc. Thesis, Universidad Simón Bolívar.

Viscarret, P., *et al.* (2009). New U-Pb zircon ages of El Baúl Massif Cojedes State, Venezuela. *Rev. Téc. Ing. Univ. Zulia* **32**(3): 210 - 221.

Watts, A. B. (1978). An analysis of isostasy in the World's Oceans 1. Hawaiian-Emperor Seamount Chain. *J. Geophys. Res.* **83**(B12): 5989-6004.

Weber, J. C., *et al.* (2001). GPS estimate of relative motion between the Caribbean and South American plates, and geologic implications for Trinidad and Venezuela. *Geology* **29**(1): 75-a-78.

Wilmes, H., *et al.* (2009). AGrav—The New International Absolute Gravity Database of BGI and BKG and its benefit for the Global Geodynamics Project (GGP). *Journal of Geodynamics* **48**(3-5): 305-309.

Wilson, J. (1965). Submarine fracture zones, aseismic ridges, and the international council of scientific unions line: Proposed western margin of the East Pacific Ridge. *Nature* **207**: 907-911.

Yépez, S. R., *et al.* (2005). *Integración geológica y geofísica del transecto "Puerto Maya-San Juan de los Morros"*. B.Sc. Thesis, Universidad Central de Venezuela.

Zarifi, Z., *et al.* (2007). An insight into the Bucaramanga nest. *Tectonophysics* **443**(1–2): 93-105.

7. Additional figures

a)

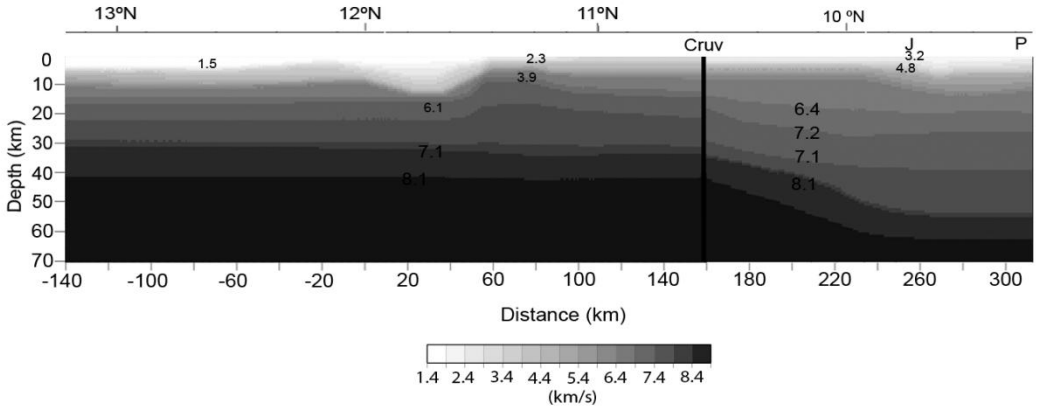

b)

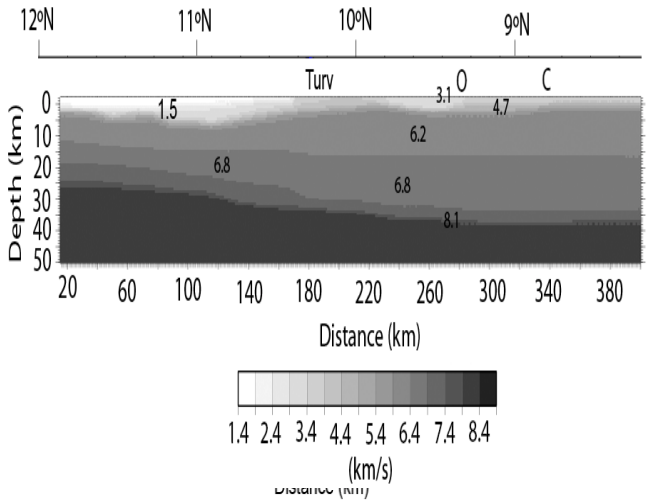

c)

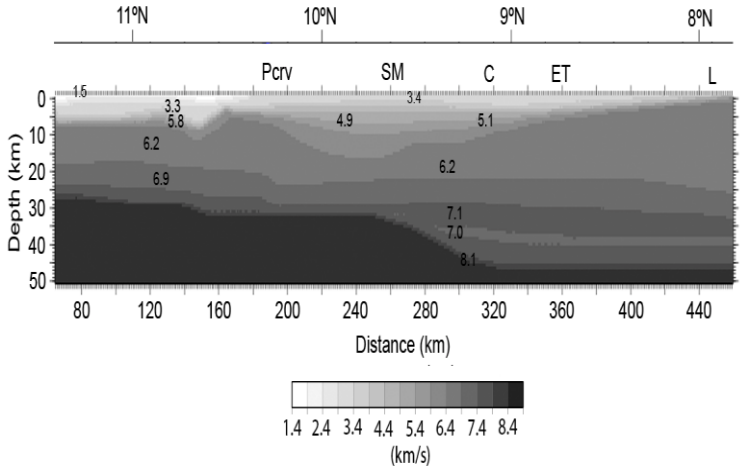

Figure 7.A

d)

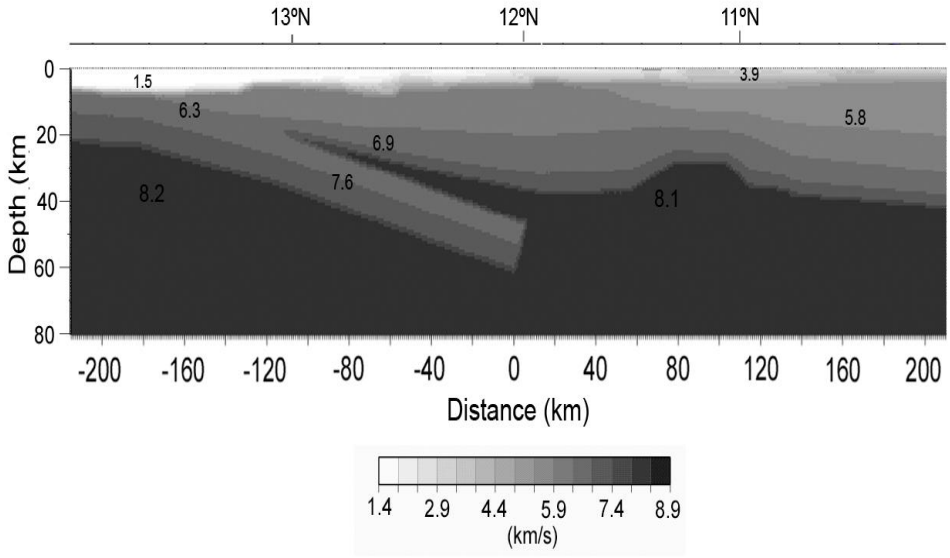

e)

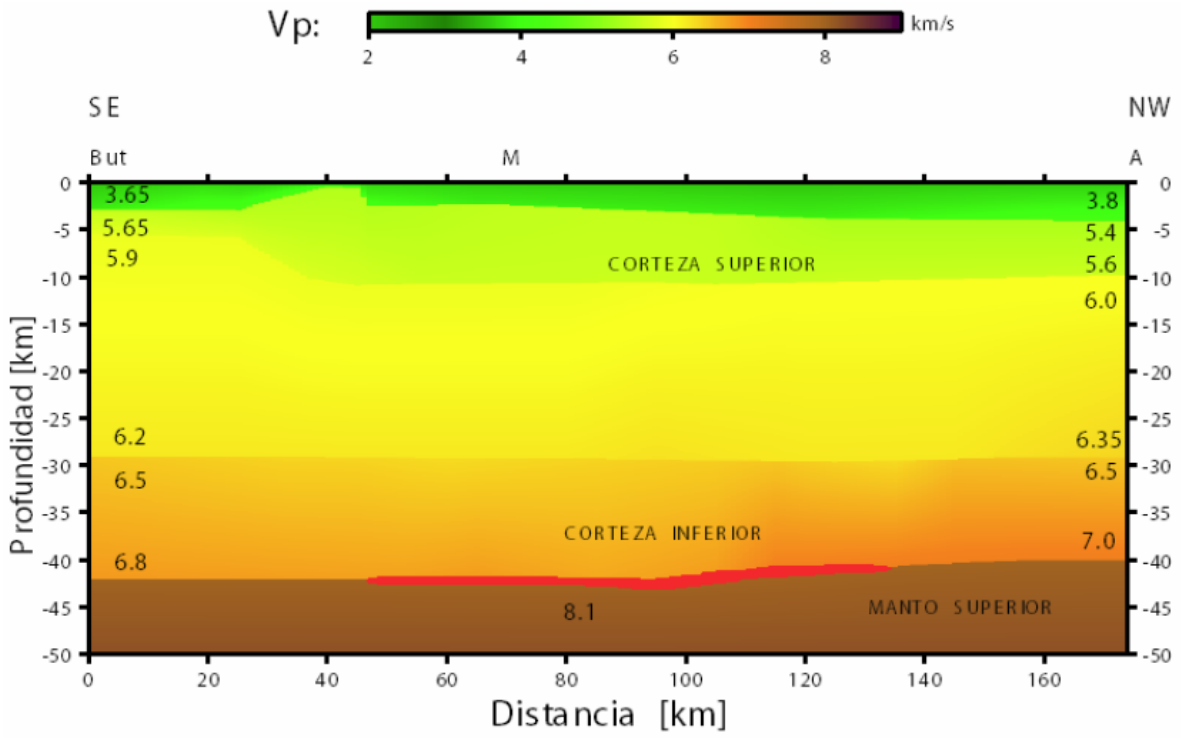

Figure 7.A (cont.) Velocity models used to estimate seismic-derived densities: a) Profile 64; b) Profile 65; c) Profile 67; d) Profile 74; and e) Profile COLM. The derived velocity model indicates an increased crustal thickness to the south with about 50 km, decreasing to 40 beneath PCRV and slight thinning towards the Caribbean Sea in the north.

a)

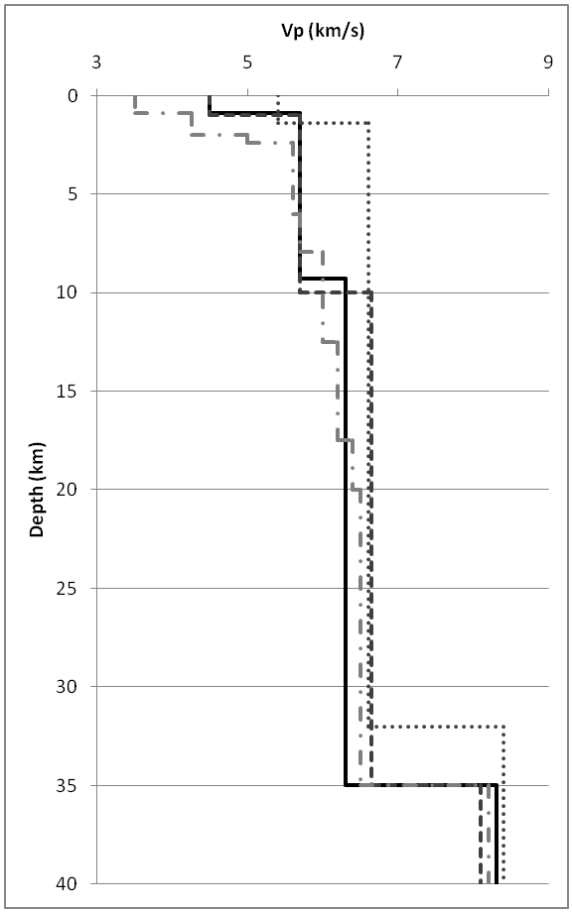

b)

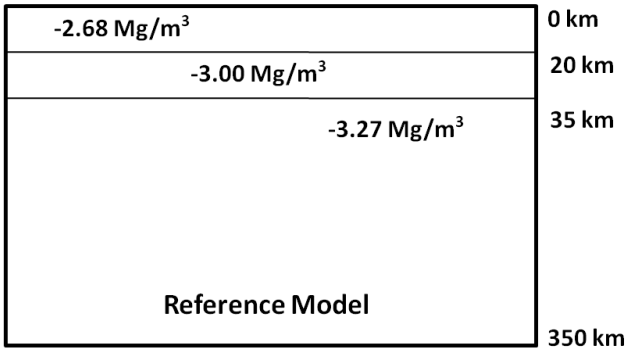

Figure 7.B a) 1-D velocity model of Venezuela used for the Hipocentral calculations. Black line RESVAC (Red Nacional de Apertura Continental), dashed line Pérez y Aggarwal (1981), doted and dashed line Franke (1994) dot line Duque (1999). b) Reference model used to calculate the background gravity field for the density model. The most used 1-D model (RESVAC) for Hipocentral calculations is the applied for FUNVISIS in Venezuela and surrounding areas. Before 1998 all hipocentral calculation used the model proposed for Pérez y Aggarwal (1981); Franke (1994) using a new data compilation, proposed a model based on 3D tomography in the eastern Venezuela which present more detailed structure up to 10 layers. That model has been considered the best approach for micro seismicity in this region (Baumbach et al. 2004). In 1999 Duque after evaluated the acelerographic records presented a new model for eastern Venezuela based on RESVAC model.

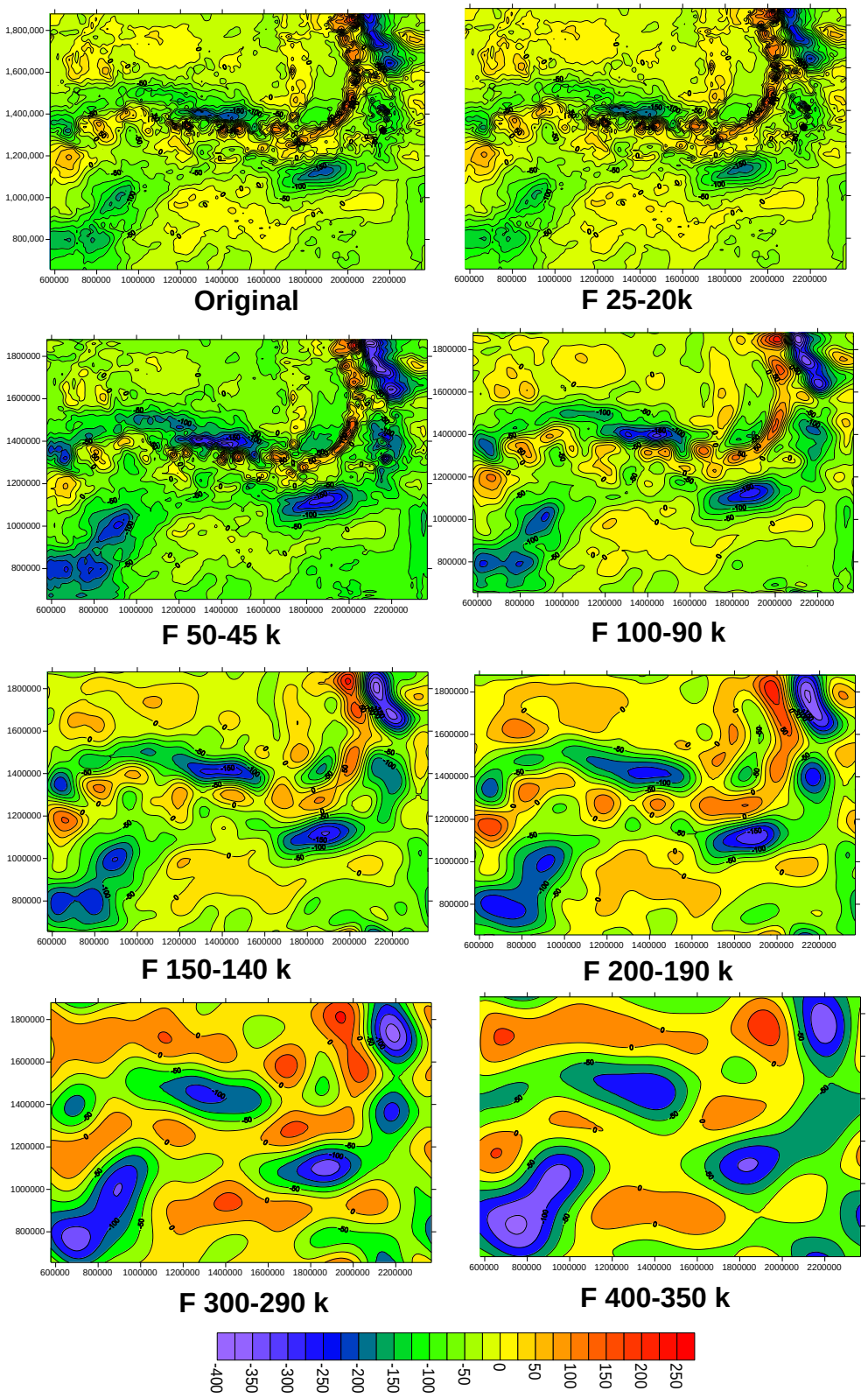

Figure 7.C Analysis a low pass filter with different cut-off wavelength (F) between 25 and 400 km of the Bouguer anomaly map of Venezuela.

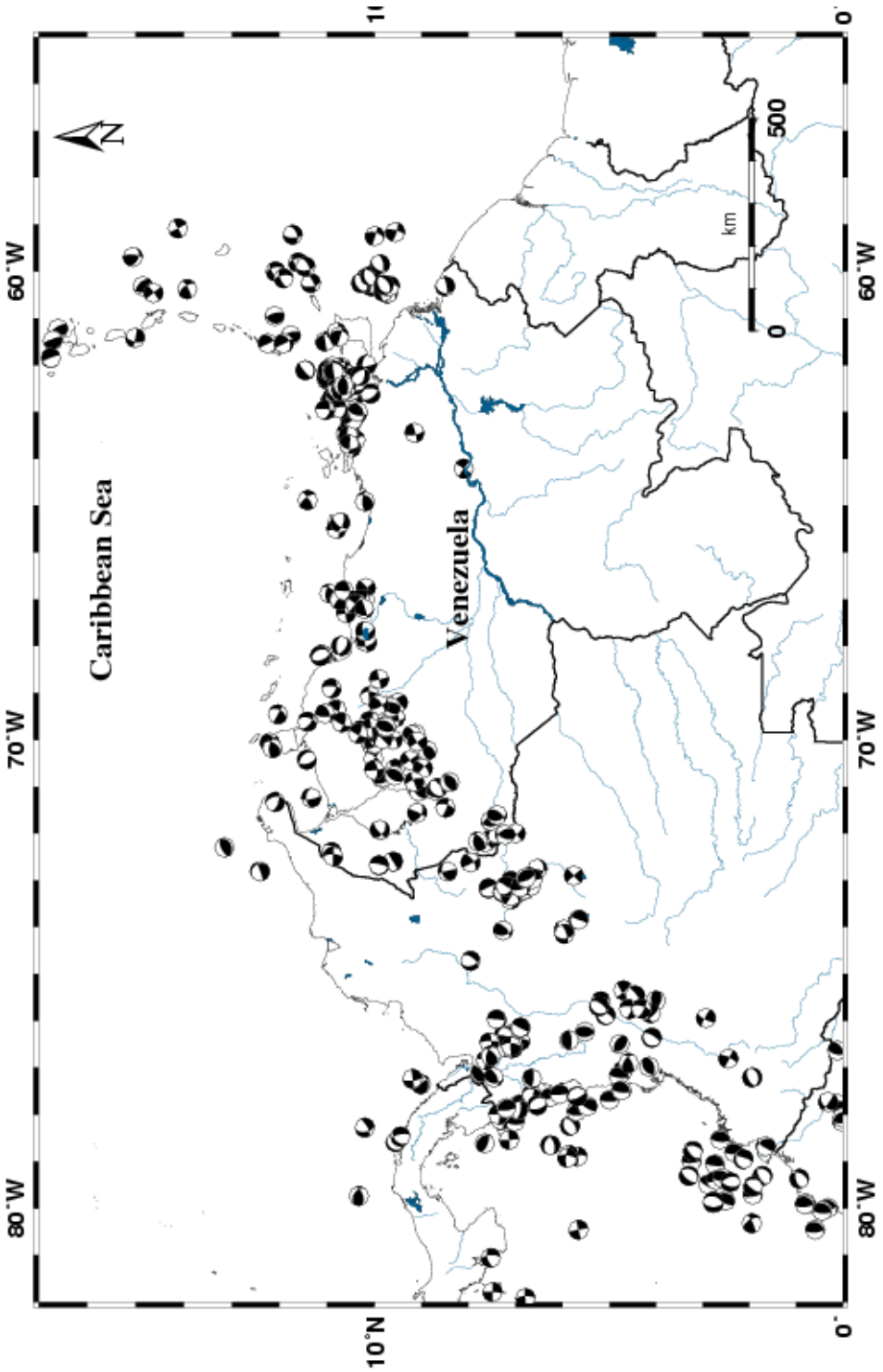

Figure 7.D Focal mechanism solutions from the Harvard and FUNVISIS catalogues (FUNVISIS 2007). Focal mechanism solutions reported by Palma et al. (2010) and Malavé and Suárez (1995). (Lower hemisphere projection).Alfonso, M. (2004). *Interpretación Geofísica Integrada de transectas Norte-Sur y Oeste-Este en la Plataforma deltana de Venezuela*. Bsc. Thesis, Universidad Simón Bolívar.

Acknowledgements

I am indebted to FUNVISIS and its people as it was there and with them that I first got involved with this project.

I would like to thank to Dr. Gustavo Malavé who support me during my race to get financial support.

I am especially grateful to Dr. Michael Schmitz who always pushed me to work hard at FUNVISIS and continued to support and challenge me during my post-graduate studies.

Special thanks to my advisor, Prof. Dr. Hans-Jürgen Götze (head of the Geophysics Department at the Christian-Albrechts-Universität zu Kiel). He supported my scientific project and the application to my scholarship.

I thank my fellow worker in CAU: Timo Damm and Ron Hackney, whom made me easier my survival during the first year at CAU.

This research would not have been possible without: Dr. Carla Braitenberg, Dr. Jörg Ebbing, Dr. Rezene Mahatsente, Dr. Zuzana Alasonati-Tasarova, Dr. Roman Pašteka, Monika Sobiesiak, Benjamin D. Gutknecht, Oscar Lücke, Dr. Sabine Schmidt, and Hans-Jürgen Götze which gave me useful comments and suggestion.

Finally, I would like to thank Maxlimer, my companion and partner in life, for her support and her unwavering confidence in my scientific ability. She is the candle which lights up my life

This work and the broader BOLIVAR and GEODINOS projects were made possible by funding from the NSF Continental Dynamics Program (grant EAR0003572 and EAR0607801) as well as FONACIT (grant G-2002000478) and PDVSA-INTEVEP-FUNVIS (project 04-141).

The work presented in this dissertation could not have been carried out without the support of the Institut für Geowissenschaften, Abteilung Geophysik, at Christian-Albrechts-Universität zu Kiel, to which I will be eternally thankful.

Eidesstattliche Erklärung

Hiermit versichere ich, dass ich vorliegende Arbeit selbständig verfaßt und keine anderen als die angegebenen Hilfsmittel benutzt habe. Die Stellen der Arbeit, die anderen Werken wörtlich oder inhaltlich entnommen sind, wurden durch entsprechende Angaben der Quellen kenntlich gemacht. Diese Arbeit hat in gleicher oder ähnlicher Form noch keiner Prüfungsbehörde vorgelegen. Hiermit versichere ich, dass die Arbeit unter Einhaltung der Regeln guter wissenschaftlicher Praxis der Deutschen Forschungsgemeinschaft entstanden ist.

I certify that this thesis is my own composition, all sources have been acknowledged and my contribution to the thesis is clearly identified. The thesis has not previously been accepted for a degree at this or another institution. I certify that the work has been undertaken in compliance with the German Research Foundation's (Deutsche Forschungsgemeinschaft, DFG) rules of good academic practice.

_____

Curriculum Vitae

Javier Sánchez Rojas

Date of Birth:	March 7, 1974
Place of Birth:	Maracay, Venezuela
Nationality:	Venezuelan.
Mother tongue	Spanish

Education

2001-1995	Bachelor of Science – Geophysical Engineering, Universidad Central de Venezuela (Zentrale Universität von Venezuela).
2007-2012	Doctorate in Natural Sciences, Christian-Albrechts-Universität zu Kiel, Kiel, Germany.

Work Experience

2001-2007	**Geophysicist III**	Venezuelan Foundation for Seismological Research (FUNVISIS),
1999	**Geophysicist**	Socororo 3D, Seismic reflection survey 1999. Westers Geophysical C.A.
1998-2001	**Teacher assistant**	.Geophysical Instrumentation. Universidad Central de Venezuela-Caracas.